Journal of Physical and Chemical Reference Data

Effective Attenuation Lengths for Different Quantitative Applications of X-ray Photoelectron Spectroscopy

Cite as: J. Phys. Chem. Ref. Data **49**, 033102 (2020); https://doi.org/10.1063/5.0008576
Submitted: 23 March 2020 • Accepted: 08 May 2020 • Published Online: 13 July 2020

A. Jablonski and C. J. Powell

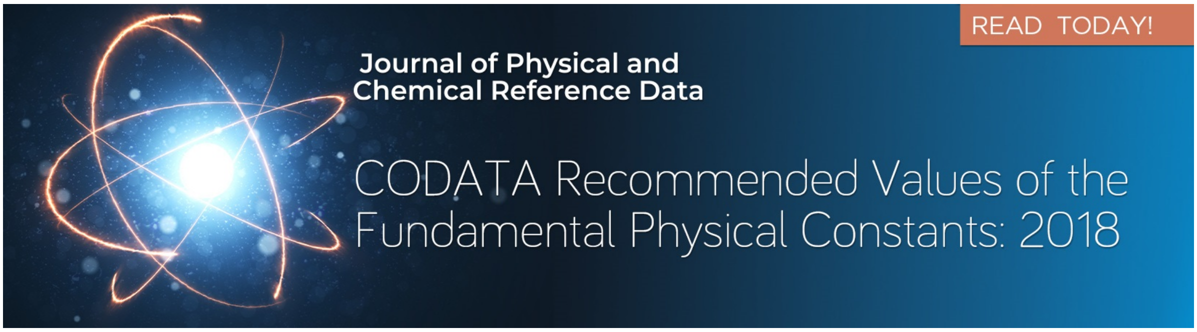

AIP Publishing

Effective Attenuation Lengths for Different Quantitative Applications of X-ray Photoelectron Spectroscopy

Cite as: J. Phys. Chem. Ref. Data 49, 033102 (2020); doi: 10.1063/5.0008576
Submitted: 23 March 2020 • Accepted: 8 May 2020 •

A. Jablonski[1] and C. J. Powell[2,a)]

AFFILIATIONS

[1] Institute of Physical Chemistry, Polish Academy of Sciences, ul. Kasprzaka 44/52, 01-224 Warsaw, Poland
[2] Materials Measurement Science Division, National Institute of Standards and Technology, Gaithersburg, Maryland 20899-8370, USA

a)**Author to whom correspondence should be addressed:** cedric.powell@nist.gov

ABSTRACT

The effective attenuation length (EAL) is a useful parameter in quantitative applications of x-ray photoelectron spectroscopy (XPS). This parameter is used in place of the inelastic mean free path (IMFP) in expressions for different XPS applications to correct those expressions for elastic scattering of the photoelectrons. We consider expressions used to determine (i) the thickness of an overlayer film on a planar substrate, (ii) the surface composition, (iii) the depth of a thin marker or delta layer, and (iv) the shell thickness of a core–shell nanoparticle. An EAL can be used for each of these applications. In general, the EAL depends on the particular defining equation as well as on the XPS configuration. Many attempts were made in the 1970s and 1980s to measure EALs for the determination of overlayer-film thicknesses, but there were often wide scatters in the reported results due to the difficulty in preparing uniform films with known thicknesses. We have therefore been motivated to calculate EALs for each application. The SRD 82 database from the National Institute of Standards and Technology (NIST) provides EALs for the measurement of overlayer-film thicknesses and of marker-layer depths. These EALs can be determined for photoelectron energies between 50 eV and 2 keV and for user-specified XPS configurations. We review EAL predictive equations for the determination of overlayer-film thicknesses on a planar substrate for XPS with unpolarized x rays and with linearly polarized x rays as well as an EAL predictive equation for quantitative analysis by XPS. These equations are simple analytical expressions that are valid for well-defined ranges of experimental conditions and for useful ranges of electron energies. We also point out that EALs for the determination of overlayer-film thicknesses can be derived from the simulated photoelectron intensities obtained from the NIST Database for the Simulation of Electron Spectra for Surface Analysis (SRD 100). Where possible, we make comparisons of the calculated EALs with illustrative experimental results. A key parameter in the EAL predictive equations is the so-called albedo, a useful measure of the strength of elastic-scattering effects in a material. The albedo is a simple function of the IMFP and the transport mean free path (TRMFP). We provide a tabulation of albedo and TRMFP values in the supplementary material for 41 elemental solids and 42 inorganic compounds for photoelectron energies between 50 eV and 30 keV. For other materials, albedo values can be determined from IMFP and TRMFP data available in the NIST SRD 82 and SRD 100 databases.

Key words: databases; effective attenuation length; predictive equations; surface analysis; x-ray photoelectron spectroscopy.

CONTENTS

List of Tables

List of Figures

1. Introduction

X-ray photoelectron spectroscopy (XPS) is in widespread use for a large variety of scientific and technological purposes. Figure 1 shows the number of papers published per year on XPS and the related technique of Auger-electron spectroscopy (AES) from 1991 to 2019 based on a Web of Science search using their acronyms and key phrases. Two sets of AES publication data are included in Fig. 1: one based on the use of "AES" in the search and the other without this term. The former dataset is an overcount (because AES is also an abbreviation for atomic emission spectroscopy), while the latter dataset is an undercount (since some Auger papers with AES in the title or abstract would be missed). Nevertheless, it appears from Fig. 1 that the number of Auger papers published per year is roughly constant or declining. In contrast, Fig. 1 clearly shows the large growth that has occurred in the number of XPS publications over the past 29 years. Nevertheless, the publication plots in Fig. 1 cannot, of necessity, represent the many unpublished practical applications of AES and XPS (e.g., from industrial laboratories) or the economic impacts of these applications.

A parameter known as the effective attenuation length (EAL) is in frequent use for certain quantitative applications of AES and XPS, as will be described in detail below. Since XPS applications are now much more common than AES applications, we will highlight the XPS applications in this review and merely point out similarities and differences relevant to AES when appropriate.

The EAL is used in place of the inelastic mean free path (IMFP) in expressions for different quantitative applications of XPS to correct those expressions for elastic scattering of the photoelectrons from their point of origin in a sample to their emission from the sample surface. Single and multiple elastic-scattering effects add complexity to models of photoelectron transport but were ignored in the early development of XPS. Use of the EAL is thus convenient in that relatively simple expressions developed when elastic-scattering effects were neglected [often referred to as being based on the straight-line approximation (SLA)] were found to be sufficiently reliable for many practical applications if the IMFP was replaced by an EAL in a particular expression. As we will see, however, different numerical EAL values are often needed for different XPS applications as well as for different instrumental configurations. It is therefore essential for an appropriate EAL to be chosen for a given application and configuration.

Technical Committee 201 on Surface Chemical Analysis of the International Organization for Standardization has defined the EAL as a "parameter which, when introduced in place of the IMFP into an expression derived for AES and XPS on the assumption that elastic-scattering effects are negligible for a given quantitative application, will correct that expression for elastic-scattering effects" (Ref. 1, Definition 4.35). Two important notes accompanying this definition have recently been revised as follows:

(1) The EAL can have different values for different quantitative applications of AES and XPS. However, the most common use of EAL is the determination of the thicknesses of overlayer films on flat substrates from measurements of the changes of overlayer and substrate Auger-electron or photoelectron signal intensities as a function of film thickness or of electron emission angle. For emission angles of up to about 60° (with respect to the surface normal), it is often satisfactory to use a single value of this parameter. For larger emission angles, the EAL can depend on this angle. EALs have also been used in equations for determining the

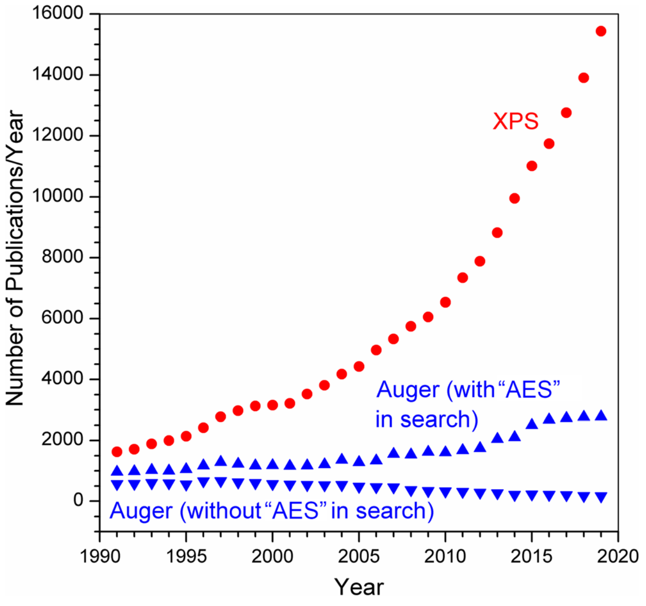

FIG. 1. Plot of the number of papers published per year on AES and XPS from 1991 to 2019 based on a Web of Science search using acronyms and key phrases for these techniques.

shell thicknesses of core–shell nanoparticles (NPs) and for quantitative analysis (to describe the changes in AES and XPS signal intensities due to elastic scattering).

(2) Since there are different uses of this term, it is recommended that users specify clearly the particular quantitative application and the definition of the parameter for that application (e.g., by giving an equation or by providing a reference to a particular source). EALs developed for one application should not be used for another application unless this usage has been validated.

We emphasize that the EAL is not a simple material parameter for a given material and electron energy such as the IMFP. Instead, the numerical value of the EAL for a material and electron energy generally depends on the defining equation for the particular application as well as on the experimental configuration. For XPS, the EAL also depends on the selected photoelectron line.

A general definition of quantitative analysis is "determination of the amounts of analytes detected in a sample" (Ref. 1, Definition 4.357). The result of such an analysis is then a number or a set of numbers that describes the composition of the volume contributing to the detected signal or of a particular phase in the sample. For AES and XPS, this information is obtained from the measured peak intensities or from the analyses of measured peak spectra.[2,3] The main purpose of a surface analysis is often to determine the average concentration of the analytes in the surface region of the sample (if this is assumed or found to be homogeneous) or otherwise to determine the concentrations of analytes laterally or as a function of depth.[3,4] Other important applications include the measurement of the thickness of an overlayer film on a substrate and the measurement of the shell thickness of a core–shell NP.

The surface sensitivity of XPS analyses arises from the small IMFPs of the detected photoelectrons, often between 0.5 nm and 5 nm for typical measurements with characteristic Mg or Al Kα x-ray sources.[5] In practical measurements, the surface sensitivity can be increased by detecting photoelectrons at more grazing emission angles or can be decreased by increasing the x-ray energy either by using x rays from x-ray tubes with Ti, Cr, Ga, or Zr anodes or from synchrotron x-ray sources. For AES, the IMFPs are typically between 0.3 nm and 6 nm for common measurement conditions, and the surface sensitivity can also be increased by detecting Auger electrons at more grazing emission angles.

In this review, we update and extend our two previous reviews on EALs.[6,7] Section 2 contains a short summary of how early measurements of EALs were made. These measurements were often difficult since they required the preparation of samples with a thin uniform film of known thickness on a planar substrate. Largely because of these difficulties, we describe in Sec. 3 how EALs can be calculated for different XPS applications. Expressions are given that enable EALs to be determined (i) for measurements of the thicknesses of overlayer films on planar substrates, (ii) for the determination of surface composition, and (iii) for the determination of marker depths (e.g., of delta layers). We also provide information on the use of EALs for determining shell thicknesses of core–shell NPs. We give examples of EAL calculations and make comparisons with illustrative experimental results. We provide information on IMFP data in Sec. 4 and give recommendations and concluding remarks in Sec. 5.

2. Early EAL Measurements

Early EAL measurements were made by depositing overlayer films of known thicknesses on a substrate and measuring changes in intensities of Auger-electron or photoelectron signals from the substrate or film as a function of film thickness. These measurements were based on the following assumptions:[8–10]

1. The surface of the substrate material is flat.
2. An overlayer film of known uniform thickness, t, can be deposited on the substrate.
3. The sample is amorphous or polycrystalline (i.e., there are no significant angular anisotropies in the photoemitted intensities due to diffraction or forward-focusing effects).
4. X-ray reflection and refraction are negligible (i.e., the x rays are not incident on the sample at a near-grazing angle of incidence).
5. The sample area irradiated by the x-ray beam is larger than the sample area viewed by the analyzer.
6. Attenuation of the x-ray beam is negligible within the information depth (ID) for the measurements.
7. Elastic scattering of photoelectrons in the sample is negligible (i.e., the SLA).

Some comments are given later on the consequences if assumptions 2, 3, and 7 are not valid.

It was then possible to derive simple expressions for the intensities of a substrate photoelectron peak, $I_s(t)$, and an overlayer photoelectron peak, $I_f(t)$, as a function of film thickness, t,

$$I_s(t) = I_s^{\infty}\exp\left\{-t/\left[\lambda_{in}^{f}(E_s)\cos\alpha\right]\right\} \tag{1a}$$

and

$$I_f(t) = I_f^{\infty}\left\{1-\exp\left[-t/(\lambda_{in}^{f}(E_f)\cos\alpha)\right]\right\}, \tag{1b}$$

where I_s^{∞} and I_f^{∞} are the corresponding peak intensities for the substrate material without an overlayer film and for the bulk overlayer material, respectively, $\lambda_{in}^{f}(E_s)$ and $\lambda_{in}^{f}(E_f)$ are the IMFPs of substrate photoelectrons with kinetic energy E_s in the overlayer film and of overlayer photoelectrons with energy E_f in the overlayer film, respectively, and α is the photoelectron emission angle with respect to the surface normal. If the IMFPs are known, Eqs. (1a) and (1b) can be rearranged to provide expressions for the film thickness as follows:

$$t = -\lambda_{in}^{f}(E_s)\cos\alpha\left[\ln I_s(t) - \ln I_s^{\infty}\right] \tag{2a}$$

and

$$t = -\lambda_{in}^{f}(E_f)\cos\alpha\ln\left\{1-\left[I_f(t)/I_f^{\infty}\right]\right\}. \tag{2b}$$

Alternatively, the values of the IMFPs can be determined from Eq. (2) if the film thicknesses are known.

Another approach was to measure the ratios of photoelectron peak intensities from the substrate and the overlayer. If the observed photoelectrons have similar energies (e.g., from an elemental solid and its oxide), $\lambda_{in}^{f}(E_s) \approx \lambda_{in}^{f}(E_f) \equiv \lambda_{in}$ and

$$t = \lambda_{in}\cos\alpha\ln(R+1), \tag{3a}$$

where

$$R = I_f(t)I_s^{\infty}/I_s(t)I_f^{\infty}. \tag{3b}$$

Many experiments were performed in the 1960s and 1970s, and Eqs. (1)–(3) were utilized to determine what were then thought to be IMFPs but are now known as EALs.[11–14] Thin films, typically of elemental solids, were deposited with varying thicknesses onto a substrate, and measurements were made on selected photoelectron peak intensities. Similar measurements were also made with Auger-electron peak intensities, but the AES formalism is more complicated in that account has to be taken of backscattering effects on the signals from the substrate and film.[15] Unfortunately, EAL data for the same material often showed considerable scatter (up to a factor of 4[11]), and it was thus difficult to determine the extent of any EAL variations from material to material.

Two major types of scientific problems are associated with the early EAL measurements by the overlayer-film method and a possible third problem also exists.[16] The first major problem is associated with the various sources of uncertainty in the experiments. These uncertainties include the lack of film uniformity (assumption 2 above), the effects of surface excitations (i.e., surface plasmons), the effects of interferences between intrinsic or shakeup excitations and extrinsic excitations, possible atomic reconstructions at the surface and the substrate/overlayer interface, intermixing at the substrate/overlayer interface, uncertainties in film-thickness determination, and the effects of possible angular anisotropies in photoelectron transport (assumption 3). When scanning tunneling and atomic force microscopes and low-energy electron microscopes became available in the 1980s, it was shown that the early stages of film growth were generally more complex than had been assumed previously. Film growth often started as islands on the substrate, which eventually coalesced as deposition proceeded. We give further comments on this topic in Secs. 3.1.2 and 5.6.

The second major problem is conceptual. As indicated by assumption 7, the effects of elastic-scattering on photoelectron trajectories were neglected in the development of Eqs. (1) and (2). It is now well known that these effects are often significant in AES and XPS and that the trajectories, on the average, are longer than would be the case if elastic scattering was insignificant (as indicated by trajectories B and C in Fig. 2). The effects are more pronounced in XPS because the photoemission process is anisotropic. The dependence of photoelectron intensities on overlayer-film thicknesses will generally not be exponential although for some common experimental conditions (to be discussed later) the dependence is approximately exponential. In these cases, the EAL is the appropriate parameter for describing the near-exponential dependences of photoelectron intensities on film thicknesses in Eqs. (1)–(3), as will be discussed later, rather than the IMFP. We will also see that the EAL can depend on the experimental configuration.

The third possible problem concerns the natural tendency of scientists to report results that are consistent with the current models. For example, if the overlayer films were not uniform, it would be reasonable to expect deviations from the exponential dependences expected from Eqs. (1) and (2). Results of these types might then be discarded. On the other hand, if exponential dependences were observed, these might not necessarily indicate that the films were uniform (as discussed in Sec. 3.1.2).

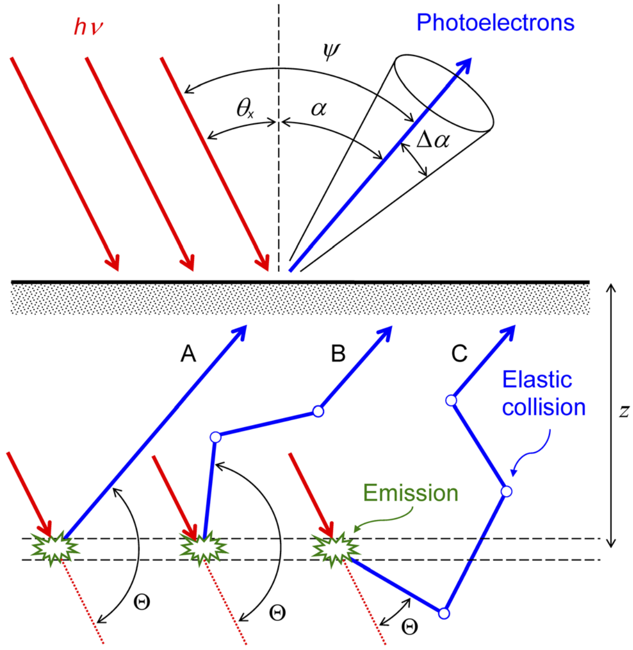

FIG. 2. (Top) Schematic outline of an XPS experiment. (Bottom) Examples of three possible photoelectron trajectories following photoemission occurring at a depth z from the sample surface.

It is difficult to estimate the uncertainties of the early EAL measurements due to the experimental and conceptual problems discussed here. We were therefore motivated to calculate EALs for different XPS applications to show how this parameter could vary with the overlayer-film thickness, the photoelectron emission angle, and the specific application. These calculations will be reviewed in Sec. 3 together with examples of experimental results.

3. EAL Calculations for Different XPS Applications

Figure 2 (top) shows a schematic outline of an XPS experiment and indicates the notation we will be using to describe this configuration. Figure 2 (bottom) illustrates possible photoelectron trajectories following photoemission at a depth z from the surface of a sample. Trajectories A, B, and C are examples of photoelectrons that are emitted from the surface at the same angle, α, with respect to the surface normal. For trajectory A, there is no elastic-scattering event before emission from the surface; this is an example of a straight-line trajectory that is assumed with the use of the SLA. Trajectory B shows two elastic-scattering events, each involving relatively small angular deflections, while trajectory C shows a large-angle elastic-scattering event as well as two such events with smaller angular deflections. Trajectories A, B, and C have widely different path lengths in the sample, and it is clear that inelastic-scattering events will be more likely to occur on the longer than the shorter trajectories.

Theoretical descriptions of photoelectron generation and of multiple elastic- and inelastic-scattering events can be complex. Nevertheless, it is useful to make these calculations for a range of solids (e.g., elemental solids with varying atomic numbers and particular compounds of interest). EALs and other useful parameters can then be derived and analyzed to determine whether useful predictive formulas can be developed to provide reasonable estimates of parameter values for other materials.

EALs and other parameters can be calculated from the so-called emission depth distribution function (EMDDF). The EMDDF has been defined as the "probability that the particle or radiation leaving the surface in a specified state and in a given direction originated from a specified depth measured normally from the surface into the material" (Ref. 1, Definition 4.161). Figure 3 shows schematically how the EMDDF for an XPS application can be calculated for a particular sample and experimental configuration with data for the relevant photoemission cross sections, IMFPs, and differential elastic-scattering cross sections. For AES, it is also necessary to calculate the excitation depth distribution function (EXDDF), the "probability that specified excitations are created at specified depths, measured normally from a surface into the material, by a beam of specified particles or radiation incident on the surface in a given direction" (Ref. 1, Definition 4.162). The EXDDF is calculated with cross sections for ionization of the shell responsible for particular Auger-electron emission, both from ionizations by the incident electrons and from possible ionizations of deeper levels and resulting vacancy transfers to the shell of interest.

We will denote EALs by L_{APP} where the subscript indicates the particular analytical application. As follows from Fig. 3, it is possible to use EMDDFs to obtain (a) EALs for determining depths of marker layers (L_{ML}), (b) EALs for determining surface composition (L_{QA}), and (c) EALs for determining thicknesses of overlayer films on planar substrates (L_{TH}). We also show additional parameters that can be affected by elastic-scattering events: (d) two measures of the sampling

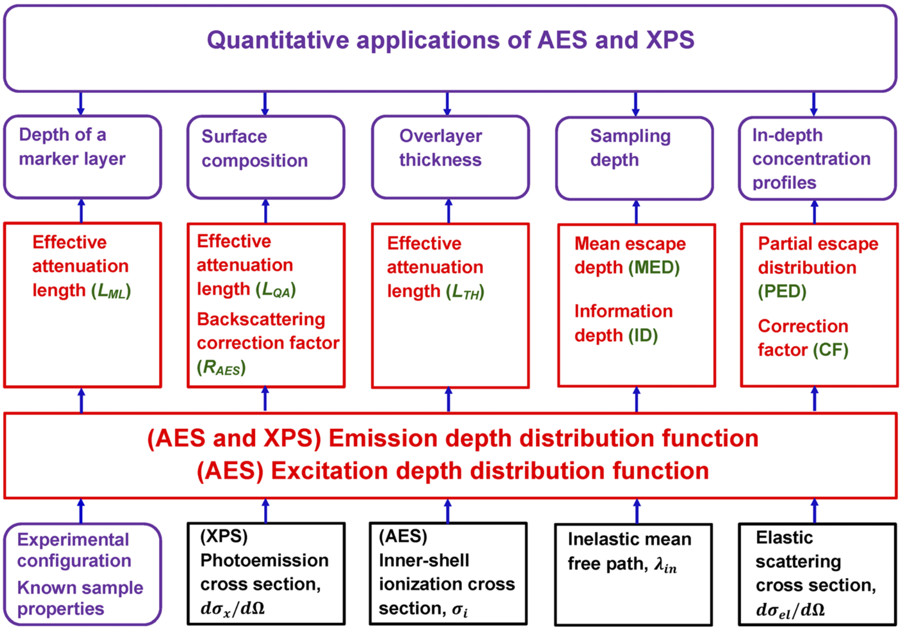

FIG. 3. Outline for calculations of the EMDDF for XPS that can be used to obtain EALs for determining depths of marker layers (L_{ML}); EALs for determining surface composition (L_{QA}); EALs for determining thicknesses of overlayer films on planar substrates (L_{TH}); measures of the sampling depth, the MED, and the ID; and in-depth concentration profiles from PEDs. For AES, it is also necessary to calculate the EXDDF.

depth for a particular measurement, the mean escape depth (MED) and the information depth (ID); and (e) in-depth concentration profiles. The latter application requires so-called partial-escape distributions (PEDs) that are defined as the "total number of electrons in an electron spectrum, originating from a given Auger transition or photoelectric transition, or associated with primary electrons backscattered from a surface, per unit of excitation or of backscattering that reach the detector after participating in a given number of inelastic interactions of a given type" (Ref. 1, Definition 4.323). We comment on the use of PED functions and the so-called Correction Factor (CF) in Subsection 3 of the Appendix.

As outlined in Fig. 3, EALs for different applications can be derived from the EMDDF. For this reason, let us identify the sources from which EMDDFs can be obtained. These sources can be grouped as follows: (a) Monte Carlo (MC) algorithms,[17–25] (b) simple predictive formulas fitted to results of MC simulations,[21,23,24,26] (c) analytical expressions derived from transport theory,[6,7,24,27] and (d) experimental data.[28–32]

The most frequently used method for determining the EMDDF involves MC calculations performed with different simulation strategies. The common features of this approach are summarized in the block diagram shown in Fig. 4. The simulation algorithms are generally based on the assumption that elastic-scattering events along the photoelectron trajectory are described by the Poisson stochastic process. Consequently, the electron path lengths between elastic collisions are described by an exponential distribution. To construct an electron trajectory that started at a given depth, we need to provide several samplers derived from the physics of electron transport. The initial photoelectron direction in XPS is defined by angles generated from a sampler based on the differential photoemission cross section. For AES, this sampler provides directions uniformly distributed in space. In addition, we need a sampler that provides angles characterizing the elastic-scattering event: the azimuthal angle (typically assumed to be uniformly distributed around an electron direction) and the polar scattering angle (derived from the differential elastic-scattering cross section). Each trajectory is followed until its length is too large to give a significant contribution to the signal intensity or until the electron leaves the solid.

For an EMDDF calculation, we first define the direction of the analyzer with respect to the sample by the photoelectron emission angle, α, with respect to the surface normal, as indicated in Fig. 2. A contribution to the EMDDF, $\Delta\phi_k(z, \alpha)$, due to the kth trajectory starting at a depth, z, is given by

$$\Delta\phi_k(z,\alpha) = \begin{cases} \exp\left(-\dfrac{x_k}{\lambda_{in}}\right) & \text{if an electron entered the analyzer} \\ 0 & \text{in all other cases,} \end{cases} \tag{4}$$

where $k = 0, 1, 2, \ldots, x_k$ is the length of the kth trajectory in the sample material, and λ_{in} is the IMFP for that material and electron energy. After generation of m trajectories, the EMDDF for depth z is estimated from

$$\phi(z,\alpha) = \frac{1}{m}\sum_{k=1}^{m}\Delta\phi_k(z,\alpha). \tag{5}$$

Details of this MC strategy are available in the literature.[17–25]

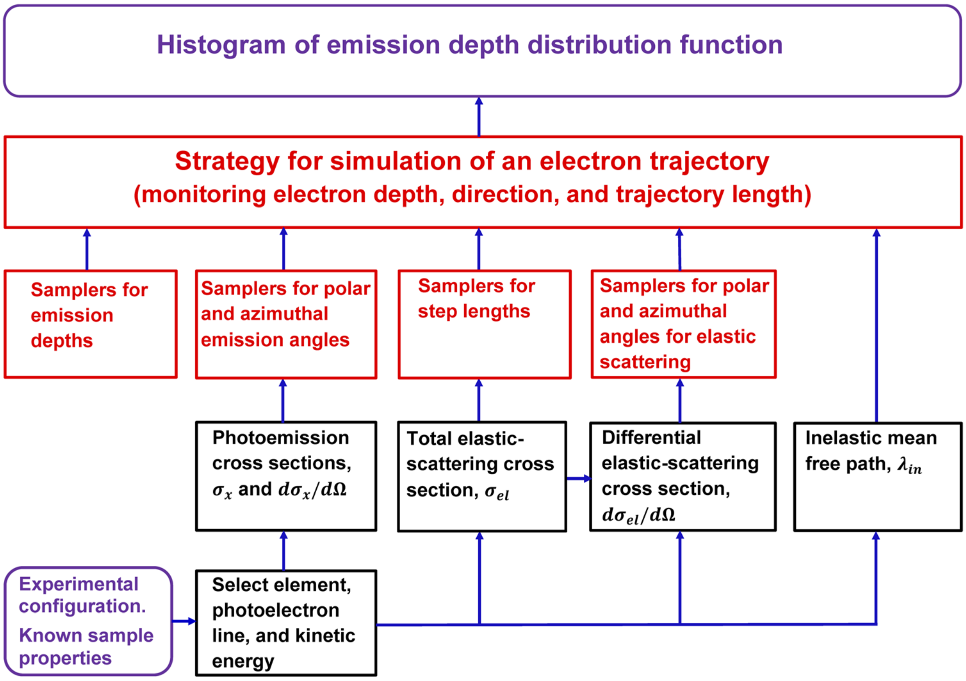

FIG. 4. Outline of calculations of the EMDDF for XPS from Monte Carlo simulations.

Selection of the number of trajectories depends on the desired precision, the sample material, and the instrumental configuration, particularly on the size of the acceptance solid angle of the analyzer. In computational practice, the number m may reach 10^7 to obtain a reasonable precision. However, the computational effort may be considerably decreased when the trajectory-reversal approach is used, i.e., when the trajectory is simulated from the exit point of the photoelectron on the sample surface to the point of origin.[18,33] This approach is particularly useful when the signal intensity is simulated for very small analyzer acceptance angles.

A second useful and universal method for calculating the EMDDF is derived from a solution of the Boltzmann equation within the transport approximation (TA). The first attempt to derive the EMDDF for AES of acceptable accuracy was published by Tilinin and Werner.[34] A more advanced expression applicable to both AES and XPS was derived by Tilinin *et al.*[27] This expression was later corrected and extended in a series of later studies.[6,7,20,24] An outline of the relevant calculations is shown in Fig. 5. An expression defining the EMDDF for XPS can generally be written in the following form:[6,7,20,24]

$$\phi(z,\alpha) = \phi_i(z,\alpha,\omega) + \frac{\beta}{4}\phi_a(z,\alpha,\theta_x,\psi,\omega), \tag{6}$$

where β is the asymmetry parameter in the differential photoemission cross section,[35–37] θ_x is the incidence angle of the x-ray beam relative to the sample normal (Fig. 2), ψ is the angle between the x ray and the analyzer directions (Fig. 2), ω is the so-called single-scattering albedo defined below, and ϕ_i and ϕ_a are the isotropic and anisotropic contributions to the EMDDF, respectively. The formulas for both contributions are rather complicated, and the interested reader is referred to the original papers for details.[6,7,20,24] One should mention that this approach requires a sufficiently accurate source of the Chandrasekhar function, $H(x, \omega)$,[38] in which x is the so-called directional variable; in the formalism of electron transport, x is frequently replaced by the parameter $\mu = \cos\alpha$. Expressions providing this function with different accuracies, together with the computer source code, were recently published.[39] However, despite the complications, a robust algorithm implementing this formalism is utilized in the National Institute of Standards and Technology (NIST) Electron Effective-Attenuation-Length Database, SRD 82.[40] We note here that the anisotropic contribution to the EMDDF, ϕ_a, is neglected for AES since it is commonly assumed that the emission of Auger electrons is uniform in space, i.e., $\beta = 0$.

We point out that elastic-scattering effects enter the formalism for Eq. (6) only through one parameter, namely, the single-scattering albedo, ω. This parameter is given by

$$\omega = \frac{\lambda_{in}}{\lambda_{in} + \lambda_{tr}}, \tag{7}$$

where λ_{tr} is the transport mean free path (TRMFP). For elemental solids, the latter parameter is defined by

$$\lambda_{tr} = (N\sigma_{tr})^{-1}, \tag{8}$$

where N is the atomic density (i.e., the number of atoms per unit volume), σ_{tr} is the transport cross section (TCS) for an atom given by

$$\sigma_{tr} = \int_{4\pi} (1 - \cos\theta)\frac{d\sigma_{el}}{d\Omega}d\Omega, \tag{9}$$

where θ is the polar elastic-scattering angle and $d\sigma_{el}/d\Omega$ is the differential elastic-scattering cross section. For a multi-component solid

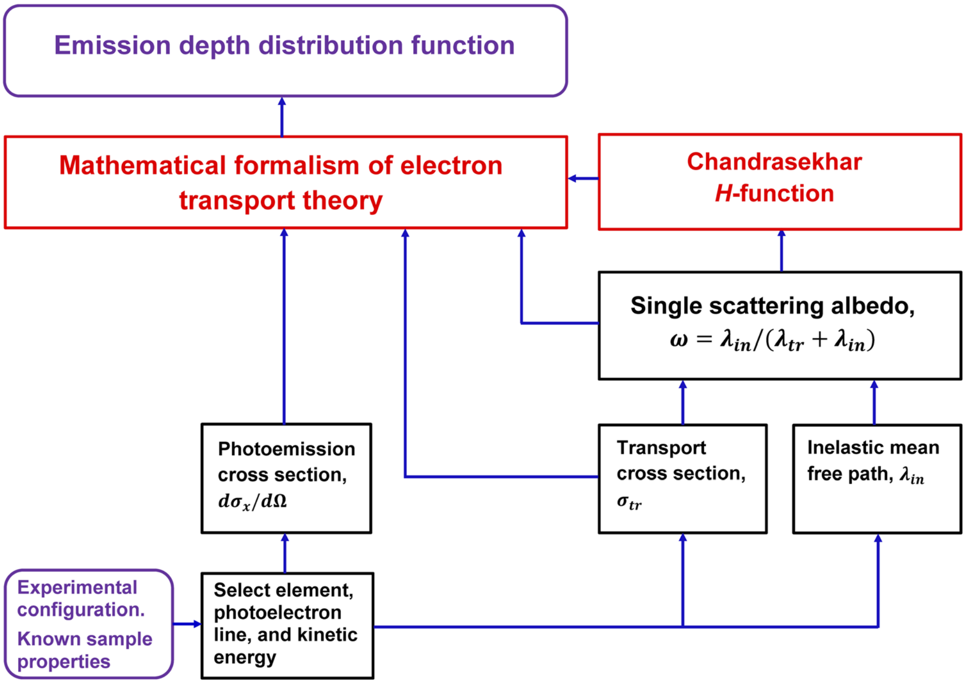

FIG. 5. Outline of calculations of the EMDDF for XPS from use of the Boltzmann equation within the transport approximation.

(i.e., an alloy or a compound), the TRMFP can be determined from Eq. (8) with an average TCS determined from the stoichiometry-weighted TCSs of the constituent elements.[5,41]

TCSs can be conveniently obtained from analytical formulas fitted to the values obtained from Eq. (9),[41] while the values of λ_{tr} are available in SRD 82 and the NIST Database for the Simulation of Electron Spectra for Surface Analysis (SESSA), SRD 100.[42,43] The values of ω can also be obtained from an analytical formula.[44] In contrast, MC strategies take the actual angular distribution of elastic-scattering events into account. For this reason, MC algorithms are considered to be more accurate than analytical transport theory. Nonetheless, EMDDFs from these two approaches compare very well.[24] Figure 6 shows the EMDDFs calculated from both models for Au $4f_{7/2}$ photoelectrons excited by Mg Kα radiation for a common XPS configuration (the so-called magic-angle configuration) in which ψ, the angle between the direction of x rays and the direction of the analyzer (Fig. 2), is 55°. We see that the EMDDFs from the MC algorithm for different photoelectron emission angles, α, are practically reproduced by the EMDDFs from the analytical transport theory.

Finally, we note that the albedo parameter from Eq. (7) has been found useful in predictive EAL formulas to be described in Subsections 3.1–3.2.

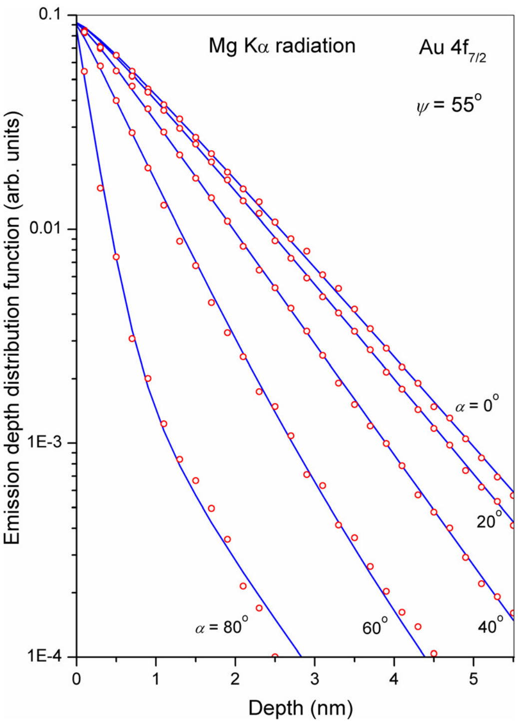

FIG. 6. Emission depth distribution function calculated for Au $4f_{7/2}$ photoelectrons emitted by Mg Kα radiation. The calculations were performed for the "magic-angle" configuration (in which the angle, ψ, between the direction of the X-ray beam and the photoelectron emission angle is fixed at 55°) and for different photoelectron emission angles, α. Solid line: transport approximation; circles: Monte Carlo simulations. Details of the theory are available in Ref. 24.

3.1. EALs for thickness measurements of an overlayer film on a planar substrate

The most common EAL application is the thickness measurement of overlayer films on a planar substrate. These measurements can be made in three ways, i.e., by the use of three different equations such as Eqs. (2a), 2(b), and (3a) based on the SLA model or the more reliable versions presented below that take elastic-scattering effects into account. As mentioned in Sec. 2, the thickness of an overlayer film can then be obtained from the following experimental procedures:

(a) Deposition of the overlayer film followed by measurement of the photoelectron signal intensity from the overlayer material. The signal intensity is also measured for a thick overlayer film (i.e., thickness much greater than the ID for the XPS measurement) or from a bulk sample of the overlayer material at the same spectrometer settings.
(b) Measurement of the photoelectron signal intensity from the substrate, followed by measurement of the same signal intensity after deposition of the overlayer film.
(c) Measurement of the signal intensities of photoelectrons emitted from both the overlayer and the substrate materials.

Generally, the EAL approach is useful when the EAL value replacing the IMFP can be easily evaluated from a simple formalism valid for a number of overlayer/substrate systems, different electronic subshells excited by commonly used x-ray sources, and a wide range of experimental configurations.

We present here a separate description of EALs for use in XPS experiments with unpolarized x rays (relevant to most laboratory XPS instruments) and with linearly polarized x rays (relevant to XPS experiments with synchrotron radiation). Most of the published EAL literature, however, refers to XPS with unpolarized x rays. These applications are described in Subsections 3.1.1.1. The mathematical formalism for quantification of XPS based on polarized x rays is more complicated due to the need to account for the direction of the polarization vector. EALs derived for this application will be described in Sec. 3.1.2.

3.1.1. *XPS with unpolarized x rays*

3.1.1.1. Introductory remarks. Many early calculations of EALs were based on the assumption that the elastic- and inelastic-scattering properties of the substrate material and overlayer film were "similar." More specifically, it was assumed that IMFPs for the substrate and film materials were identical and similarly that TRMFPs for these materials were also identical. These assumptions enabled EAL calculations for a film material on a substrate of the same material by the transport approximation. Although such calculations might not seem to be of direct practical relevance, they have been validated by the more realistic Monte Carlo simulations. The major benefits of EAL calculations from the transport approximation are that they can readily be made for any material and that they are much faster than Monte Carlo simulations.

We first give general expressions for the photoelectron intensities from a thin film and a substrate based on the straight-line approximation (i.e., the neglect of elastic scattering). We then show how the expression for the substrate intensity can be corrected for elastic-scattering effects by replacing the IMFP with the EAL for overlayer-thickness measurement, L_{TH}. An example is given of how such an EAL could vary with the film thickness and the photoelectron emission angle, and we point out how useful average EAL values can be determined for particular ranges of film thicknesses and emission angles. The average EAL values have been determined in this way for many materials by the TA, and these results have been validated for representative materials by MC simulations. A major benefit of these average EAL calculations is that they have led to useful predictive formulas for L_{TH}. Finally, we note that the SLA expressions for the photoelectron intensities from the film and the substrate will be used as the basis for more detailed discussions of EAL calculations and measurements in Subsections 3.1.1.2–3.1.1.4.

We consider a sample consisting of a thin uniform overlayer film deposited on a planar substrate. We assume that the film thickness is less than the sampling depth (i.e., the ID) for the chosen XPS measurement[45] and that we wish to determine the film thickness from measurements of the attenuation of a selected photoelectron line from the substrate, s, by the overlayer film.

To simplify the discussion, we initially assume that the IMFP for the chosen photoelectron line from the substrate material in the overlayer film, λ_{in}^{f}, is approximately equal to the IMFP for that line in the substrate, λ_{in}^{s},

$$\lambda_{in}^{f} \approx \lambda_{in}^{s} = \lambda_{in}. \tag{10}$$

The substrate-signal intensity based on the SLA model for an overlayer-film thickness t is then given by

$$I_s^{SLA}(t) = S\Delta\Omega F_x \left(\frac{d\sigma_x}{d\Omega}\right) N\lambda_{in} \exp\left(-\frac{t}{\lambda_{in}\cos\alpha}\right), \tag{11}$$

where S is a constant comprising properties of the analyzer optics and the detector efficiency for the chosen operating conditions, $\Delta\Omega$ is the solid acceptance angle of the analyzer, F_x is the flux of incident x rays, and $d\sigma_x/d\Omega$ is the differential photoemission cross section. The corresponding signal intensity from a clean substrate is

$$I_s^{\infty,SLA} = S\Delta\Omega F_x \left(\frac{d\sigma_x}{d\Omega}\right) N\lambda_{in}. \tag{12}$$

From Eqs. (11) and (12), we can calculate the overlayer-film thickness based on the SLA,

$$t = -\lambda_{in}\cos\alpha \ln\left[\frac{I_s^{SLA}(t)}{I_s^{\infty,SLA}}\right], \tag{13}$$

as also shown in Eq. (2a). Consequently, we need to measure the ratio of the substrate-signal intensity after deposition of the overlayer film, $I_s(t)$, to the corresponding intensity prior to deposition, I_s^{∞}.

The accuracy of a film-thickness measurement can be improved if account is taken of elastic-scattering effects on the photoelectron intensities. We make use of the EAL definition and replace the IMFP in Eq. (13) with the corresponding EAL for film-thickness measurements, L_{TH},

$$t = -L_{TH}\cos\alpha \ln\left[\frac{I_s(t)}{I_s^{\infty}}\right], \tag{14}$$

where L_{TH} is the EAL for overlayer-thickness measurements. It has been shown the this EAL is related to the EMDDF by the following relation:[6,7,25,46]

$$L_{TH} = \frac{1}{\cos\alpha}\frac{t}{\ln\int_0^\infty \phi(z)dz - \ln\int_t^\infty \phi(z)dz}. \tag{15}$$

The above formalism is valid if the elastic-scattering effects in the overlayer and substrate materials are similar. This criterion can also be expressed by stating that the values of the TRMFPs for the two materials should be comparable. Since we initially assumed that IMFP values for the two materials should be similar, the values of the albedo, ω, will also be similar. We will summarize some useful results from these assumptions before describing results obtained from a model in which the overlayer and substrate materials have distinctly different electron-transport properties.

Many EAL calculations have been made with Eq. (15) from both Monte Carlo simulations and the transport approximation model for elemental solids and compounds, a wide range of photoelectron energies, and a wide range of experimental configurations.[45–47] Ideally, EALs should be independent of the overlayer thickness and the instrumental configuration, particularly the photoelectron emission angle. In fact, the EAL values can vary with both the film thickness and emission angle. In situations where these variations are relatively small, averaging procedures provide the average EALs for a useful range of measurement conditions. These procedures will now be described for XPS with unpolarized x rays, while similar procedures for XPS with polarized x rays are described in Sec. 3.1.2.

We illustrate the averaging procedure for XPS with unpolarized x rays using the Au $4f_{7/2}$ photoelectron line emitted from Au by Mg Kα radiation as an example. The EALs obtained from Eq. (15) for different overlayer thicknesses t are referred to as "practical EALs."[6,7,20,46] These values, calculated with the algorithms of Ref. 46 for different overlayer depths and emission angles, are shown in Fig. 7. We see that L_{TH} varies weakly with the overlayer thickness and with the emission angle for emission angles less than about 50°. For larger

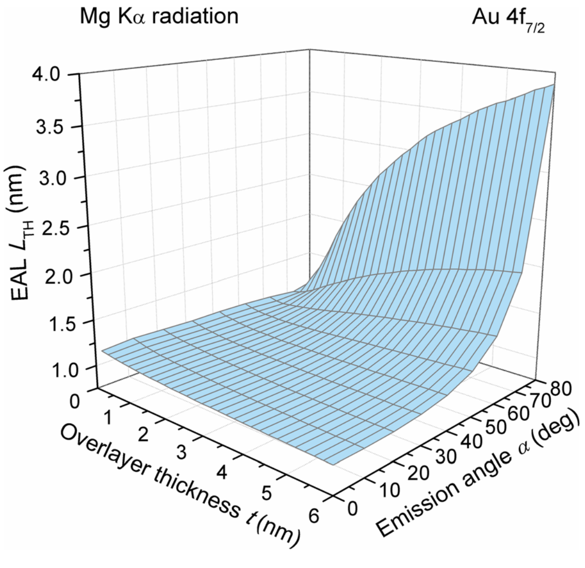

FIG. 7. A 3D plot of the EAL, L_{TH}, calculated from Eq. (15) for Au $4f_{7/2}$ photoelectrons excited by Mg Kα radiation assuming different overlayer thicknesses and photoelectron emission angles. The EALs were obtained from the MC algorithm described in Ref. 45.

emission angles, however, L_{TH} varies much more strongly with the emission angle.

In analytical practice, we do not know in advance the actual thickness of the overlayer film. Instead, we need EALs for some expected range of thicknesses. Our recommended procedure for obtaining an average practical EAL, L_{TH}^{ave}, over a potentially wide range of thicknesses is the following:[7,45,46]

$$L_{TH}^{ave} = \frac{1}{n_{TH}} \sum_{i=1}^{n_{TH}} \frac{1}{\cos\alpha} \frac{t_i}{\ln\int_0^\infty \phi(z)dz - \ln\int_{t_i}^\infty \phi(z)dz}, \quad 0 < t_i \le t_{max}, \tag{16}$$

where n_{TH} is the number of thicknesses and t_{max} is the maximum considered thickness. It is reasonable to assume that t_{max} is the thickness from which most of the substrate-signal intensity is emitted (i.e., the information depth[45] for the particular emission angle). For our convenience, we consider an information depth from which 99% of the substrate signal is emitted or, equivalently, a maximum overlayer-film thickness at which the substrate signal intensity is reduced to 1% of its maximum value (i.e., for an uncovered substrate).

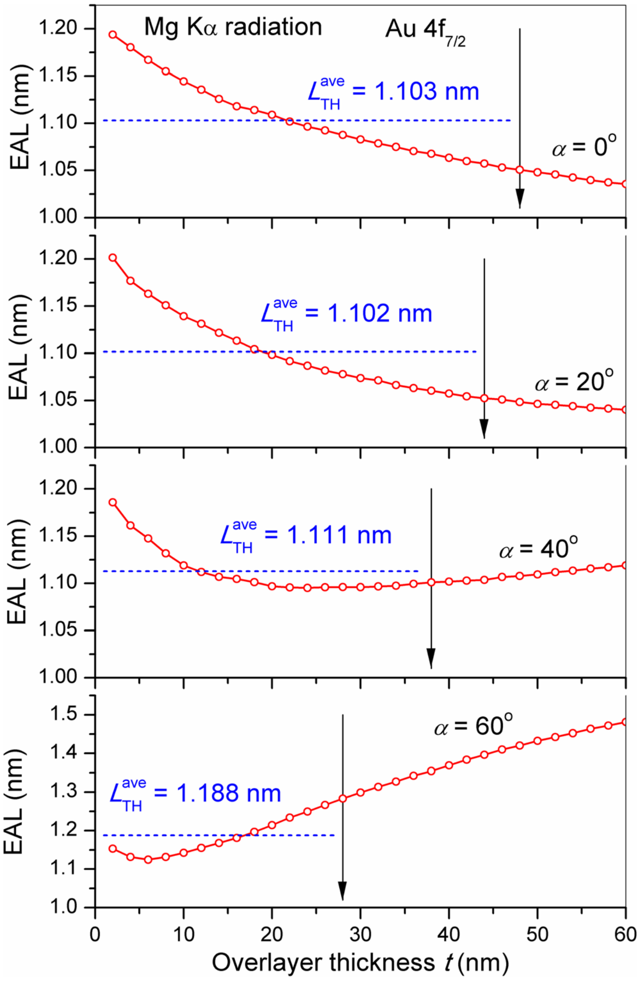

FIG. 8. Dependence of the EAL, L_{TH}, on the overlayer thickness for Au 4f$_{7/2}$ photoelectrons excited by Mg Kα radiation and for different photoelectron emission angles, α. The EALs were obtained from MC simulations.[24,45] The dashed lines show the average EALs, L_{TH}^{ave}, obtained from Eq. (16). The vertical arrows indicate the values of the 99% ID (overlayer thicknesses from which 99% of the signal intensity is emitted) for a given emission angle.

EALs for Au 4f$_{7/2}$ photoelectrons excited by Mg Kα x rays are shown in Fig. 8 as a function of overlayer thickness for emission angles of 0°, 20°, 40°, and 60°. We see that the EALs can vary by up to about 15% with the overlayer thickness. The average EALs, L_{TH}^{ave}, from Eq. (16) are indicated by the horizontal dashed lines for the values of t_{max} (information depths for 99% of the signal) indicated by the vertical arrows. The values of L_{TH}^{ave} are plotted as a function of emission angle in Fig. 9(a). We see that the average EALs depend weakly on the emission angle in the range $0 \le \alpha \le 50°$. This observation seems to hold for many solids and for a wide range of photoelectron energies from about 150 eV to 10 keV.[7,45–47] Consequently, emission angles up to $\alpha = 50°$ can be recommended for the determination of the overlayer thickness. A further small variation of L_{TH}^{ave} with the emission angle can be further averaged using the following formula:

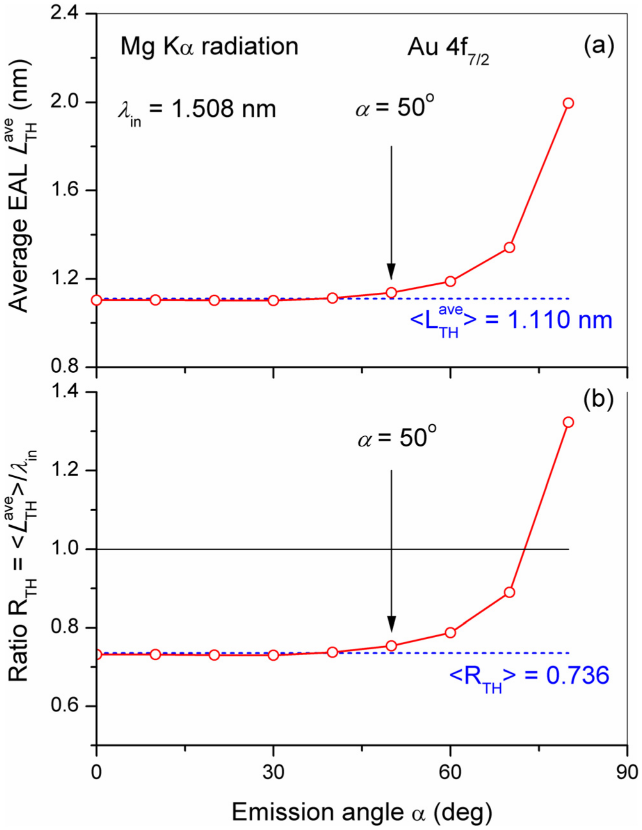

FIG. 9. (a) Dependence of the average EALs, L_{TH}^{ave}, on the emission angle, α, obtained from MC simulations for Au 4f$_{7/2}$ photoelectrons emitted by Mg Kα radiation (open circles and solid line). The horizontal dashed line indicates the value of the mean average EAL, $\langle L_{TH}^{ave} \rangle$, calculated from Eq. (17) for emission angles between $\alpha = 0°$ and $\alpha = 50°$. (b) Dependence of the ratio of the mean average EAL to the IMFP, R_{TH}, calculated from Eq. (18) for the same photoelectron line. The horizontal dashed line indicates the ratio, $\langle R_{TH}^{ave} \rangle$, from the average of the R_{TH} values over the angular range from $\alpha = 0°$ to $\alpha = 50°$.

$$\langle L_{TH}^{ave} \rangle = \frac{1}{n_\alpha} \sum_{i=1}^{n_\alpha} L_{TH}^{ave}, \tag{17}$$

where n_α is the number of emission angles in the range $0 \leq \alpha \leq 50°$. This procedure is also implemented in the NIST SRD 82 database.[40] Of course, if the thickness of the overlayer film is known or expected to be less than the information depth, the averaging of Eq. (16) can be performed over a smaller range of thicknesses. It is possible for a user of SRD 82 to select a maximum overlayer-film thickness to determine $\langle L_{TH}^{ave} \rangle$ for the intended application.

To visualize the elastic-scattering effects, it is useful to determine the ratios

$$R_{TH} = \frac{\langle L_{TH}^{ave} \rangle}{\lambda_{in}} \tag{18}$$

as a function of emission angle. These ratios for Au $4f_{7/2}$ photoelectrons excited by Mg Kα x rays are shown in Fig. 9(b) where we have used λ_{in} = 1.508 nm in Eq. (18).[48] The average of the R_{TH} values for $0° \leq \alpha \leq 50°$, $\langle R_{TH} \rangle$, was 0.736. In this example, elastic-scattering effects are relatively strong, and $\langle L_{TH}^{ave} \rangle$ is 26.4% less than the IMFP. Further information on the magnitude of elastic-scattering effects for different materials and different electron energies is given in the supplementary material.

It has been found that the values of R_{TH} for different photoelectron lines, x-ray energies, and materials are a linear function of the single-scattering albedo, ω,[6,7,45,46]

$$R_{TH} = 1 - A_{EAL}\omega. \tag{19}$$

We recently reported an analysis of EALs calculated for Si $2s_{1/2}$, Cu $2p_{3/2}$, Ag $3d_{5/2}$, and Au $4f_{7/2}$ photoelectrons excited by Mg Kα, Al Kα, Zr Lα, and Ti Kα x rays where the photoelectron energies ranged from 321 eV to 4426 keV.[46] The values of L_{TH} were calculated from both the TA formalism and from MC simulations using photoionization cross sections from the dipole approximation (DA) and non-dipole approximation (NDA). The EAL calculations were made for a fixed angle of 55° between the angle of x-ray incidence and the photoelectron emission angle and for maximum overlayer-film thicknesses corresponding to attenuations of the substrate signal intensity to 1%, 5%, and 10% of the signal from an uncovered substrate. Satisfactory consistency was found between EALs determined from the TA formalism and from MC simulations, while differences between EALs for Au $4f_{7/2}$ photoelectrons from the DA and NDA were between 1% (for Mg and Al Kα x rays) and 2.5% (for Ti Kα x rays) for photoelectron emission angles ≤50°.[46]

We found that $A_{EAL} = 0.729$ for $\langle R_{TH} \rangle$ values obtained with the transport approximation [with a root-mean-square (rms) deviation of the percentage deviations between EALs from the transport approximation and the fitted values from Eq. (19) of 1.00%], while $A_{EAL} = 0.748$ for $\langle R_{TH} \rangle$ values obtained from MC simulations (with a corresponding rms deviation of 1.75%).[46] If the EAL values from the transport approximation and Monte Carlo simulations were combined, A_{EAL} = 0.738 with an rms deviation of 1.44%. Thus, the following equation can be recommended as a predictive formula for R_{TH} and consequently for the EAL:

$$R_{TH} = 1 - 0.738\ \omega. \tag{20}$$

The values of R_{TH} calculated from the transport approximation and Monte Carlo algorithms[46] and from the predictive formula given by Eq. (20) are compared in Fig. 10.

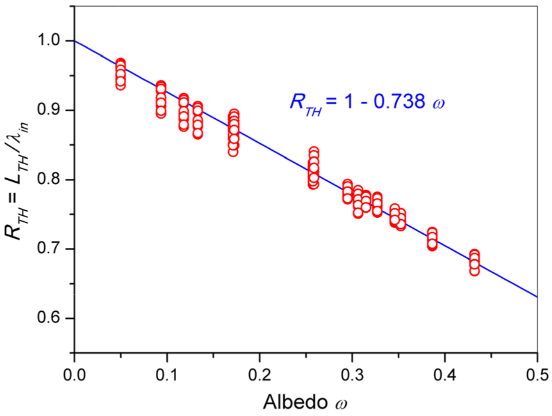

FIG. 10. Dependence of average values (symbols) of the ratio R_{TH} from Eq. (18) on the single-scattering albedo, ω, from EALs calculated from Monte Carlo simulations and the transport approximation for Si $2s_{1/2}$, Cu $2p_{3/2}$, Ag $3d_{5/2}$, and Au $4f_{7/2}$ photoelectrons excited by Mg Kα, Al Kα, Zr Lα, and Ti Kα x rays. The EALs were further averaged from the values obtained for emission angles between $\alpha = 0°$ and $\alpha = 50°$ (after Ref. 46). The solid line shows the fitted function [Eq. (20)].

The slope A_{EAL} = 0.738 is essentially identical to the A_{EAL} value we obtained previously (A_{EAL} = 0.735) from the transport approximation formalism for photoelectron and Auger-electron lines from another group of materials and for a smaller energy range (61 eV–2016 eV).[45] Equation (20) is believed to be useful as a convenient means for estimating R_{TH} values in other materials. We will comment further on Eq. (20) and two other EAL predictive equations[49,50] in Sec. 3.1.1.5.

We based the above analysis on the assumptions that the IMFPs for the overlayer and substrate materials are similar and that transport mean free paths for the two materials are also similar. These assumptions simplified the formalism and facilitated calculations of EALs that could be conveniently used in practical applications. Let us now analyze the general situation in which the IMFPs for a given electron energy could be different for the overlayer and substrate materials. We also consider the case where the energy of the substrate photoelectrons, E_s, is different from the energy of overlayer photoelectrons, E_f. If elastic-scattering effects are neglected, the signal intensity from the substrate can be written in the following form [cf. Eq. (11)]:

$$I_s^{SLA}(t) = S(E_s)\Delta\Omega F_x \left(\frac{d\sigma_x}{d\Omega}\right)_s N_s \lambda_{in}^s(E_s) \exp\left(-\frac{t}{\lambda_{in}^f(E_s)\cos\alpha}\right), \tag{21}$$

where $\lambda_{in}^s(E_s)$ is the IMFP of photoelectrons emitted and moving in the substrate material, while $\lambda_{in}^f(E_s)$ denotes the IMFP of photoelectrons emitted in the substrate but moving in the overlayer material. For the bulk substrate material, i.e., for $t \to 0$, we have

$$I_s^{SLA}(t) \to I_s^{\infty,SLA} = S(E_s)\Delta\Omega F_x \left(\frac{d\sigma_x}{d\Omega}\right)_s N_s \lambda_{in}^s(E_s) \tag{22}$$

and

$$I_s^{SLA}(t) = I_s^{\infty,SLA} \exp\left(-\frac{t}{\lambda_{in}^f(E_s)\cos\alpha}\right). \tag{23}$$

The signal intensity of photoelectrons emitted in the overlayer is expressed by

$$I_f^{SLA}(t) = S(E_f)\Delta\Omega F_x\left(\frac{d\sigma_x}{d\Omega}\right)_f \times N_f\lambda_{in}^f(E_f)\left[1-\exp\left(-\frac{t}{\lambda_{in}^f(E_f)\cos\alpha}\right)\right], \tag{24}$$

where $\lambda_{in}^f(E_f)$ denotes the IMFP of photoelectrons emitted and moving in the overlayer material. For the bulk overlayer material, i.e., for $t \to \infty$, Eq. (24) becomes

$$I_f^{SLA}(t) \to I_f^{\infty,SLA} = S\left(E_f\right)\Delta\Omega F_x\left(\frac{d\sigma_x}{d\Omega}\right)N_f\lambda_{in}^f\left(E_f\right). \tag{25}$$

In Subsections 3.1.1.2–3.1.1.4, we will review the theoretical background and applicability of this EAL approach for three types of measurements to determine the thicknesses of an overlayer film on a planar substrate. For each type of measurement, there is a separate equation to determine the film thickness in terms of measured photoelectron intensities, an EAL, and the cosine of the photoelectron emission angle. In each case, the EAL replaces the IMFP in a similar equation that had been derived on the assumption that elastic-scattering effects could be neglected. In principle, the EALs could be different for each of these three equations. In most applications, however, it appears that the same EAL (for a given material and electron energy) is valid for the three applications. We will therefore use the same notation, L_{TH}, to refer to EALs for these applications. We will also apply and test the predictive EAL equation [Eq. (20)] that we have developed for the three applications. Information on other predictive EAL equations will be given in Sec. 3.1.1.5.

3.1.1.2. Analysis of overlayer photoelectron intensities. If elastic-scattering effects are neglected, the photoelectron signal intensity from the overlayer increases with increasing overlayer thickness and reaches a saturation value corresponding to the bulk overlayer material, as expected from Eq. (24). Note that no information on the substrate is needed in this formalism. We have

$$I_f^{SLA}(t) = I_f^{\infty,SLA}\left[1-\exp\left(-\frac{t}{\lambda_{in}^f(E_f)\cos\alpha}\right)\right] \tag{26a}$$

or

$$R_f^{SLA} = \frac{I_f^{SLA}(t)}{I_f^{\infty,SLA}} = \left[1-\exp\left(-\frac{t}{\lambda_{in}^f(E_f)\cos\alpha}\right)\right]. \tag{26b}$$

Let us replace the ratio R_f^{SLA} with the ratio of the measured photoelectron intensity from the overlayer material, I_f, to the intensity measured for the bulk overlayer material, I_f^{∞}, i.e., by the ratio $R_f^{expt} = I_f/I_f^{\infty}$. We then obtain

$$t = -\lambda_{in}^f\left(E_f\right)\cos\alpha\ln\left(1-R_f^{expt}\right). \tag{27}$$

Thus, in principle, the overlayer thickness can be determined from Eq. (27) [or the equivalent equation (2b)]. However, elastic-scattering effects cannot be neglected and a photoelectron emitted in the overlayer could enter the substrate and could eventually be backscattered toward the analyzer.

We will now investigate the validity and utility of replacing the IMFP in Eq. (26) with the corresponding EAL, $L_{TH}(E_f)$,

$$t = -L_{TH}\left(E_f\right)\cos\alpha\ln\left(1-R_f^{expt}\right). \tag{28}$$

A series of Monte Carlo simulations have been performed for an overlayer material deposited with different thicknesses on different substrates to study the magnitude of elastic-scattering effects.[51–53] Jablonski and Tougaard[51] performed simulations of Ag $3d_{5/2}$ photoelectrons emitted by Mg Kα radiation for an Ag overlayer deposited on elemental substrates with atomic numbers varying over a wide range (Be, Al, Pd, and Au) and determined EAL values from Eq. (28). They found that the influence of the substrate was noticeable only in the case of beryllium. This effect occurs because the contribution to the signal intensity from photoelectrons backscattered from each substrate was distinctly smaller in the case of beryllium than for other substrates with larger atomic numbers.

Similar simulations were performed for Cu $2p_{3/2}$ photoelectrons from Cu overlayers on Si, Ni, Ag, and Au substrates and for Ag $3d_{5/2}$ photoelectrons from Ag overlayers on Si, Cu, Pd, and Au substrates.[52] These calculations were performed for a typical XPS experimental configuration (an x-ray incidence angle of 60° with respect to the surface normal and normal emission of the photoelectrons). The Cu $2p_{3/2}$ and Ag $3d_{5/2}$ signal intensities were calculated as a function of overlayer thickness from three theoretical models: Monte Carlo (MC) simulations, the transport approximation (TA), and the straight-line approximation (SLA) model.[52] It was found that the $R(t) = I_f(t)/I_f^{\infty}$ values from the MC simulations and the TA did not change appreciably for the four considered substrates with atomic numbers varying from 14 to 79. Furthermore, the differences between the $R(t)$ values from the MC and TA calculations were typically between 1% and 3% with slightly larger differences (up to 5%) for Ag films on Si and film thicknesses less than 2 nm. In contrast, the $R(t)$ values from the SLA model (with no account taken of elastic-scattering effects) differed from those from the MC calculations by up to 25%. Use of the SLA approach can thus lead to systematic errors. As an example, suppose that an experiment provided the measured ratio $R_{exp}(t)$ equal to 0.8 for an Ag overlayer on a particular substrate. We would then obtain an Ag film thickness of 2.48 nm from the SLA model, while the TA model (which took elastic collisions into account) would yield a film thickness of 1.99 nm. The results reported in Ref. 52 support the applicability of the TA model in calculations of EALs for the determination of film thicknesses using photoelectron intensities from the overlayer. While the TA model is based on the assumption that the overlayer and substrate materials are identical, these results indicate that this assumption is well justified, that is, photoelectron intensities from the overlayer are generally insensitive to the substrate material.

In the later work of Ref. 53, the validity of the EAL approach for describing photoelectron intensities was analyzed in detail by performing advanced MC calculations of the dependence of the overlayer photoelectron intensity on the overlayer-film thickness. Unlike earlier investigations, the elastic- and inelastic-scattering properties of both substrate and overlayer materials were included in these calculations. In particular, the structure in the differential elastic-scattering cross section as a function of polar scattering angle was included. Different overlayer materials (Al, Ag, and Au) deposited on a number of substrates (Al, Si, Cu, Pd, Ag, and Au) were investigated. MC simulations were performed for an XPS configuration in which the angle, ψ, between the direction of the Al Kα x-ray beam and the photoelectron emission angle was fixed at 55° and for photoelectron emission angles of 0° and 50°. Exemplary results are shown as symbols in Fig. 11 for $\alpha = 0°$.

We note that the IMFP, $\lambda_{in}^{f}(E_f)$, was used twice in Eq. (24), which was derived from the SLA model. The question addressed in Ref. 53 was to test if replacement of both IMFPs in Eq. (24) with an EAL, L_{TH}, from the predictive formula [Eqs. (18) and (20)] would correct this equation for elastic-scattering effects. The answer was negative. However, if the IMFP in the prefactor of Eq. (24) was replaced by the EAL for the determination of surface composition, L_{QA}, the photoelectron intensities from the MC calculations were practically reproduced for all overlayer/substrate systems considered, as illustrated by the solid lines in Fig. 11. Thus, Eq. (24) should be corrected for the effects of elastic scattering as follows:

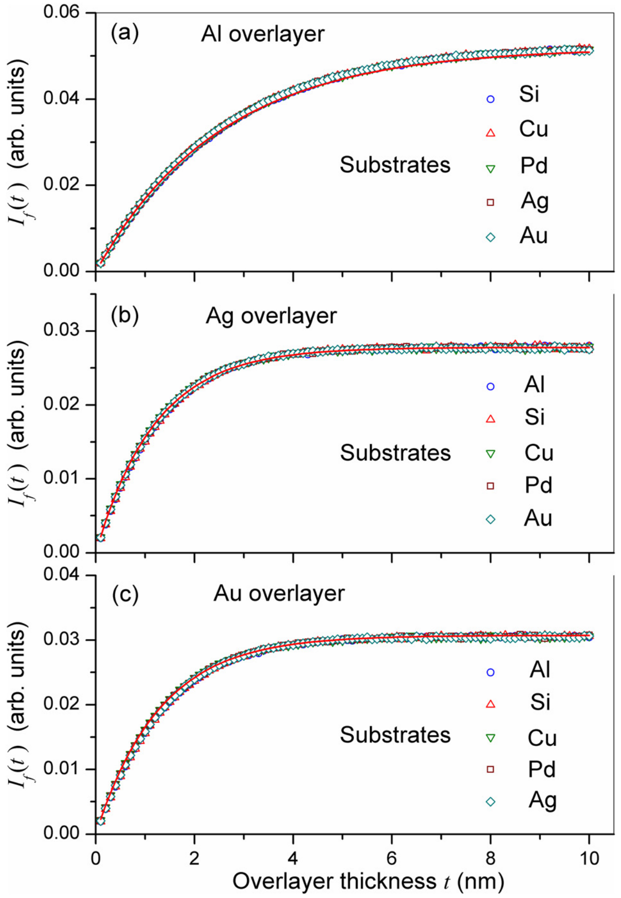

FIG. 11. Dependence of the (a) Al $2s_{1/2}$, (b) Ag $3d_{5/2}$, and (c) Au $4f_{7/2}$ photoelectron signal intensities excited by Al Kα x rays from (a) Al, (b) Ag, and (c) Au overlayers deposited on different substrates as a function of overlayer thickness.[53] Solid line: common formalism with the IMFPs replaced with two EALs, $L_C^f(E_f)$ and $L_{TH}^f(E_f)$, from the predictive formulas [Eqs. (18), (20), (30), and (31)]; symbols: Monte Carlo calculations for the substrates specified in a particular panel.

$$I_f(t) = S(E_f)\Delta\Omega F_x\left(\frac{d\sigma_x}{d\Omega}\right)_f \times N_f L_{QA}^f(E_f)\left[1-\exp\left(-\frac{t}{L_{TH}^f(E_f)\cos\alpha}\right)\right]. \tag{29}$$

The predictive formula for the EAL for surface composition, L_{QA}, has the following form:[54]

$$L_{QA} = R_{QA}^{pred}\lambda_{in}, \tag{30}$$

where

$$R_{QA}^{pred} = 1 - 0.147\omega - 0.164\omega^2. \tag{31}$$

Further details on the EAL for the determination of surface composition, L_{QA}, are provided in Sec. 3.2.

In Fig. 11, the solid lines represent Eq. (29) with the EALs, $L_{TH}^f(E_f)$ and $L_{QA}^f(E_f)$, calculated from the corresponding predictive formulas [Eqs. (18), (20), (30), and (31)]. One can see essentially perfect agreement.

The values of $L_{TH}^f(E_f)$ for a particular overlayer thickness and photoelectron emission angle can be calculated from

$$L_{TH}^f(E_f) = -\frac{1}{\cos\alpha}\frac{t}{\ln\left[1 - I_f(t)/I_f^{\infty}\right]} \tag{32}$$

and with the values of $I_f(t)$ and I_f^{∞} from Monte Carlo simulations.[53] The EALs were calculated in this way for Al $2s_{1/2}$ photoelectrons from Al overlayers on Si, Cu, Pd, Ag, and Au substrates, Ag $3d_{5/2}$ photoelectrons from Ag overlayers on Al, Si, Cu, Pd, and Au substrates, and Au $4f_{7/2}$ photoelectrons from Au overlayers on Al, Si, Cu, Pd, and Ag substrates. These calculations were made for XPS with Al Kα x rays, $\psi = 55°$, $\alpha = 0°$, and a wide range of overlayer thicknesses from 0.3 nm to a maximum value corresponding to 95% of the signal for the bulk overlayer material. The maximum deviations of these EALs from the average EAL values determined from Eq. (16) varied between 1.36% and 3.78%. Similar results were obtained for additional simulations with $\alpha = 50°$. This work indicates that average EALs are useful for determining overlayer thicknesses for a wide range of film thicknesses and for emission angles between 0° and 50°. Note that Eq. (29) in the limit of large overlayer thicknesses approaches the signal intensity from the bulk overlayer material, I_f^{∞},[54]

$$I_f^{\infty} = S(E_f)\Delta\Omega F_x\left(\frac{d\sigma_x}{d\Omega}\right)_f N_f L_{QA}^f(E_f). \tag{33}$$

From Eqs. (29) and (33), we obtain

$$R_f = \frac{I_f(t)}{I_f^{\infty}} = \left[1-\exp\left(-\frac{t}{L_{TH}^f(E_f)\cos\alpha}\right)\right]. \tag{34}$$

Consequently, the overlayer thickness can be determined from the measured ratios R_f^{expt} using

$$t = -L_{TH}^f(E_f)\cos\alpha\ln\left(1 - R_f^{expt}\right). \tag{35}$$

As follows from Eqs. (34) and (35), no information on the electron-scattering properties of the substrate is needed in this formalism, which has already been corrected for elastic-scattering effects.

One should be aware of a limitation in using EALs derived from the predictive formula given by Eqs. (19) and (20). This formula was derived for the "magic-angle" experimental configuration, i.e., for configurations in which the angle between the x-ray beam and the analyzer axis, ψ, is close to 55° (see Fig. 2). Furthermore, we assumed that the overlayer and substrate materials were identical, that the overlayer thickness was uniform, and that the interface in a given overlayer/substrate system was sharp. Reference 53 indicated that the predictive formula gave satisfactory results even when the substrate and overlayer materials were different. It has also been found that the EALs from the predictive formula do not show any substantive dependence on the photoelectron emission angle in the range $0° \le \alpha \le 50°$.[45,46] Thus, the above procedure for the determination of overlayer thickness is recommended for this range of photoelectron emission angles. For values of ψ appreciably different from 55° and for emission angles exceeding 50°, the EALs should be taken from other sources, e.g., the NIST Electron Effective-Attenuation-Length Database.[40]

3.1.1.3. Analysis of substrate photoelectron intensities. We described a formalism in Sec. 3.1.1.2 for the determination of overlayer-film thicknesses from substrate photoelectron intensities, which was based on the assumption that the electron-scattering properties of the overlayer and substrate materials were similar. This assumption is roughly equivalent to assuming that the IMFPs and transport mean free paths for a photoelectron signal in the substrate were each roughly similar to the corresponding values in the overlayer film. We then expect that the overlayer thickness could be calculated from Eq. (21) in which the IMFP, $\lambda^f_{in}(E_s)$, is replaced by the EAL, $L^f_{TH}(E_s)$, from the predictive EAL formula [Eq. (20)]. This expectation is based on the fact that the predictive formula was derived on the assumption that the electron-scattering properties of both materials were identical. We now address the general case where this assumption is not valid.

A systematic analysis of EALs for overlayer and substrate material combinations having appreciably different elastic- and inelastic-scattering properties was recently published by Jablonski.[53] As in Sec. 3.1.1.2, this analysis was based on the expression describing the photoelectron signal intensity from a substrate derived within the SLA model. In Eq. (21), we see two IMFPs, $\lambda^s_{in}(E_s)$ and $\lambda^f_{in}(E_s)$, which should be replaced by the EALs when the elastic-scattering events are taken into account. Jablonski utilized the advanced Monte Carlo strategy described earlier and found essentially perfect agreement between the simulated photoelectron intensities and the corresponding intensities from Eq. (21) after the IMFP, $\lambda^s_{in}(E_s)$, was replaced by the EAL, $L^s_{QA}(E_s)$, while the IMFP, $\lambda^f_{in}(E_s)$, was replaced by the EAL, $L^f_{TH}(E_s)$. Both EAL values were taken from the respective predictive formulas [Eqs. (20) and (31)]. We note that the Monte Carlo simulations were performed for various overlayer and substrate materials with similar and different electron-scattering properties. Thus, we have

$$I_s(t) = S(E_s)\Delta\Omega F_x\left(\frac{d\sigma_x}{d\Omega}\right)_s N_s L^s_{QA}(E_s)\exp\left(-\frac{t}{L^f_{TH}(E_s)\cos\alpha}\right). \tag{36}$$

The photoelectron signal intensity from an uncovered substrate after correcting for elastic-scattering effects is expressed by

$$I^\infty_s = S(E_s)\Delta\Omega F_x\left(\frac{d\sigma_x}{d\Omega}\right)_s N_s L^s_{QA}(E_s), \tag{37}$$

and thus, Eq. (36) can be written as follows:

$$I_s(t) = I^\infty_s \exp\left(-\frac{t}{L^f_{TH}(E_s)\cos\alpha}\right). \tag{38}$$

If the EAL, $L^f_{TH}(E_s)$, is calculated from the predictive formula [Eq. (20)], the photoelectron intensities from Eq. (38) were found to be very close to the corresponding results of Monte Carlo calculations for any combination of the overlayer and substrate materials, including cases of a low-atomic-number overlayer deposited on a high-atomic-number substrate.[53]

As an example, the symbols in Fig. 12 show the dependence of the photoelectron intensities from Si, Pd, and Au substrates on the Ag overlayer thickness obtained from Monte Carlo simulations.[53]

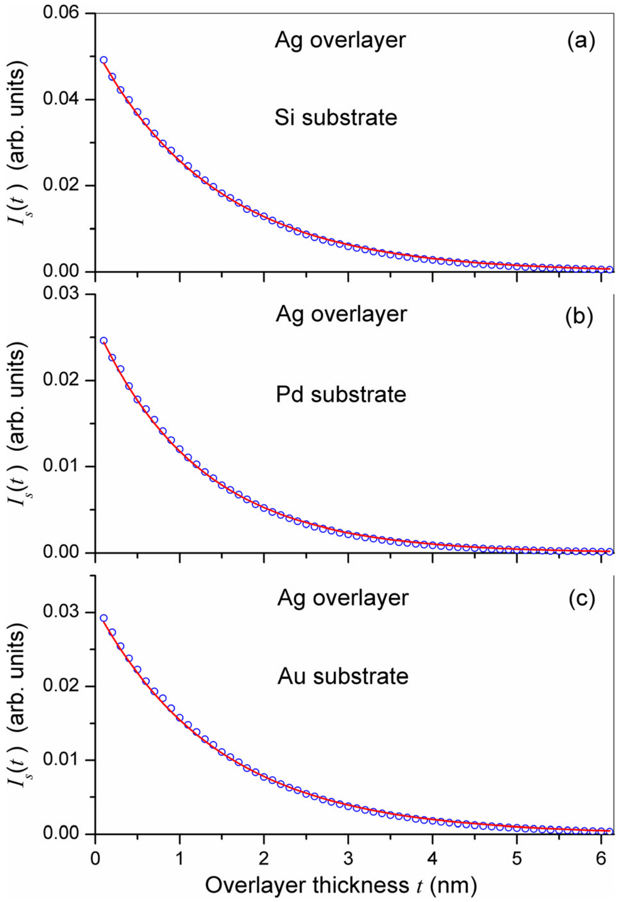

FIG. 12. Dependence of the (a) Si $2s_{1/2}$, (b) Pd $3d_{5/2}$, and (c) Au $4f_{7/2}$ photoelectron signal intensities excited by Al Kα x rays from (a) Si, (b) Pd, and (c) Au substrates covered by an Ag overlayer as a function of overlayer thickness.[53] Solid line: common formalism with IMFPs replaced with two EALs, $L^s_{QA}(E_s)$ and $L^f_{TH}(E_s)$, from the predictive formulas [Eqs. (18), (20), (30), and (31)]; symbols: Monte Carlo calculations.

These simulations were made for the Si $2s_{1/2}$, Pd $3d_{5/2}$, and Au $4f_{7/2}$ photoelectron lines emitted by Al Kα x rays in an XPS configuration with $\psi = 55^\circ$. We see essentially perfect agreement with the solid lines that were calculated from Eq. (36) and with the EALs, $L_{TH}^{f}(E_s)$ and $L_{QA}^{s}(E_s)$, calculated from the corresponding predictive formulas [Eqs. (18), (20), (30), and (31)].

Measurements of photoelectron intensities from the covered and uncovered substrate provide the ratio $R_s^{expt} = I_s/I_s^{\infty}$. The overlayer thickness can then be calculated from Eq. (38) modified as follows:

$$t = -L_{TH}^{f}(E_s)\cos\alpha\ln(R_s^{expt}). \tag{39}$$

The values of $L_{TH}^{f}(E_s)$ for a particular overlayer thickness and photoelectron emission angle can be calculated from

$$L_{TH}^{f}(E_s) = -\frac{1}{\cos\alpha}\frac{t}{[\ln I_s(t) - \ln I_s^{\infty}]} \tag{40}$$

and with the values of $I_s(t)$ and I_s^{∞} from the MC simulations.[53] The EALs were calculated for Al overlayers on substrates of Si (Si $2s_{1/2}$), Cu (Cu $2p_{3/2}$), Pd (Pd $3d_{5/2}$), Ag (Ag $3d_{5/2}$), and Au (Au $4f_{7/2}$), for Ag overlayers on substrates of Al (Al $2s_{1/2}$), Si (Si $2s_{1/2}$), Cu (Cu $2p_{3/2}$), Pd (Pd $3d_{5/2}$), and Au (Au $4f_{7/2}$), and for Au overlayers on substrates of Al (Al $2s_{1/2}$), Si (Si $2s_{1/2}$), Cu (Cu $2p_{3/2}$), Pd (Pd $3d_{5/2}$), and Ag (Ag $3d_{5/2}$). The selected photoelectron lines from each substrate are indicated in parentheses. The Monte Carlo simulations were made for $\alpha = 0^\circ$ and for a wide range of overlayer thicknesses from 0.3 nm to a maximum value corresponding to the reduction of the substrate signal to 5% of its maximum value (for an uncovered substrate). The maximum deviations of these EALs from the average EALs determined from Eq. (16) varied between 0.98% and 6.49%. Similar results were found from additional simulations with $\alpha = 50^\circ$, again showing that the average EALs can be used to determine overlayer thicknesses for a wide range of film thicknesses and for emission angles between 0° and 50°.

The above procedure seems to be a reliable way of extending the formalism based on the straight-line approximation (SLA) to take elastic-scattering effects into account. We also see that it is justified to use the EALs from the predictive formulas [Eqs. (18) and (20)] that were developed from the EAL calculations for substrate/overlayer material combinations with similar electron-scattering properties and to apply these EALs to substrate/overlayer material combinations having substantially different electron-scattering properties.

The same limitations on the use of Eq. (39) are to be observed as for the use of overlayer-signal intensities, which was discussed in Sec. 3.1.1.2. The XPS configuration should be close to the "magic-angle" geometry ($\psi = 55^\circ$), and the photoelectron emission angles should be in the range $0^\circ \le \alpha \le 50^\circ$. When these requirements are not satisfied, EALs can be obtained from the NIST EAL database.[40] Alternatively, Monte Carlo simulations can be performed to calculate the dependence of substrate-signal intensity on the overlayer thickness for a given material combination and experimental configuration.[55,56] If this dependence can be approximated by a relatively simple analytical expression, this expression can be utilized to determine film thicknesses from the measured changes in substrate intensities.

As an example of this approach, Jablonski and Zemek[55] measured the dependence of the Au $4f_{7/2}$ photoelectron intensity emitted by Mg Kα radiation from an Au substrate covered by Ni overlayers of varying thicknesses. These measurements were performed with an x-ray incidence angle, θ_x, equal to 70° and with $\alpha = 0^\circ$. Thus, the angle $\psi = 70^\circ$ differs considerably from the magic angle (55°) considered above. Monte Carlo simulations were performed for these conditions, and they showed that the dependence of the calculated Au $4f_{7/2}$ intensity, $I_s(t)$, on Ni film thickness, t, could be well approximated by[55]

$$I_s(t) = (a + bt)\exp\left(-\frac{t}{c}\right), \tag{41}$$

where a, b, and c are fitted constants. For $t \to 0$, the signal intensity $I_s(t) \to I_s^{\infty}$, and Eq. (41) could be transformed to

$$R_s(t) = \frac{I_s(t)}{I_s^{\infty}} = \left(1 + \frac{bt}{a}\right)\exp\left(-\frac{t}{c}\right). \tag{42}$$

For a given thickness, the experiment provided the ratio

$$(I_s/I_s^{\infty})_{expt} = R_s^{expt}. \tag{43}$$

The overlayer thickness could then be conveniently obtained by solving Eq. (42) with $R_s(t)$ replaced by R_s^{expt}. For example, the measured ratio $(I_s/I_s^{\infty})_{expt} = 0.012\,97$ leads to a Ni film thickness of 5.231 nm, while a Ni thickness of 7.248 nm results from the straight-line approximation.[55] This example shows that neglect of elastic-scattering effects leads to a Ni thickness that is 38.6% larger than the value found when a correction is made for these effects.

The NIST SESSA database[42] can also be used to perform Monte Carlo simulations of the type just described. Powell *et al.*[56] calculated EALs describing intensity changes of Si-substrate 2p photoelectrons for $SiO_{1.6}N_{0.4}$ and $HfO_{1.9}N_{0.1}$ overlayer films of varying thicknesses and for different XPS configurations.

We would now like to present an example of EAL measurements for thin films of an organic molecular solid, perylene-3,4,9,10-tetracarboxylic dianhydride (PTCDA), by Graber *et al.*[57] PTCDA has been shown to grow layer-by-layer when deposited on Ag(111) at a substrate temperature between 210 K and 250 K.[58] The Ag(111) substrate was cleaned by several cycles of sputtering with 700 eV Ar^+ ions and a well-established annealing procedure to produce an atomically flat surface. PTCDA is thus an exemplary model system that satisfies most of the assumptions listed in Sec. 2 for valid EAL measurements. It is, however, possible that the crystalline substrate and the ordered PTCDA films[58] could modulate the photoelectron intensities at particular energies and directions.[59–62] In one spectacular example, Egelhoff[59] showed that the Ni $2p_{3/2}$ signal from 0.3 monolayers of Ni on a Cu(100) surface *increased* (in a particular direction) rather than decreased following the deposition of 1.5 monolayers of copper.

Some of the Graber *et al.* EAL measurements were made with a laboratory XPS instrument equipped with Al and Mg Kα x-ray sources (i.e., XPS with unpolarized x rays), while other EAL measurements were made with linearly polarized x rays from a synchrotron-radiation source with energies between 395 eV and 900 eV.[57] Additional EAL measurements were made with He I and He II ultraviolet radiation (to produce photoelectrons with energies between 15 eV and 35 eV), and one measurement was made with a two-photon photoemission experiment to produce a photoelectron energy of 5.3 eV.

Graber *et al.* reported EALs for electron energies between 5.3 eV and 1480 eV based on attenuation measurements of Ag photoelectron and Auger-electron signals from the substrate and on growth measurements of the C 1s signal from PTCDA as a function of PTCDA film thickness.[57] Figure 13 shows the EALs and their uncertainties reported by Graber *et al.* as a function of electron energy. The error bars in Fig. 13 were determined by the authors based on the quality of the fits to exponential functions of the signal intensities as a function of PTCDA thickness. We also show the plots of IMFPs in PTCDA calculated from the TPP-2M predictive IMFP equation of Tanuma *et al.*,[63] Eqs. (93) and (94), and the EALs expected from the predictive EAL formulas of Jablonski and Powell [Eq. (20)] for XPS with unpolarized x rays and Eq. (62) for XPS with linearly polarized x rays. While there is some scatter of the experimental points beyond that expected from the error bars, the measured EALs generally follow the trends expected from the predictive EAL formulas. Nevertheless, there is a group of points at energies between 242 eV and 690 eV with the EALs that are systematically smaller than the predicted EALs. This EAL decrease as well as the increased EALs at energies of 82 eV and 135 eV could be the result of diffraction or forward-focusing effects on the photoelectron transport.[59–62]

The example of EALs for PTCDA in Fig. 13 is also instructive in that the elastic-scattering effects are relatively small at high energies and relatively large at low energies. Figure 14 shows the plots as a function of electron energy of IMFPs for PTCDA ($C_{24}H_8O_6$) from the TPP-2M equation[63] [Eqs. (93) and (94) described in Sec. 4] and of TRMFPs based on TCSs for the elemental constituents (weighted according to the stoichiometry of the molecule) from the ELSEPA database.[64] The inset in Fig. 14 is a plot of ω from Eq. (7) as a function of electron energy. We see that $\omega = 0.0618$ for an energy of 1500 eV, and there is only a small difference between the IMFP and EAL for unpolarized radiation (4.6%) and for polarized radiation (5.17%) as shown in Fig. 13 at this energy. In contrast, $\omega = 0.583$ for an energy of 50 eV, and there is a much larger difference (43%) between the IMFP and EAL for XPS with unpolarized x rays at this energy. For XPS with polarized x rays, there is an even larger difference (49%) between the IMFP and the predicted EAL.

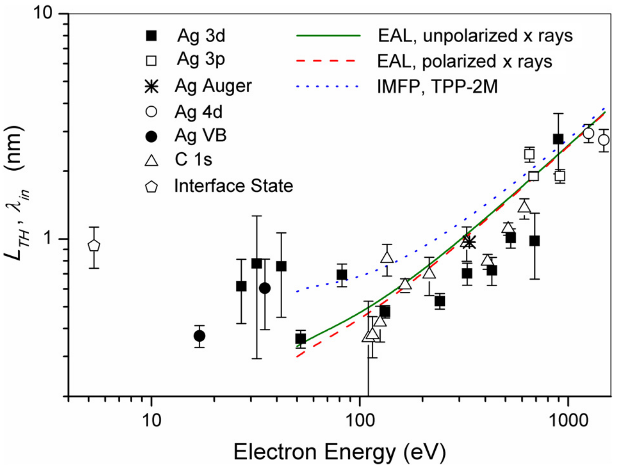

FIG. 13. Plot of measured EALs, L_{TH}, vs electron energy reported by Graber *et al.*[57] for PTCDA. The experiments were performed with thin films of PTCDA deposited on an Ag(111) substrate, and the symbols denote attenuation measurements of various Ag photoelectron and Auger-electron signals from the substrate and the growth of the C 1s signal from PTCDA. "VB" refers to the Ag valence band, and "interface state" indicates excitation of a photoelectron with an energy of 5.3 eV from an interface state in a two-photon photoemission experiment. The dotted line shows the IMFPs for PTCDA calculated from the TPP-2M IMFP predictive formula [Eqs. (93) and (94)] of Tanuma *et al.*[63] The solid and dashed lines show the calculated EALs for PTCDA from the predictive formulas of Jablonski and Powell for XPS with unpolarized x rays [Eqs. (18) and (20)] and linearly polarized x rays [Eq. (62)], respectively.

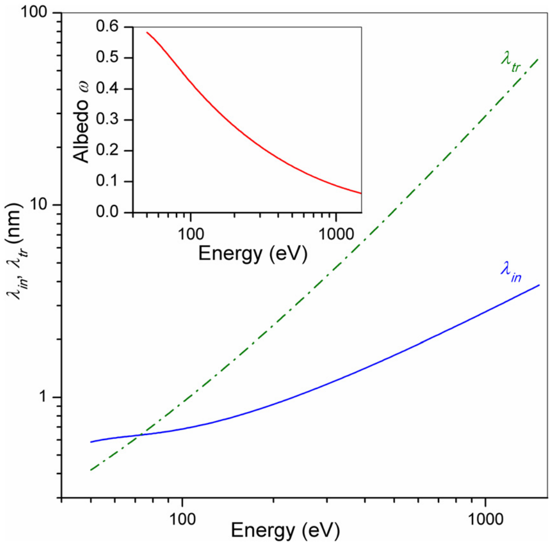

FIG. 14. The solid line shows IMFPs for PTCDA calculated from the TPP-2M IMFP predictive formula [Eqs. (93) and (94)] of Tanuma *et al.*[63] The dot-dashed line shows transport mean free paths for PTCDA calculated from Eqs. (8) and (9) using transport cross sections from the ELSEPA database.[64] The inset shows a plot of the single-scattering albedo, ω, for PTCDA from Eq. (7) as a function of electron energy.

3.1.1.4. Analysis of the ratio of substrate and overlayer photoelectron intensities. As in Subsections 3.1.1.1–3.1.1.3, we first consider the SLA model. The ratio of peak intensities from an overlayer and a substrate is given by

$$\frac{I_f^{SLA}(t)}{I_s^{SLA}(t)} = \frac{S(E_f)\Delta\Omega F_x\left(\frac{d\sigma_x}{d\Omega}\right)_f N_f\lambda_{in}^f(E_f)\left[1-\exp\left(-\frac{t}{\lambda_{in}^f(E_f)\cos\alpha}\right)\right]}{S(E_s)\Delta\Omega F_x\left(\frac{d\sigma_x}{d\Omega}\right)_s N_s\lambda_{in}^s(E_s)\exp\left(-\frac{t}{\lambda_{in}^s(E_s)\cos\alpha}\right)}$$

$$= \frac{I_f^{\infty,SLA}}{I_s^{\infty,SLA}}\frac{\left[1-\exp\left(-t/\lambda_{in}^f(E_f)\cos\alpha\right)\right]}{\exp\left(-t/\lambda_{in}^f(E_s)\cos\alpha\right)}. \tag{44}$$

Let us denote

$$R^{SLA} = \frac{I_f^{SLA}(t)}{I_s^{SLA}(t)}\frac{I_s^{\infty,SLA}}{I_f^{\infty,SLA}}. \tag{45}$$

This ratio can be measured experimentally, and thus, we obtain the equation

$$R_{expt} = R^{SLA} = \frac{\left[1-\exp\left(-t/\lambda_{in}^f(E_f)\cos\alpha\right)\right]}{\exp\left(-t/\lambda_{in}^f(E_s)\cos\alpha\right)}. \tag{46}$$

In general, the IMFPs $\lambda_{in}^{f}(E_f)$ and $\lambda_{in}^{f}(E_s)$ may be different, and consequently, Eq. (46) cannot be solved analytically with respect to the thickness, t. However, the method based on measurements of signal intensities from an overlayer and a substrate is very convenient in experimental practice. It is also advantageous in that the ratio R_{expt} does not depend on the presence of any surface contamination.[65] Let us now analyze the conditions for this EAL approach to be useful.

As mentioned earlier, the formalism based on the straight-line approximation (SLA) is considerably simplified when the IMFPs of photoelectrons from the overlayer and substrate materials in the overlayer are identical or almost identical,

$$\lambda_{in}^{f}\left(E_f\right) \cong \lambda_{in}^{f}(E_s) = \lambda_{in}^{f}. \tag{47}$$

One can satisfy this condition by selecting photoelectron peaks with similar energies, $E_f \approx E_s$. In one very useful application of this approach to be described in more detail later in this section, measurements have been made of Si 2p photoelectron intensities from a native SiO_2 film and the Si substrate. In this example case, the kinetic energies of the Si 2p photoelectrons differ by about 4 eV. We follow the procedure of Subsections 3.1.1.2 and 3.1.1.3 and initially assume that the SLA model is valid. From Eqs. (46) and (47), we obtain Eq. (3a) written as follows:

$$t = \lambda_{in}^{f} \cos\alpha \ln\left[\frac{R(t)}{R^{\infty}} + 1\right], \tag{48}$$

where

$$R(t) = \frac{I_f(t)}{I_s(t)} \tag{49}$$

and

$$R^{\infty} = \frac{I_f^{\infty}}{I_s^{\infty}}. \tag{50}$$

The superscript SLA is omitted here to simplify the notation. The ratio R^{∞} can be determined from separate measurements of I_f^{∞} and I_s^{∞}. Measurements of the ratio $R(t)$ are relatively easy to perform, and the thickness can be readily calculated from Eq. (48). In order to take elastic scattering of the photoelectrons into account, we use an EAL instead of the IMFP in Eq. (48). However, an additional condition should also be satisfied, namely, the elastic-scattering properties of the overlayer and substrate materials should be similar. These properties can be evaluated with the transport mean free paths (TRMFPs). If these values are similar for both materials, a single value of the EAL, L_{TH}, for the overlayer material can be determined from the predictive formula [Eq. (20)]. One can tentatively suggest here, as an "educated guess," that the TRMFP difference should not exceed 10%. Equation (48) then takes the following form:

$$t = L_{TH} \cos\alpha \ln\left[\frac{R(t)}{R^{\infty}} + 1\right]. \tag{51}$$

We now consider the more general case where the IMFPs of photoelectrons in the substrate and overlayer materials could be different and the TRMFPs of these photoelectrons could also be different in the two materials. In a recent analysis of the procedure for overlayer-thickness determination from the intensities of two lines for the magic-angle configuration ($\psi = 55°$),[53] it was found that the overlayer thickness could be calculated from the SLA formalism [Eq. (46)] with the IMFPs replaced by the EALs for the overlayer material, $L_{TH}^{f}(E_f)$ and $L_{TH}^{f}(E_s)$, which were obtained from the predictive formulas [Eqs. (18) and (20)]. Suppose that experiments provided the ratio

$$R_{expt} = \frac{I_f}{I_s}\frac{I_s^{\infty}}{I_f^{\infty}}. \tag{52}$$

Equation (46) can be then written in the following form:

$$R_{expt} = \frac{\left[1 - \exp\left(-t^{pred}/L_{TH}^{f}(E_f)\cos\alpha\right)\right]}{\exp\left(-t^{pred}/L_{TH}^{f}(E_s)\cos\alpha\right)}, \tag{53}$$

where t^{pred} indicates the overlayer thickness. The validity of Eq. (53) was tested by performing extensive simulations with the advanced MC program described in Ref. 53. For an assumed overlayer thickness, t, the intensities I_f, I_s, I_f^{∞}, and I_s^{∞} were calculated, and the thickness t^{pred} was determined from Eq. (53). Calculations were performed for three overlayer materials (Al, Ag, and Au) deposited on five different substrate materials (Al on Si, Cu, Pd, Ag, and Au; Ag on Al, Si, Cu, Pd, and Au; and Au on Al, Si, Cu, Pd, and Ag). The most pronounced photoelectron lines from each solid were considered (Al $2s_{1/2}$, Si $2s_{1/2}$, Cu $2p_{3/2}$, Pd $3d_{5/2}$, Ag $3d_{5/2}$, and Au $4f_{7/2}$). The results of these calculations are shown in Fig. 15 for XPS with Al Kα x rays, $\psi = 55°$, and $\alpha = 0°$. It was found that, irrespective of the overlayer/substrate combination, the values of t^{pred} practically reproduced the assumed thicknesses, t. The average difference between the predicted and assumed overlayer thicknesses was less than 3%. Similar results were obtained with $\alpha = 50°$.

Table 1 shows the electron-scattering properties (IMFPs, λ_{in}, TRMFPs, λ_{tr}, and albedo values, ω) for the Al-overlayer/Pd-substrate, Ag-overlayer/Cu-substrate, and Au-overlayer/Si-substrate systems. Suppose we wished to measure the thickness of Au overlayers deposited on Si. In this relatively extreme case, the IMFPs of Au $4f_{7/2}$ photoelectrons in Au and Si differ by a factor close to 2, the TRMFPs by a factor of about 7, and the ω values by a factor of around 3. Similarly, the IMFPs of Si $2s_{1/2}$ photoelectrons in Au and Si differ by a factor of almost 2, the TRMFPs by a factor of about 7, and the ω values by a factor of around 3. Nonetheless, satisfactory overlayer thicknesses were obtained for this combination and the other substrate/overlayer combinations. The analytical relation given by Eq. (53) with the simple predictive formula for the EALs practically reproduces the results obtained from Monte Carlo simulations that implement the actual properties of the overlayer and substrate materials. Note that, in Eq. (53), the scattering properties of the substrate are ignored; the EALs, $L_{TH}^{f}(E_f)$ and $L_{TH}^{f}(E_s)$, must be calculated only for the overlayer material. One should stress, however, that the approach based on Eq. (53) is applicable only for experimental configurations close to the magic-angle configuration, i.e., when the angle ψ between the analyzer axis and the direction of the x-ray beam is close to 55° (see Fig. 2). Furthermore, the emission angle, α, should not exceed 50°. For other configurations and for $\alpha > 50°$, EALs can be determined from the NIST EAL database[40] or from simulated photoelectron intensities from SESSA[42] or other software.[55]

For simplicity, we did not previously indicate the dependence of the ratio R^{SLA} in Eq. (46) on emission angle α, and we now designate this ratio and the ratio $R(t)$ from Eq. (49) as $R_{t,\alpha}$. Powell *et al.*[56] utilized the NIST SESSA database[42] to simulate Si $2p_{3/2}$ photoelectron

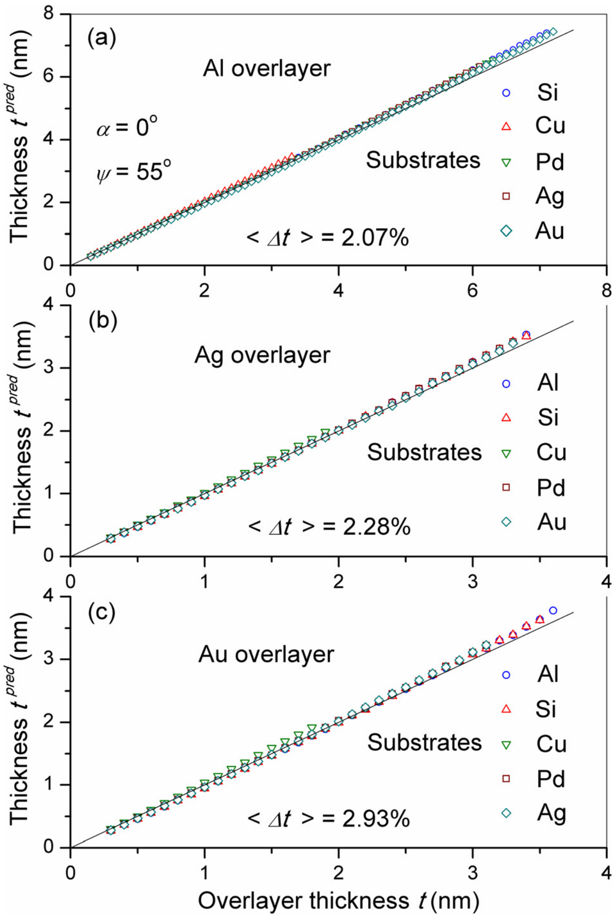

FIG. 15. Predicted overlayer thicknesses, t^{pred}, as a function of assumed overlayer thickness, t, from Monte Carlo simulations that were obtained from solution of the nonlinear equation [Eq. (53)] involving the EALs from the predictive formulas [Eqs. (18) and (20)]. The simulations were performed for the magic-angle XPS configuration, $\alpha = 0°$, and excitation by Al Kα x rays.[53] See the text for other details. (a) Al overlayer, (b) Ag overlayer, and (c) Au overlayer. Substrates are identified by symbols in a particular panel. The values $\langle \Delta t \rangle$ are the mean percentage deviations of the calculated thicknesses from the assumed thicknesses.

intensities (excited by Al Kα x rays) from thin films of $SiO_{1.6}N_{0.4}$ on a Si substrate as a function of t and α. These simulations were performed for two XPS configurations. For the first configuration (the sample-tilting configuration), the angle between the direction of x rays and the axis of the electron energy analyzer was fixed at 55° (the magic-angle configuration), and the sample was tilted to vary the photoelectron emission angle. For the second configuration (the Theta Probe configuration[66]), the sample is fixed, and photoelectron intensities are measured in parallel for emission angles between 20° and 80°. The x-ray incidence angle is 30° in the latter configuration, and the plane of x-ray incidence is at 70° with respect to the emission plane (defined by the electron energy analyzer). The angle between the direction of x-ray incidence and a particular emission angle for the detected photoelectrons thus varies with the emission angle. At this point, we need to define an EAL, L_{TH}^{ratio}, that would be specific to the determination of overlayer thicknesses with Eq. (51),

$$t = L_{TH}^{ratio} \cos\alpha \ln\left[\frac{R_{t,\alpha}}{R^{\infty}} + 1\right], \tag{54}$$

since we will show an application where the values of L_{TH}^{ratio} could differ from the values of L_{TH} obtained from the predictive formula [Eq. (20)]. Figure 16 shows the plots of $\ln[1 + (R_{t,\alpha}/R_0)]/t$ from the simulated Si $2p_{3/2}$ intensities from the substrate and the film vs $1/\cos\alpha$ for each of five film thicknesses (0.5 nm, 1.5 nm, 2.5 nm, 3.5 nm, and 4.5 nm) for the sample-tilting configuration.[56] The values of R_0 were determined from separate simulations of the Si $2p_{3/2}$ intensities for a bare Si substrate and a 100 nm $SiO_{1.6}N_{0.4}$ film for each emission angle. We see that the plots in Fig. 16 appear to be linear for emission angles up to 55° ($\sec\alpha = 1.74$). For $\alpha \geq 60°$ ($\sec\alpha = 2$), the plots show increasing amounts of curvature with increasing film thickness due to the effects of elastic scattering. We note that the plot in Fig. 16 for the 3.5 nm $SiO_{1.6}N_{0.4}$ film is qualitatively similar to a plot based on the measured Si 2p intensities for a 3.9 nm SiO_2 film on Si.[67]

The solid line in Fig. 17(a) is a plot of $L_{TH}^{ratio}/\lambda_{in}$ vs $SiO_{1.6}N_{0.4}$ film thickness where L_{TH}^{ratio} is the average EAL determined from one-parameter linear fits through the origin to the plotted data in Fig. 16 for emission angles between 0° and 55°. Error bars on each point indicate the one-standard-deviation uncertainties. The values of L_{TH}^{ratio} in Fig. 17(a) were fitted with the following three-parameter single-exponential equation:[56]

$$L_{TH}^{ratio} = e + f\exp(-gt). \tag{55}$$

The solid line in Fig. 17(a) shows this fit for $SiO_{1.6}N_{0.4}$ with the sample-tilting configuration, while the dashed line shows a similar fit based on simulations for the Theta Probe configuration. The values of L_{TH}^{ratio} at the average Si $2p_{3/2}$ photoelectron energy of 1385.4 eV can then be obtained from Eq. (51) and the fit parameters for a desired film thickness (in nanometers) and the average IMFP (3.895 nm) for $SiO_{1.6}N_{0.4}$ at this energy.[56]

Similar SESSA simulations were made for thin films of $HfO_{1.9}N_{0.1}$ on Si.[56] In this case, the ratios of Hf $4f_{7/2}$ and Si $2p_{3/2}$ intensities were determined, again as a function of t and α. Since the kinetic energies of these photoelectrons differ by 85 eV, Eq. (47) cannot be used. If we again use the SLA, Eq. (48) becomes

$$t = \lambda_{in}\cos\alpha \ln\left(\frac{R_{t,\alpha}}{R^{\infty}} + F\right), \tag{56}$$

where

$$F = \frac{\exp(-t/\lambda_{Hf}\cos\alpha)}{\exp(-t/\lambda_{Si}\cos\alpha)} \tag{57}$$

and λ_{Hf} and λ_{Si} are IMFPs for Hf $4f_{7/2}$ and Si $2p_{3/2}$ photoelectrons, respectively, in $HfO_{1.9}N_{0.1}$. The average values of F from Eq. (57) for emission angles between 0° and 55° ranged from 1.015 for a film thickness of 0.5 nm to 1.144 for a film thickness of 4.5 nm. If we now use the EAL instead of the IMFP to account for elastic-scattering effects, Eq. (56) becomes

$$t = L_{TH}^{ratio}\cos\alpha \ln\left(\frac{R_{t,\alpha}}{R^{\infty}} + F\right). \tag{58}$$

Figure 18 shows the plots of $\ln[F + (R_{t,\alpha}/R_0)]/t$ vs $1/\cos\alpha$ from the simulated Si $2p_{3/2}$ photoelectron intensities from the substrate and the Hf $4f_{7/2}$ intensities from the $HfO_{1.9}N_{0.1}$ film with the

TABLE 1. Comparison of IMFPs, λ_{in}, transport mean free paths, λ_{tr}, and albedo values, ω, in selected overlayer/substrate systems for photoelectrons emitted in both materials by Al Kα radiation

Overlayer/substrate	Kinetic energy (eV)	λ_{in} (nm)	λ_{tr} (nm)	ω
Al/Pd system, Al $2s_{1/2}$ photoelectron line from the overlayer				
Al	1368.8	2.761	22.207	0.1106
Pd	1368.8	1.684	4.143	0.2890
Al/Pd system, Pd $3d_{5/2}$ photoelectron line from the substrate				
Al	1151.4	2.406	17.037	0.1237
Pd	1151.4	1.476	3.364	0.3050
Ag/Cu system, Ag $3d_{5/2}$ photoelectron line from the overlayer				
Ag	1118.6	1.542	3.689	0.2949
Cu	1118.6	1.839	4.184	0.3053
Ag/Cu system, Cu $2p_{3/2}$ photoelectron line from the substrate				
Ag	554.1	0.941	1.769	0.3473
Cu	554.1	1.118	1.776	0.3863
Au/Si system, Au $4f_{7/2}$ photoelectron line from the overlayer				
Au	1402.7	1.731	3.272	0.3459
Si	1402.7	3.220	24.925	0.1144
Au/Si system, Si $2s_{1/2}$ photoelectron line from the substrate				
Au	1336.9	1.669	3.129	0.3479
Si	1336.9	3.099	23.159	0.1180

sample-tilting configuration for each of the five film thicknesses.[56] The values of R_0 were determined from separate simulations of the Si $2p_{3/2}$ intensities for a bare Si substrate, as before, and of the Hf $4f_{7/2}$ intensities for a 100 nm $HfO_{1.9}N_{0.1}$ film. Appropriate values of F were utilized for each emission angle and film thickness.[56] The plots in Fig. 18 are qualitatively similar to those in Fig. 16 for $SiO_{1.6}N_{0.4}$ although the effects of elastic scattering are stronger in two ways. First, as shown in the inset of Fig. 18, there is a clearer dispersion of the curves for emission angles less than 60° than in the inset of Fig. 16. Second, the curves are linear for smaller ranges of emission angles, as shown in the inset for emission angles between 0° and 55°. One-parameter linear fits through the origin to the data in Fig. 18 were judged satisfactory for angular ranges between 0° and 55° for film thicknesses of 0.5 nm and 1.5 nm, between 0° and 50° for a film thickness of 2.5 nm, and between 0° and 45° for film thicknesses of 3.5 nm and 4.5 nm.

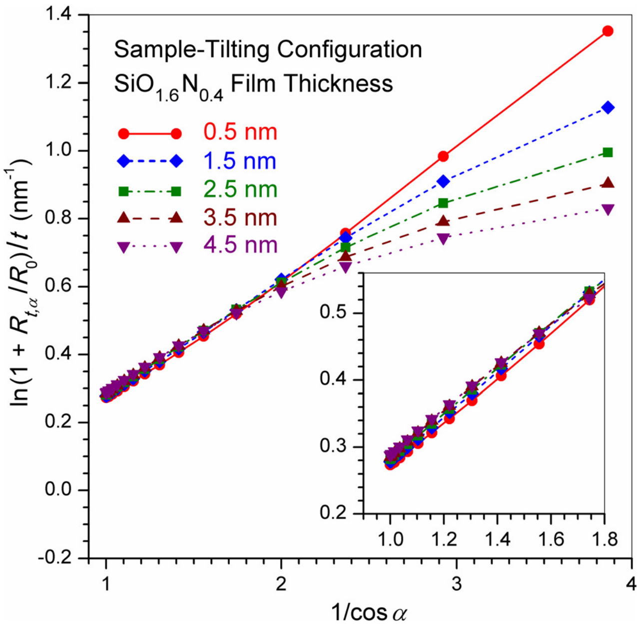

FIG. 16. Plots of $\ln[1 + (R_{t,\alpha}/R_0)]/t$ vs 1/cos α for thin films of $SiO_{1.6}N_{0.4}$ on Si for the sample-tilting configuration, the indicated film thicknesses, and an average photoelectron energy of 1385.4 eV.[56] The values of $R_{t,\alpha}$ for a particular film thickness, t, and emission angle, α, were obtained from the ratio of Si $2p_{3/2}$ photoelectron intensities for the film and substrate, while R_0 is the ratio of these intensities for a thick film and a bare substrate. The inset shows an enlarged view of the plots for emission angles between 0° and 55°.

Figure 17(b) shows the plots of the resulting $L_{TH}^{ratio}/\lambda_{in}$ values for the sample-tilting configuration (solid squares) and the Theta Probe configuration (solid circles) and their one-standard-deviation uncertainties vs $HfO_{1.9}N_{0.1}$ film thickness where L_{TH}^{ratio} is here the average EAL for 1429.9 eV photoelectrons in $HfO_{1.9}N_{0.1}$. The lines in Fig. 17(b) are again fits to the plotted points with Eq. (55). The relatively stronger dependence of $L_{TH}^{ratio}/\lambda_{in}$ values for $HfO_{1.9}N_{0.1}$ on the film thickness in Fig. 17(b) compared to those for $SiO_{1.6}N_{0.4}$ in Fig. 17(a) is an indication of the relatively larger effects of elastic scattering in $HfO_{1.9}N_{0.1}$ compared to $SiO_{1.6}N_{0.4}$.

The horizontal dotted-dashed lines in Fig. 17 show the plots of L_{TH}/λ_{in} from the EAL predictive formulas [Eqs. (18) and (20)]. We see that the values of $L_{TH}^{ratio}/\lambda_{in}$ are close to the L_{TH}/λ_{in} values for both $SiO_{1.6}N_{0.4}$ and $HfO_{1.9}N_{0.1}$ at $t = 0.5$ nm, but there are divergences of up to about 7% when $t = 4.5$ nm.

We now describe examples of EAL determination based on the measurements of the ratio of substrate and overlayer photoelectron intensities, as first proposed by Hill *et al.*[68] Seah *et al.*[69,70] conducted an extensive study among National Measurement Institutes to determine the absolute thicknesses of ultra-thin layers of SiO_2 on Si. Samples of silicon oxide on (100) and (111) oriented silicon wafers with nominal thicknesses between 1.5 nm and 8 nm were distributed

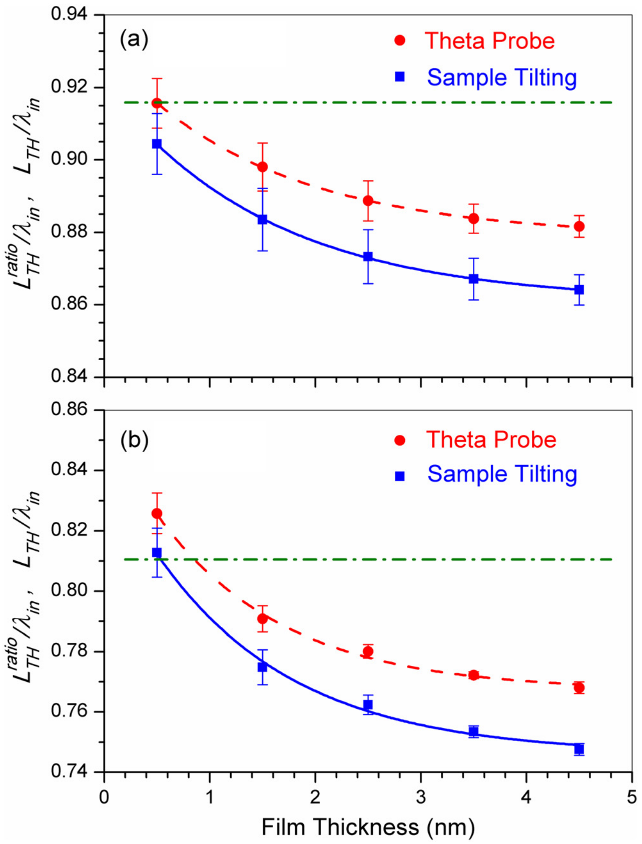

FIG. 17. Plots of $L_{TH}^{ratio}/\lambda_{in}$ (symbols) for (a) $SiO_{1.6}N_{0.4}$ (average photoelectron energy = 1385.4 eV) and (b) $HfO_{1.9}N_{0.1}$ (average photoelectron energy = 1429.9 eV) as a function of film thickness for the Theta Probe configuration (red circles) and the sample-tilting configuration (blue squares).[56] The values of $L_{TH}^{ratio}/\lambda_{in}$ were derived from one-parameter linear fits to the plots in Figs. 16 and 18 and similar plots for the Theta Probe configuration for the selected ranges of emission angles as described in the text, with the error bars indicating their one-standard-deviation uncertainties. The lines show fits to the $L_{TH}^{ratio}/\lambda_{in}$ data with Eq. (55). The horizontal dotted-dashed lines show plots of L_{TH}/λ_{in} from the EAL predictive formula [Eqs. (18) and (20)].

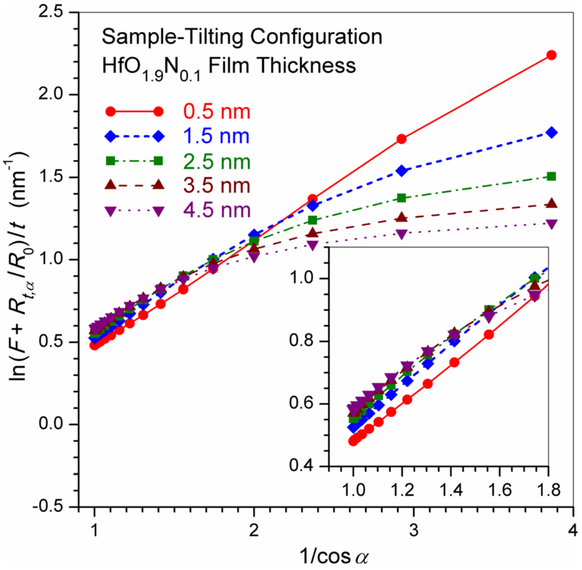

FIG. 18. Plots of $\ln[F + (R_{t,\alpha}/R_0)]/t$ vs $1/\cos\alpha$ for thin films of $HfO_{1.9}N_{0.1}$ on Si for the sample-tilting configuration, the indicated film thicknesses, and an average photoelectron energy of 1429.9 eV.[56] The values of $R_{t,\alpha}$ for a particular film thickness, t, and emission angle, α, were obtained from the ratio of the Hf $4f_{7/2}$ photoelectron intensity from the film to the substrate Si $2p_{3/2}$ photoelectron intensity for the film, while R_0 is the ratio of these intensities for a thick film and a bare substrate. The parameter F was calculated from Eq. (57) for each film thickness and emission angle. The inset shows an enlarged view of the plots for emission angles between 0° and 55°.

to participating laboratories, and oxide thicknesses were determined by XPS and nine other methods. While some of the larger systematic offsets found in this comparison (of up to 1 nm) could be reasonably attributed to surface contamination, the authors found that the XPS thickness measurements had a near-zero offset.

The XPS measurements of silicon oxide thickness were based on a generalization of Eq. (51) to account for the presence of interfacial oxides (Si_2O_3, SiO, and Si_2O) between the Si substrate and the SiO_2 film. Measurements were made of the Si 2p photoelectron intensities from the Si substrate and from SiO_2 and each intermediate oxide after subtraction of a Shirley inelastic background.[69,70] In an earlier work, Seah and Spencer[71] summarized the measured EALs for SiO_2 found from overlayer experiments, i.e., values of L_{TH}. The average values of the reported EALs were 2.85 ± 0.46 nm and 3.14 ± 0.31 nm for XPS experiments with Mg Kα and Al Kα x-ray sources, respectively, where the indicated uncertainties represent standard deviations. Seah and Spencer also used the Seah and Gilmore predictive equation (described in Sec. 3.1.1.5) to estimate the corresponding EALs from the calculated IMFPs of Tanuma *et al.*,[72] 2.964 nm and 3.448 nm, for XPS with Mg Kα and Al Kα x-ray sources, respectively. These EALs are close to the values reported by Powell and Jablonski,[73] between 2.905 nm and 3.036 nm and between 3.392 nm and 3.546 nm, for XPS with Mg Kα and Al Kα x-ray sources, respectively. Oxide thickness measurements made by XPS, and other methods were compared with the reference values from XPS measurements at the National Physical Laboratory (NPL).[69] These comparisons showed excellent linearity.

While the XPS results gave a near-zero intercept, the thicknesses from the other methods resulted in finite offsets of up to about 0.8 nm.[71] These offsets could reasonably be interpreted as being due to surface contamination or due to difficulties in defining interface positions in transmission electron microscopy (TEM) images.[69] The XPS thicknesses could, in effect, be recalibrated with respect to the thicknesses from the other methods by adjusting the EALs to 2.923 nm and 3.400 nm for XPS with Mg Kα and Al Kα x-ray sources, respectively. In a later reanalysis with an improved method for setting the chosen photoelectron emission angle for the NPL XPS measurements, the EALs were revised to 2.996 ± 0.016 nm and 3.448 ± 0.019 nm for XPS with Mg Kα and Al Kα x-ray sources, respectively.[74] These experimental EAL values are thus consistent with the corresponding calculated EALs of Powell and Jablonski.[73] We also point out that the experimental EALs are traceably calibrated for use with a specific procedure to provide accurate values of

SiO_2 film thicknesses. It is therefore possible that they might not be consistent with the calculated EALs that are defined differently. For example, the calculated EALs relate to peak intensities that include shake-up or intrinsic excitations, while these contributions are excluded in the protocol for EAL measurements through the use of the Shirley background.

We note here that Shinotsuka *et al.*[75] have made new IMFP calculations for SiO_2 and a group of 41 other inorganic compounds with an improved algorithm over that used previously.[72] The new IMFPs for SiO_2 are an average of 1.6% larger than the previous IMFPs for Si 2p photoelectrons excited by Mg Kα and Al Kα x-ray sources.

At first sight, it is gratifying that there is satisfactory consistency between the extremely careful EAL determinations for Si 2p photoelectrons excited in SiO_2 by Mg and Al Kα x-ray sources[74] and the corresponding calculated EALs.[71,73] Nevertheless, we need to point out that these experimental EALs are the values of the parameter L_{TH}^{ratio} from Eq. (54), while the calculated EALs are the values of the parameter L_{TH} from Eqs. (14) and (15). As discussed earlier, Powell *et al.*[56] reported SESSA simulations for thin films of $SiO_{1.6}N_{0.4}$ and $HfO_{1.9}N_{0.1}$ on Si. They determined values of L_{TH}^{ratio}andL_{TH} and found them to be generally similar although there were some variations in the L_{TH}^{ratio} values with the film thickness, as illustrated in Fig. 17. Similar results were found for thin films of SiO_2 on Si where the values of L_{TH}^{ratio} changed by about 7% for film thicknesses between 1.5 nm and 7.5 nm.[76]

In contrast, Kim and Seah[77] found experimentally from XPS with Mg Kα x rays that the previously derived value[74] of $L_{TH}^{ratio} = 2.996\,\text{nm}$ was independent of SiO_2 film thickness within the experimental uncertainty of ±0.016 nm. There is thus an inconsistency between the thickness dependence of the calculated L_{TH}^{ratio} values[76] for SiO_2 with the thickness independence of the experimentally determined values of L_{TH}^{ratio} for SiO_2.[77] This inconsistency is believed to arise from variation in the fraction of intrinsic or shakeup intensity accompanying Si 2p photoionization with SiO_2 thickness and/or from variation of inelastic-scattering probabilities in the vicinity of the Si/SiO_2 and SiO_2/vacuum interfaces, also as a function of SiO_2 thickness.[76] Although the procedures for determining the film thickness by XPS are empirically useful for SiO_2, further investigations are needed of shakeup and inelastic scattering in thin films. For SiO_2, it appears that any thickness dependence of the EAL in the experiments of Seah *et al.* is masked by the need to subtract a "short-range" background such as the Shirley background and by possible variations of shakeup fractions and inelastic-scattering probabilities with the film thickness.[76]

The procedures developed by Seah *et al.*[69] for the measurement of SiO_2 film thicknesses by XPS have been further extended by Kim *et al.*[78–80] This group proposed what they called a mutual calibration method for determining overlayer-film thicknesses by XPS based on comparison measurements with TEM. As noted previously, measurements of SiO_2 film thicknesses by XPS with Eq. (51) are not affected by the presence of surface contamination but can have large uncertainties due to the uncertainties in the measured or calculated EALs.[71] In contrast, similar measurements by TEM can be adversely affected by the presence of surface contamination or by difficulties in location of interface positions. Kim *et al.* showed that XPS can be used to correct the offset error in thickness measurements by transmission electron microscopy (TEM), while TEM can be used to refine the thickness scale of XPS thickness measurements.

In their first paper, Kim *et al.*[78] reported XPS and TEM thickness measurements of SiO_2 films on a Si(100) substrate with nominal thicknesses of 2 nm, 3 nm, 4 nm, 5 nm, and 6 nm. For the TEM measurements, the oxide films were covered with a Ge capping layer, and the SiO_2 film thicknesses were determined with respect to the distance between 50 Si(111) lattice planes in the TEM images. TEM thicknesses, t_{TEM}, were determined from an average of eight positions in the TEM images. XPS thicknesses, t_{XPS}, were obtained from experiments with Mg Kα x rays and with the procedures and data recommended by Seah *et al.*[69,70,74]

Figure 19(a) is a plot of the SiO_2 film thicknesses determined from TEM experiments vs those obtained by XPS.[78] The dashed line in Fig. 19(a) is the calibration relation between the oxide film thickness measured by TEM, t_{TEM}, and the corresponding thickness measured by XPS, t_{XPS},

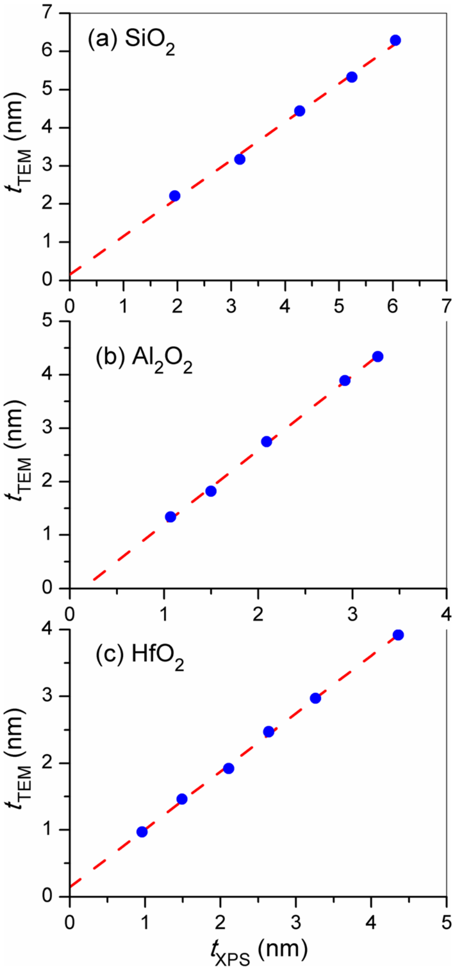

FIG. 19. Plot of measurements of (a) SiO_2 (b) Al_2O_3, and (c) HfO_2 film thicknesses by transmission electron microscopy, t_{TEM}, vs the corresponding film-thickness measurements by XPS, t_{XPS}, from the experiments of Kim *et al.*[78–80] The experimental values are shown as solid circles, while the dashed lines are the mutual calibration lines [Eq. (59)] described in the text.

$$t_{TEM} = mt_{XPS} + c. \tag{59}$$

A plot of t_{TEM} vs t_{XPS} ideally should be linear with the slope m equal to unity and the intercept c equal to zero. Kim *et al.* found from their experiments that $m = 0.999 \pm 0.038$ and $c = 0.154 \pm 0.165$ nm. Their value for the average EAL for Si 2p photoelectrons from the SiO_2 film and the Si substrate of $L_{TH}^{ratio} = 2.994$ nm ± 0.0114 nm (for XPS with Mg Kα x rays) is consistent with the earlier result of 2.996 nm ± 0.0116 nm recommended by Seah and Spencer.[74]

In their second paper, Kim *et al.*[79] used the same approach for determining the average EALs for thin films of Al_2O_3 deposited on a Si(100) substrate that had a thin SiO_2 surface layer. Prior to film deposition, the Si(100) substrate was amorphized by ion-beam sputtering to a depth of about 10 nm. For TEM measurements, the Al_2O_3 films were covered with a Ge capping layer. Kim *et al.* considered the use of the term F in Eq. (58) but decided not to include it in their evaluations since the difference in kinetic energies of Si 2p photoelectrons in Si and of Al 2p photoelectrons in Al_2O_3 was only about 24 eV; the corresponding difference in IMFPs is only about 1.6%.[75] The initial XPS measurements by Kim *et al.* with Eq. (58) indicated an EAL, L_{TH}^{ratio}, of 1.746 nm at the average kinetic energy of 1166 eV for these photoelectrons.

Figure 19(b) is a plot of the Al_2O_3 film thicknesses determined by TEM vs the corresponding thicknesses obtained by XPS. The dashed line shows the calibration line with $m = 1.390$ and $c = -0.188$ nm (but no uncertainties were reported for these values). Kim *et al.* multiplied their initial EAL by the value of m and reported that $L_{TH}^{ratio} = 2.4334$ nm (with no estimate of uncertainty).[79] This value is 15% larger than the value of $L_{TH} = 2.11$ nm expected from the calculated IMFP of 2.47 nm at the average Al 2p and Si 2p photoelectron energy[75] of 1166 eV[75] and the Jablonski–Powell predictive equation for L_{TH} [Eq. (20)]. We note here that the calculated IMFPs of Shinotsuka *et al.*[75] for Al_2O_3 agree generally within 10% with the IMFPs measured by elastic-peak electron spectroscopy for electron energies between 200 eV and 2000 eV.[81]

In their third paper, Kim *et al.*[80] reported the average EALs for Hf 4f and Si 2p photoelectrons from thin films of HfO_2 deposited on a 3 nm film of SiO_2 that had been deposited on a Si(100) substrate. TEM measurements were made after the films were covered with a Si capping layer. In the XPS experiments (again using Mg Kα x rays), the average kinetic energies of the Hf 4f and Si 2p photoelectrons were 1238 eV and 1152 eV, respectively. For simplicity, Kim *et al.* used Eq. (51) to determine HfO_2 film thicknesses from their XPS measurements. This procedure seems reasonable since the IMFPs calculated from the TPP-2M equation [Eqs. (93) and (94) in Sec. 4] for HfO_2 at the two photoelectron energies differ by less than 6%. The initial XPS measurements with Eq. (51) indicated an EAL, L_{TH}^{ratio}, of 2.386 nm at the average kinetic energy of 1195 eV for the Hf 4f and Si 2p photoelectrons.

Figure 19(c) is a plot of the HfO_2 film thicknesses determined by TEM vs the corresponding thicknesses obtained by XPS. The dashed line shows the calibration line with $m = 0.867$ and $c = 0.142$ nm (again, no uncertainties were reported for these values). Kim *et al.* multiplied their initial EAL by the value of m and reported that $L_{TH}^{ratio} = 2.069$ nm (with no estimate of uncertainty).[80] This value is 33% larger than the value of $L_{TH} = 1.55$ nm expected from the calculated IMFP of 1.92 nm at the average Hf 4f and Si 2p photoelectron energy of 1195 eV and the Jablonski–Powell predictive equation for L_{TH} [Eq. (20)].

We conclude this section by pointing out that the most accurate EAL measurements have been made by Seah *et al.*[69,74] and Kim *et al.*[78] for Si 2p photoelectrons from thin films of SiO_2 on Si using Eq. (51). Seah *et al.* reported values of L_{TH}^{ratio} of 2.996 ± 0.016 nm and 3.448 ± 0.019 nm for the average photoelectron energies of 1150 eV and 1383 eV from XPS experiments with Mg and Al Kα x-ray sources, respectively, while Kim *et al.* reported an L_{TH}^{ratio} value of 2.994 nm ± 0.0114 nm for XPS experiments with Mg Kα x rays. These EAL results were consistent with the corresponding L_{TH} values calculated by Powell and Jablonski.[73] Nevertheless, the subsequent measurements of L_{TH}^{ratio} for Al_2O_3 and HfO_2 by Kim *et al.*[79,80] were reported without any estimate of the experimental uncertainties. They are also larger than the corresponding calculated values of L_{TH} by 15% and 33%, respectively. Systematic differences between L_{TH}^{ratio} and L_{TH} of up to about 7%, depending on film thickness, have been reported by Powell *et al.*[56] from SESSA simulations for thin films of $HfO_{1.9}N_{0.1}$ on Si, as shown in Fig. 17. It is also possible that the procedures developed by Seah *et al.* for the measurement of Si 2p photoelectron peak intensities might not be satisfactory when used for Al_2O_3 and HfO_2.[76] We note here that useful information on the sample morphology in the surface region (i.e., within the XPS sampling depth) can be obtained from the QUASES software[66,82] as well as from the NIST SESSA database.[42,83]

3.1.1.5. Other predictive EAL formulas for L_{TH}.

We reported in Sec. 3.1.1.1 on our development of a predictive equation [Eq. (20)] for L_{TH}, the EAL needed to determine the thickness of an overlayer film on a planar substrate by XPS with unpolarized x rays. We now mention two additional predictive EAL equations for this application.

Seah and Gilmore[49] proposed a relation similar to Eq. (20) that was based on fits to earlier EAL calculations by Cumpson and Seah,[84]

$$R_{TH}^{SG} = L_{TH}/\lambda_{in} = 0.979\,[1 - \omega\,(0.955 - 0.0777\ln Z)]. \tag{60}$$

This equation has a weak dependence on the atomic number, Z, and becomes stronger with increasing ω.[46] As described in Sec. 3.1.1.1, Jablonski and Powell compared their calculated EALs from the transport approximation and Monte Carlo approaches for Si, Cu, Ag, and Au photoelectrons excited by Mg Kα, Al Kα, Zr Lα, and Ti Kα x rays and found satisfactory agreement.[46] There was similar agreement between EALs calculated from MC simulations with photoionization cross sections from the dipole approximation and the non-dipole approximation. These EALs were used to determine the values of R_{TH}^{MC} that are plotted in Fig. 20 as a function of ω for photoelectron energies between 321 eV and 4426 keV. We also show the values of R_{TH}^{SG} from Eq. (60) for Si, Cu, Ag, and Au. The rms difference of the R_{TH}^{MC} values from the R_{TH}^{SG} values was 1.71%, a result similar to that found with Eq. (20) (1.44%).

Seah[50] later proposed an analytical expression for L_{TH} that was designated as the S3 equation. This equation was designed to be applicable to complex and non-stoichiometric materials where data for the parameters in the TPP-2M equation were likely to be not available. Seah based his S3 equation, in part, on his predictive IMFP equation [Eq. (95) in Sec. 4] and, in part, from averaging over the elastic-scattering effects as a function of Z,

$$L_{TH}^{S3} = \frac{(5.8 + 0.0041Z^{1.7} + 0.088E^{0.93})a^{1.82}}{Z^{0.38}\,(1 - W)} \quad (\text{in nm}), \tag{61a}$$

where Z is the atomic number (or the average atomic number for a compound). The parameter a is the average atomic spacing given by

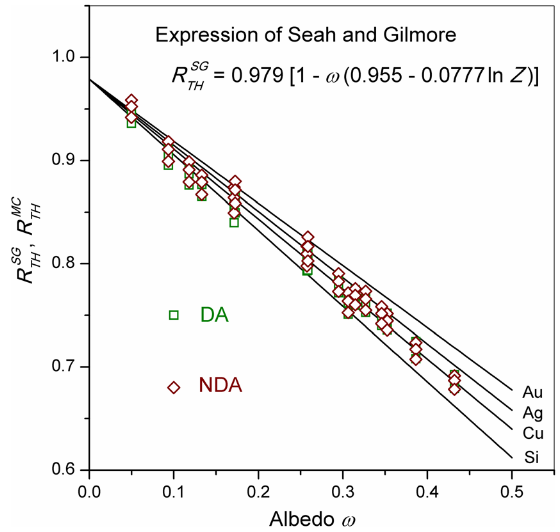

FIG. 20. Plots of the ratios, R^{SG}_{TH}, calculated from the Seah and Gilmore[49] expression [Eq. (60)] (solid lines for Si, Cu, Ag, and Au) as a function of the single-scattering albedo, ω, with the corresponding ratios R^{MC}_{TH} calculated from MC simulations with photoionization cross sections from the dipole approximation, shown as squares, and the non-dipole approximation, shown as diamonds.[46]

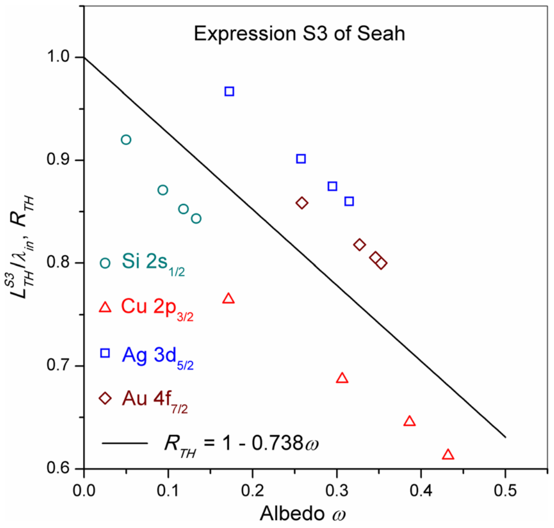

FIG. 21. Plots of the ratios L^{S3}_{TH}/λ_{in} (symbols) for EALs calculated from the Seah S3 equation [Eq. (61)] for Si 2s$_{1/2}$, Cu 2p$_{3/2}$, Ag 3d$_{5/2}$, and Au 4f$_{7/2}$ photoelectrons excited by Mg Kα, Al Kα, Zr Lα, and Ti Kα x rays to the corresponding IMFPs of Tanuma *et al.*[48] as a function of the single-scattering albedo, ω. The solid line is a plot of Eq. (20).[46]

$$a^3 = \frac{10^{21} M}{\rho N_A (g+h)} \quad (\mathrm{nm}^3), \tag{61b}$$

where M is the atomic or molecular weight, N_A is the Avogadro constant, and g and h are the stoichiometry coefficients if the material of interest is a binary compound G_gH_h. For an elemental solid, $g = 1$ and $h = 0$. The average atomic number for a binary compound is

$$Z = \frac{gZ_g + hZ_h}{(g+h)}, \tag{61c}$$

where Z_g and Z_h are the atomic numbers of the constituent elements. The term W in Eq. (61a) is given by $W = 0.06H$ or $W = 0.02E_g$, where H is the heat of formation of a compound (in eV per atom) and E_g is the bandgap energy (in eV).[50] Sources of data for E_g and H are described in Sec. 4.

Figure 21 shows a plot of the ratios, L^{S3}_{TH}/λ_{in}, for EALs calculated from Eq. (61) for the photoelectron lines and x-ray sources considered by Jablonski and Powell[46] to the corresponding IMFPs of Tanuma *et al.*[48] as a function of ω. These ratios are compared with R_{TH} values from Eq. (20). We see a pronounced scatter of the L^{S3}_{TH}/λ_{in} values about the predicted values of R_{TH} from Eq. (20). This scatter is believed to be associated with the residuals from the use of the simple dependence of L^{S3}_{TH} on Z in Eq. (61) to describe the more complicated dependence of L_{TH}/λ_{in} on Z shown in Fig. 3 of Ref. 50. The rms deviation of the L^{S3}_{TH}/λ_{in} values in Fig. 21 from the R_{TH} values from Eq. (20) was 9.29%.[46] Although Eq. (61) is easy to use, particularly as it does not include any dependence on ω, it is not as accurate as either Eq. (20) or (60). That is, the relatively simple dependences on Z in Eq. (61) does not fully represent the complex dependences of ω on Z found for some materials, as shown in Figs. S1 and S2 of the supplementary material.

Early EAL measurements were often described by simple empirical expressions such as $L_{TH} = kE^p$, where the electron energy was expressed in electron volts and k and p were material-specific parameters. In 1980, Wagner *et al.*[85] fitted EAL measurements for a range of energies in a single laboratory. They found that the exponent p was material dependent (as was k) and ranged from 0.54 to 0.81. Powell[86] analyzed later EAL measurements in 1985 and found similar results. These results are now believed to be associated with different effects of island growth in the deposited overlayer films.[83] That is, exponential decreases of substrate photoelectron intensities or exponential increases of overlayer-film intensities could occur for a non-uniform overlayer film, and the resulting EAL values would not necessarily be reliable for other XPS applications. We also note that valid film-thickness measurements using EALs similarly depend on whether the film of interest is known or can be expected to be uniform.

3.1.2. XPS with linearly polarized x rays

XPS measurements are generally performed using spectrometers equipped with laboratory sources of unpolarized x rays. Three sources of characteristic radiation are commonly available: Mg Kα ($h\nu$ = 1253.6 eV), unmonochromated Al Kα ($h\nu$ = 1486.6 eV), and monochromated Al Kα ($h\nu$ = 1486.7 eV).[87] In recent years, interest in so-called hard x-ray photoelectron spectroscopy (HAXPES) has grown with x-ray energies up to 15 keV.[88–90] Some laboratory XPS instruments are equipped with x-ray sources providing characteristic radiation with energies up to about 10 keV: Zr Lα$_1$ ($h\nu$ = 2043.1 eV), Ag Lα$_1$ ($h\nu$ = 2984.6 eV), Ti Kα$_1$ ($h\nu$ = 4510.4 eV), Cr Kα$_1$ ($h\nu$ = 5413.9 eV), Cu Kα$_1$ ($h\nu$ = 8048.1 eV), and Ga Kα$_1$ ($h\nu$ = 9251.9 eV).[91] In addition, XPS experiments are performed with synchrotron radiation where the x rays are linearly polarized. HAXPES experiments have useful advantages compared to conventional XPS in that the measurements are less sensitive to surface contamination on the sample and that thicker films or deeper interfaces can be characterized (due to the larger information depths). Variation of the incident x-ray energy is also useful for varying the surface/bulk sensitivity of the experiments and for ensuring that Auger-electron features do not overlap photoelectron peaks.

There are two main complications in the calculation of photoelectron intensities in HAXPES compared to conventional XPS with Al Kα or Mg Kα x ray sources. First, non-dipole contributions to the photoionization cross section need to be included for x-ray energies above about 2 keV.[46] Second, the position of the polarization vector needs to be specified for XPS with linearly polarized x rays from synchrotron-radiation sources.[92,93]

The following experimental conditions should be satisfied in HAXPES experiments with linearly polarized x rays to facilitate comparisons with available theory:[92,93]

(a) The polarization vector should be located in the plane perpendicular to the sample surface.
(b) The analyzer axis and, consequently, the photoelectron emission angle should be perpendicular to the direction of the x-ray beam.
(c) The x-ray incidence angle should be near glancing to the sample surface.

Figure 22 shows a schematic outline of a typical HAXPES experiment.

Jablonski[92] has calculated emission depth distribution functions and EALs from MC simulations for 13 photoelectron lines (Si: $2s_{1/2}$ and $2p_{3/2}$; Cu: $2s_{1/2}$, $2p_{3/2}$, and $3p_{3/2}$; Ag: $3s_{1/2}$, $3p_{3/2}$, $3d_{5/2}$, and $4s_{1/2}$; and Au: $4s_{1/2}$, $4p_{3/2}$, $4d_{5/2}$, and $4f_{7/2}$) from the corresponding elemental solids for the configuration of Fig. 22. The angle of incidence of the linearly polarized x rays was 5° with respect to the surface plane, and the photoelectron emission angle was varied from 5° to 80° in steps of 5°. Simulations were performed with various x-ray energies such that there were six photoelectron kinetic energies: 100 eV, 500 eV, 1 keV, 3 keV, 5 keV, and 10 keV. The EALs were determined from changes of substrate photoelectron intensities by an overlayer of the same material with varying thicknesses. As for the EALs with unpolarized x rays discussed in Sec. 3.1.1,[46] the EALs for XPS with linearly polarized x rays were weakly dependent on the photoelectron emission angle for $5° \le \alpha \le 50°$. The average practical EALs were calculated for this range of emission angles.

Figure 23 is a plot of the ratio $R_{TH} = L_{TH}/\lambda_{in}$ (symbols) on the single-scattering albedo, ω, where the L_{TH} values are the results from the MC simulations and the IMFPs were taken from the calculations of Tanuma *et al.*[48] The solid line in Fig. 23 is a linear fit to the plotted points,

$$R_{TH} = 1 - 0.836\ \omega. \tag{62}$$

Equation (62) can be considered as an EAL predictive formula for linearly polarized x rays and the experimental configuration shown in Fig. 22. The average rms percentage deviations of the points in Fig. 23 from the solid line was 1.85%. The dashed line in Fig. 23 shows a plot of Eq. (20), the EAL predictive equation for XPS with unpolarized x rays.

Figure 24 shows EALs measured for Au with linearly polarized x rays by Rubio-Zuazo and Castro (RZC).[94] They deposited thin films of Au on a Cu substrate and measured the intensities of various Cu and Au photoelectron lines excited by synchrotron x rays. The nine EALs in Fig. 24 for energies between 1029 eV and 9694 eV were obtained from experiments in which the attenuation of Cu photoelectron lines was measured as a function of Au film thickness or in

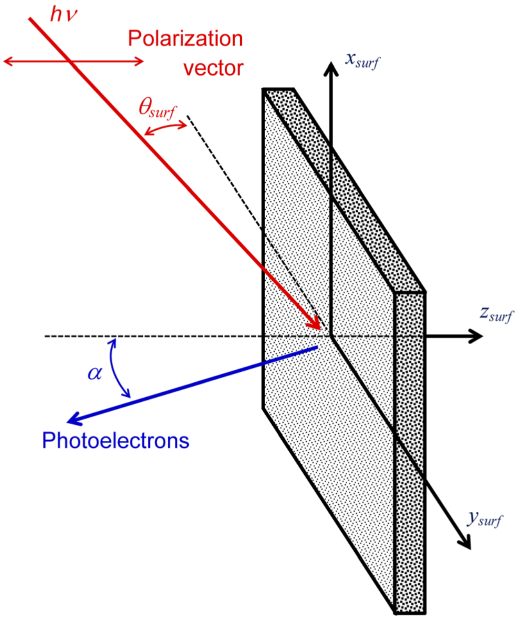

FIG. 22. Schematic outline of a typical XPS configuration used for HAXPES experiments (after Ref. 25). The beam of polarized x rays, the surface normal, and the direction toward the analyzer are located in the horizontal plane.

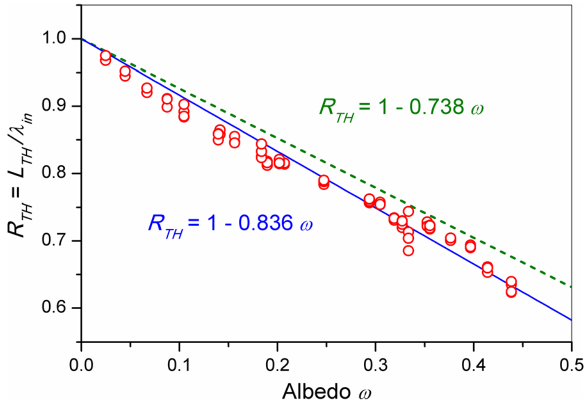

FIG. 23. Dependence of the ratio $R_{TH} = L_{TH}/\lambda_{in}$ on the single-scattering albedo, ω, for HAXPES with linearly polarized x rays.[92] The EALs, L_{TH}, were obtained from MC simulations for 13 photoelectron lines (Si: $2s_{1/2}$ and $2p_{3/2}$; Cu: $2s_{1/2}$, $2p_{3/2}$, and $3p_{3/2}$; Ag: $3s_{1/2}$, $3p_{3/2}$, $3d_{5/2}$, and $4s_{1/2}$; and Au: $4s_{1/2}$, $4p_{3/2}$, $4d_{5/2}$, and $4f_{7/2}$) from the corresponding elemental solids for the configuration of Fig. 22. The x-ray energies were varied such that there were six photoelectron kinetic energies: 100 eV, 500 eV, 1 keV, 3 keV, 5 keV, and 10 keV. The IMFPs were taken from the calculations of Tanuma *et al.*[48] The symbols show the R_{TH} values from the simulations. The solid line shows a linear fit to these results [Eq. (62)], and the dashed line is a plot of Eq. (20), the corresponding result for unpolarized x rays.

which the increase in Au photoelectron lines was similarly measured with exponential decreases or increases of the photoelectron intensities with the Au film thickness. The RZC experiments are noteworthy in that the EALs were determined over a wide energy range and that x-ray reflectivity (XRR) measurements on their sample could be performed during deposition of the Au films and without moving the Cu substrate from the XPS analysis position. Analysis of the XRR data yielded the film thickness with an accuracy better than 1% of the film thickness and the rms roughness with an accuracy better than 10% of the roughness value.[94]

The dotted line in Fig. 24 shows IMFPs for Au from the calculations of Tanuma *et al.*,[48] and the solid line shows the predicted EALs from Eq. (62). The five EALs in Fig. 24 for energies between 8752 eV and 9694 eV are less than the corresponding IMFPs, as expected, and are also close to the values expected from Eq. (62). However, the four EALs at lower energies are larger than the predicted values, and two of the EAL values, for energies of 1029 eV and 2921 eV, are larger than the calculated IMFPs. While it is possible that the calculated IMFPs for Au could be incorrect, these values are consistent with other IMFP calculations and measurements.[48]

Powell and Jablonski have recently reinterpreted the RZC experiments.[83] RZC derived their EALs with the assumption that their Au films were of uniform thickness (i.e., layer-by-layer film growth). We considered two other forms of film growth: island formation (Volmer–Weber film growth) and island growth on a continuous monatomic Au wetting layer (Stranski–Krastanov film growth). Simulations were made with the NIST SESSA database[42] to find relative Au island areas for each Au film thickness that matched the exponential intensity changes reported by RZC. Figure 25 shows a comparison of relative Au island areas as a function of Au film thickness for Volmer–Weber film growth (no wetting layer) and Stranski–Krastanov film growth (Au wetting layer). These comparisons were made for photoelectron energies of (a) 1029 eV and (b) 6583 eV. We show uncertainties in some points based on the results of SESSA simulations in which relative Au island areas were determined for ±5% variations in the calculated IMFPs of Tanuma *et al.* We see consistent results for growth in the relative Au island areas for the two photoelectron energies from the simulations with an Au wetting layer. No such consistency is found for the simulations without a wetting layer. An important conclusion of this work is that exponential growth of overlayer intensity or decay of substrate intensity with increasing overlayer-film thickness does not necessarily mean that the film is uniform. The conditions listed in Sec. 2 for reliable measurements of L_{TH} also apply to reliable measurements of overlayer-film thicknesses.

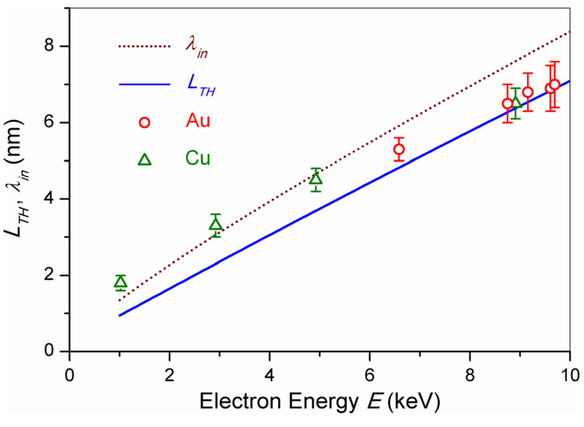

FIG. 24. Dependence of the IMFP and the EAL for Au on photoelectron kinetic energy.[83] Solid line: predictive EAL formula for polarized x rays [Eq. (62)]; dashed line: predictive EAL formula for unpolarized x rays [Eq. (20)]; dotted line: IMFPs from Tanuma *et al.*[48] Symbols indicate experimentally determined EALs.[91] Circles: photoelectrons emitted from the Au overlayer; triangles: photoelectrons emitted from the Cu substrate and attenuated by the Au overlayer.

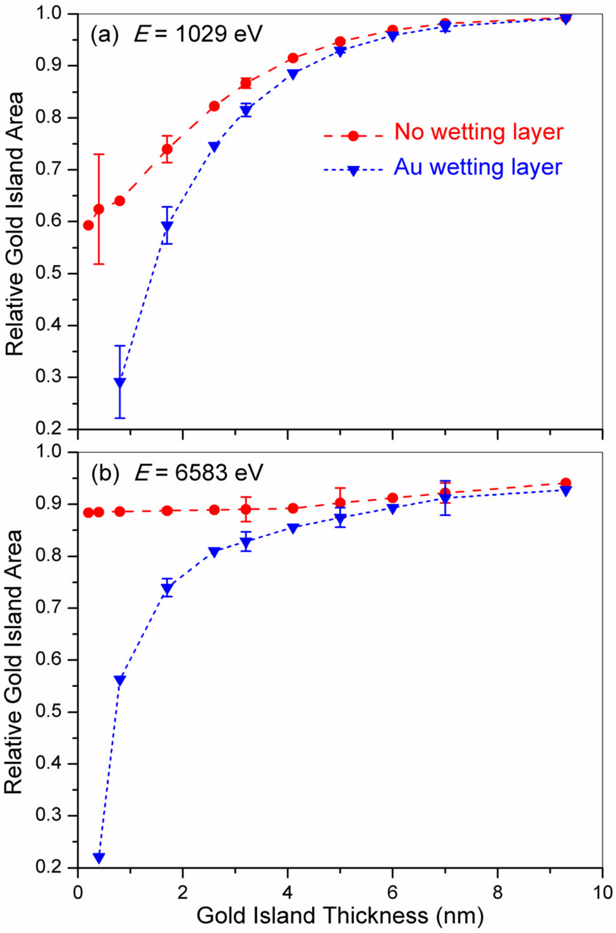

FIG. 25. Comparisons of relative gold island areas as a function of gold island thickness for Volmer–Weber film growth (no wetting layer) and for Stranski–Krastanov film growth (Au wetting layer) for photoelectron energies, E, of (a) 1029 eV and (b) 6583 eV.[83] Uncertainties are indicated for some points based on the assumed uncertainties of ±5% in the calculated IMFPs of Tanuma *et al.*[48] Lines are shown between points to guide the eye.

3.2. EALs for the determination of surface composition

A frequent XPS application is the determination of elemental concentrations in the surface region of a sample. The common approach for such measurements implicitly involves use of the straight-line approximation (and the assumptions listed in Sec. 2 that may be satisfactory for some samples and XPS configurations). It is also assumed that the sample is homogeneous over the sampling depth or information depth for the sample of interest and XPS instrument configuration. The information depth for a particular experiment can be obtained from Eq. (A12) in the Appendix.

However, the accuracy of the results can be improved if account is taken of elastic-scattering effects on the photoelectron trajectories. According to the ISO definition of the EAL,[1] given in the Introduction, Eq. (12) would be expected to provide a more accurate value of the signal intensity if the IMFP was replaced by an appropriate EAL. We denote this EAL, L_{QA}, as the EAL for the determination of surface composition and define it by rewriting Eq. (12),

$$I_x = S\Delta\Omega F_x\left(\frac{d\sigma_x}{d\Omega}\right)NL_{QA}. \tag{63}$$

From Eqs. (12) and (63), we then have

$$L_{QA} = \lambda_{in}\frac{I_x}{I_x^{SLA}}. \tag{64}$$

The value of L_{QA} can be calculated from the EMDDF. We first normalize the EMDDF from the SLA model as follows:

$$\phi^{SLA}(z,\alpha) = \frac{d\sigma_x/d\Omega}{\sigma_x}\exp\left(-\frac{z}{\lambda_{in}\cos\alpha}\right). \tag{65}$$

Consequently, we may express the XPS signal intensity from the SLA model by this EMDDF,

$$I_x^{SLA} = S\Delta\Omega N\frac{\sigma_x}{\cos\alpha}\int_0^\infty \phi^{SLA}(z,\alpha)dz. \tag{66}$$

The corresponding signal intensity from a model in which elastic-scattering effects are accounted for can be obtained from the EMDDF for this model,

$$I_x = S\Delta\Omega\; N\frac{\sigma_x}{\cos\alpha}\int_0^\infty \phi(z,\alpha)dz. \tag{67}$$

Thus, Eq. (64) may be rewritten as[54]

$$L_{QA} = \lambda_{in}\frac{\int_0^\infty \phi(z,\alpha)dz}{\int_0^\infty \phi^{SLA}(z,\alpha)dz}. \tag{68}$$

We note that the EAL for the determination of surface composition by AES is given by the same expression as for XPS.[54]

In the early literature on elastic-scattering effects in quantitative analysis by XPS,[95–97] it was postulated that the SLA formalism could be corrected by replacing the photoemission cross section,

$$\frac{d\sigma_x}{d\Omega} = \sigma_x W(\psi,\beta) = \sigma_x\frac{1}{4\pi}\left[1-\frac{\beta}{4}3\cos^2\psi - 1\right], \tag{69}$$

with the cross section modified by two correction factors, Q_x and β_{eff},

$$\left(\frac{d\sigma_x}{d\Omega}\right)_{mod} = \sigma_x Q_x W\left(\psi,\beta_{eff}\right) = \sigma_x\frac{Q_x}{4\pi}\left[1-\frac{\beta_{eff}}{4}3\cos^2\psi - 1\right]. \tag{70}$$

Numerous analytical expressions for these two parameters have been published based on the results of MC calculations[49,97–99] or from analytical transport theory.[54,100,101]

Among the different analytical expressions for the correction parameters, Q_x and β_{eff}, the most universal and accurate seem to be the formulas proposed by Seah and Gilmore[49] and by Jablonski and Powell,[98] which were based on a large number of MC calculations. The following equations were proposed by Seah and Gilmore:[49]

$$Q_x = Q_x(0)\left(0.863 + 0.308\cos\alpha - 0.171\cos^2\alpha\right), \tag{71}$$

where $Q_x(0)$ is the value of Q_x at normal emission, i.e., at $\alpha = 0°$. Seah and Gilmore[49] recommended the following equations for the parameter $Q_x(0)$:

$$Q_x(0) = (1-\omega)^{1/2}\left[0.091 + \frac{2.684}{1+1.908(1-\omega)^{1/2}}\right] \tag{72}$$

for $\omega \geq 0.245$ or

$$Q_x(0) = (1-\omega)^{1/2}(1+0.412\omega) \tag{73}$$

for $\omega < 0.245$. A similar expression was derived for the modified asymmetry parameter, β_{eff},

$$\beta_{eff} = \beta_{eff}(0)\left(0.0868\cos^2\alpha - 0.208\cos\alpha + 1.121\right), \tag{74}$$

where $\beta_{eff}(0)$ is the value of β_{eff} at $\alpha = 0°$,

$$\beta_{eff}(0) = 0.876\beta[1-\omega(0.955 - 0.0777\ln Z)], \tag{75}$$

and Z is the atomic number.

Jablonski and Powell[98] derived the following equations for Q_x and β_{eff}:

$$Q_x = \frac{1+h_Q\cos\alpha}{(1-\omega)^{-1/2}+h_Q\cos\alpha} - \frac{g_Q\omega}{\cos\alpha}, \tag{76}$$

$$\beta_{eff} = \beta\left[\frac{(1-\omega)^{-1/2}+(1-\omega)h_\beta\cos\alpha}{1+h_\beta\cos\alpha} - g_\beta\omega^{1/2}(1-\omega)^2\right], \tag{77}$$

where $h_Q = 2.570$, $g_Q = 0.010\,97$, $h_\beta = 0.5075$, and $g_\beta = 0.2546$. These equations were derived from the results of MC simulations for 584 photoelectron lines in 39 elemental solids that could be excited by Mg Kα and Al Kα x rays in 315 different XPS configurations. Equations (76) and (77) seem to be preferable in practical applications over Eqs. (71)–(75) proposed by Seah and Gilmore.[49] The theoretical model implemented in the latter analysis was less advanced than the model of Jablonski and Powell.[98] Furthermore, $\beta_{eff}(0)$ from Eq. (75) does not reach β for albedo values, ω, approaching zero. Thus, the formalism of Seah and Gilmore is not recommended for materials in which the elastic-scattering effects are weak.

One can prove that the EAL approach for correcting the SLA formalism for elastic-scattering effects is equivalent to the correction procedure described above. Introducing Eqs. (12) and (63) and following the notation used in Eqs. (69) and (70), we obtain[6,54,102,103]

$$L_{QA} = \lambda_{in}\frac{d\sigma_x/d\Omega}{(d\sigma_x/d\Omega)_{mod}} = \lambda_{in}Q_x\frac{W(\psi,\beta_{eff})}{W(\psi,\beta)}. \tag{78}$$

Jablonski and Powell[54] derived a universal formula for the EAL, L_{QA}, from the transport approximation described in Sec. 3.1.1.1,

$$L_{QA} = \lambda_{in}(1-\omega)\left[1 - \frac{1-(1-\omega)^{-1/2}H(\mu,\omega)}{1-\left(\frac{\beta}{4}\right)(3\cos^2\psi - 1)}\right], \tag{79}$$

where $H(\mu, \omega)$ is the Chandrasekhar function[38,39] that depends on the variables $\mu = \cos\alpha$ and ω. In numerous applications, it is justified to use the following approximate expression for the Chandrasekhar function:[39,100,101]

$$H(\mu,\omega) = \frac{1+1.9078\mu}{1+1.9078\mu(1-\omega)^{1/2}}. \tag{80}$$

Its accuracy is typically better than 2.3%.[39]

For AES, we assume that the asymmetry parameter, β, approaches zero, and then, the resulting EAL no longer depends on the angle ψ so that

$$L_{QA} = \lambda_{in}(1-\omega) = \lambda_{in}Q_{QA}^{AES}. \tag{81}$$

The notation $Q_{QA}^{AES} = Q_A$ is frequently encountered in the literature.[6,7,101,102]

Jablonski and Powell[54] reported calculations of L_{QA} for the selected photoelectron lines of Si ($2s_{1/2}$, $2p_{3/2}$), Cu ($2s_{1/2}$, $2p_{3/2}$, $3p_{3/2}$), Ag ($3s_{1/2}$, $3p_{3/2}$, $3d_{5/2}$, $4s_{1/2}$), and Au ($4s_{1/2}$, $4p_{3/2}$, $4d_{5/2}$, $4f_{7/2}$) excited by Mg Kα and Al Kα x rays for photoelectron emission angles between 0° and 85°. It was found that the values of L_{QA}/λ_{in} calculated for the magic-angle geometry varied weakly with the photoelectron emission angle in the range $0° \le \alpha \le 50°$, similar to the case of L_{TH} discussed in Sec. 3.1.1. It was thus again useful to calculate the average values of L_{QA}, $\langle L_{QA}\rangle$, for this range and then to determine

$$R_{QA} = \langle L_{QA}\rangle/\lambda_{in}. \tag{82}$$

The symbols in Fig. 26 show a plot of R_{QA} values as a function of the single-scattering albedo, ω. We see that the data points are located along a curve that deviates slightly from linearity. The data points were therefore fitted with a second-order polynomial,

$$R_{QA} = 1 - A_{QA}\omega - B_{QA}\omega^2, \tag{83}$$

with $A_{QA} = 0.147$ and $B_{QA} = 0.164$, as indicated in Eq. (31). This fit is shown as the solid line in Fig. 26. Since the rms deviation of the R_{QA} values from the curve was 0.085%, Eq. (81) can be used as a predictive formula for determining the values of L_{QA} for other materials.

Equation (83) is valid for XPS configurations close to the magic-angle configuration, i.e., for ψ between 50° and 60°. For other configurations, L_{QA} should be calculated from Eq. (79). Although Eq. (83) was derived from calculations for XPS with Mg Kα and Al Kα x rays, similar calculations for larger x-ray energies should take non-dipolar effects into account.[46,47,88,99,104] Nevertheless, the addition of non-dipole contributions to the photoionization cross sections had minor effects on the calculated values of L_{TH} for x-ray energies up to 5 keV so that it is possible that Eqs. (79) and (83) might also be useful for similar x-ray energies.[46,54] We note that Eq. (83) can be used to provide L_{QA} values for quantitative AES applications and for any AES configuration.[54]

The dotted-dashed line in Fig. 26 shows a plot of R_{TH} from Eq. (20). We see that there is a clear difference between values of R_{QA} and R_{TH} for a given value of ω. EALs for one quantitative application should obviously not be used for another unless this use has been justified, as discussed further in Sec. 3.4.

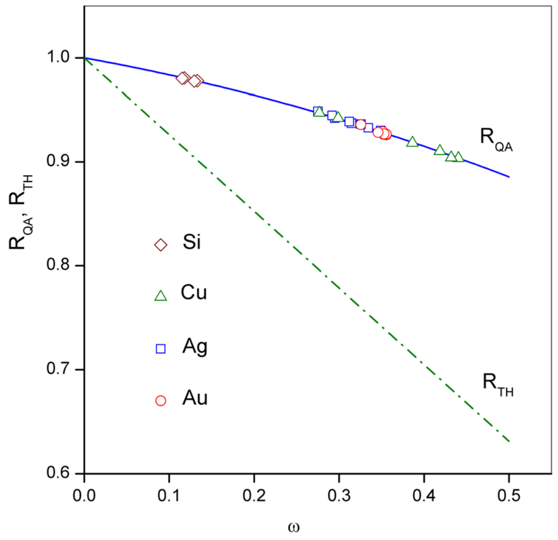

FIG. 26. Comparison of predictive formulas for EALs for quantitative analysis by AES and XPS and for overlayer-thickness determination.[54] Symbols: ratios R_{QA} of the average EALs for quantitative analysis by AES and XPS to the IMFPs from Eq. (82) as a function of the single-scattering albedo, ω; solid line: fit of Eq. (83) to the R_{QA} values; dotted-dashed line: predictive formula for EAL for measurements of overlayer thickness according to Eq. (20).

Suzuki *et al.*[105] reported EALs for liquid water from XPS experiments with synchrotron radiation. They measured the relative intensities of O 1s photoelectrons from liquid water in a microjet and from water vapor surrounding the microjet for photoelectron energies between 10 eV and 600 eV. They considered relevant geometrical factors, different photoelectron angular distributions for liquid and vapor, different photoionization cross sections near threshold, and variations of x-ray polarization with x-ray energy to derive EAL values. In effect, they utilized Eq. (63) for the O 1s signal intensity from the water microjet and a similar equation for the signal from the water vapor.

Suzuki *et al.* reported two sets of EAL values in Fig. 4 of their paper, and these are plotted in Fig. 27. The set of smaller values, designated EAL1 here, was based on the assumption of strong elastic-scattering effects in liquid water that would lead to an isotropic angular distribution of the O 1s photoelectrons in the liquid. These values are included in the supplementary material of the work of Suzuki *et al.* The other set of EAL values, designated EAL2 here, was based on the assumption of negligible elastic-scattering effects and the analysis of Winter and Faubel[106] for a geometrical correction factor. The latter factor ($\pi/2$) accounts for different MEDs of the photoemitted electrons in the limits of strong and negligible elastic scattering.[106] The EAL2 values would thus correspond to IMFPs for the O 1s photoelectrons in the limit of negligible elastic scattering and, as expected, would be larger than the first set of values. Suzuki *et al.* pointed out that the actual EALs (i.e., their values of L_{QA}) for liquid water should be close to the EAL1 values at low electron energies

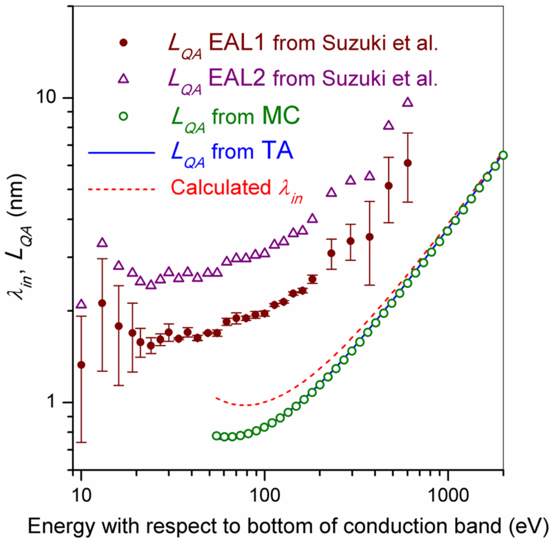

FIG. 27. Plot of measured EALs, L_{QA}, for water vs electron energy reported by Suzuki *et al.*[105] (solid circles). The EALs calculated from MC simulations [open circles, Eqs. (76)–(78)], the EALs from the transport approximation [solid line, Eq. (79)], and the IMFPs for water (dashed line) from Shinotsuka *et al.*[75,107]

where elastic-scattering effects are strong and close to the EAL2 values or IMFPs at high electron energies where the elastic-scattering effects are weak. Suzuki *et al.* showed a thick green line in their Fig. 4 as a plausible EAL curve, which is close to the EAL1 values at low energies and close to the EAL2 values at high energies.

We show the statistical uncertainties of the Suzuki *et al.* EAL1 results in Fig. 27 that were associated with replicate measurements on different days. There could be additional uncertainties in the reported EALs. For example, Suzuki *et al.* noted that an uncertainty of 5 K in the vapor temperature could lead to an uncertainty in the saturated vapor density of up to 38% that would directly affect the derived EAL values. Another possible source of uncertainty is that Suzuki *et al.* measured the intensities of the main O 1s peaks from liquid water and water vapor and did not consider possible differences in shakeup fractions for the two phases or possible variations in the shakeup fractions as a function of photoelectron energy.

Figure 27 also includes plots of the calculated values of L_{QA} values for liquid water. These calculations were made for the XPS configuration of Suzuki *et al.* and were based on MC simulations using Eqs. (76)–(78) (open circles) and with Eq. (79) based on the transport approximation (solid line). We see perfect agreement of the L_{QA} values from these two sources. However, we cannot make a direct comparison between the calculated L_{QA} values and the EAL1 and EAL2 values of Suzuki *et al.* for two reasons. First, Suzuki *et al.* used linearly polarized x rays, while the L_{QA} calculations were made for unpolarized x rays. Second, the experiments were performed with a cylindrical sample, but the calculations were made for a planar sample. Nevertheless, the solid line in Fig. 27 shows calculations of L_{QA} using Eq. (79) for the Suzuki *et al.* XPS configuration. Additionally, we plot the IMFPs for water from the calculations of Shinotsuka *et al.*[75,107] We see that the L_{QA} values from Eq. (79) are less than the corresponding IMFPs as expected. However, the EAL1 values of Suzuki *et al.* are more than double the IMFPs for energies between 50 eV and 600 eV, while their three EAL2 values at energies between 373 eV and 601 eV are more than three times the corresponding calculated IMFPs. While it is possible that the IMFPs of Shinotsuka *et al.* for water are incorrect, the same algorithm has been used to calculate IMFPs for 42 inorganic compounds, and generally, satisfactory agreement has been found with other IMFP calculations and measurements.[75] Finally, we note that elastic-scattering effects are stronger for the Suzuki *et al.* configuration than for the magic-angle XPS configuration, that is, there is a larger difference between the calculated values of L_{QA} and λ_{in} at low energies than would be expected from the plot of R_{QA} in Fig. 26.

It is, of course, difficult to make IMFP or EAL measurements with liquid water, and it is perhaps not surprising that substantial differences exist among the experimental values.[107] There are also large differences among the calculated IMFPs.[107,108] It is expected that additional IMFP and EAL measurements and calculations for water can be made to establish consistent datasets since such data are of considerable importance for radiation dosimetry and for investigations of surface reactions on atmospheric aerosols.

To assist future investigations, we show plots of the IMFPs of liquid water calculated by Shinotsuka *et al.*[75] as a function of electron energy in Fig. 28 together with the transport mean free paths calculated from transport cross sections (appropriately weighted for H and O) from the ELSEPA database.[64] The inset in Fig. 28 is a plot of ω from Eq. (7) as a function of electron energy. We find that ω = 0.076 at an energy of 992 eV so that elastic-scattering effects are weak and EALs such as L_{TH} and L_{QA} should be close to the IMFP. At an energy of 55 eV, however, ω = 0.53, elastic-scattering effects are strong, and EALs such as L_{QA} should be appreciably smaller than the IMFP, as shown in Fig. 27.

We also make comparisons of several recent IMFP calculations[75,107–109] for liquid water in Fig. 29 for electron energies

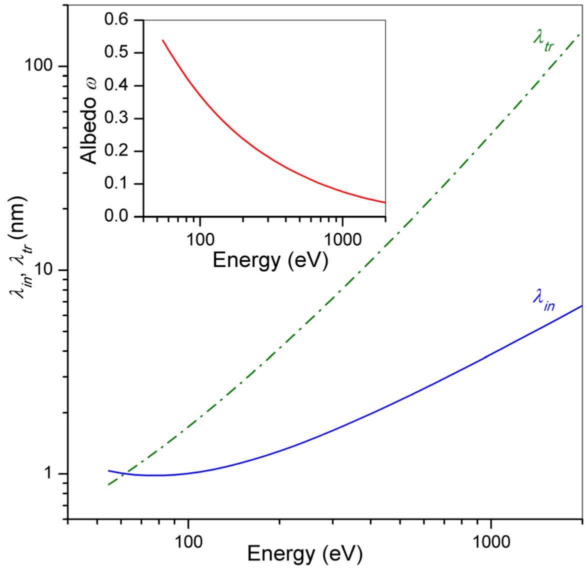

FIG. 28. The solid line shows IMFPs for water from Shinotsuka *et al.*[75,107] The dotted-dashed line shows transport mean free paths for water calculated from Eqs. (8) and (9) using properly weighted transport cross sections from the ELSEPA database.[64] The inset shows a plot of the single-scattering albedo, ω, for water from Eq. (7) as a function of electron energy.

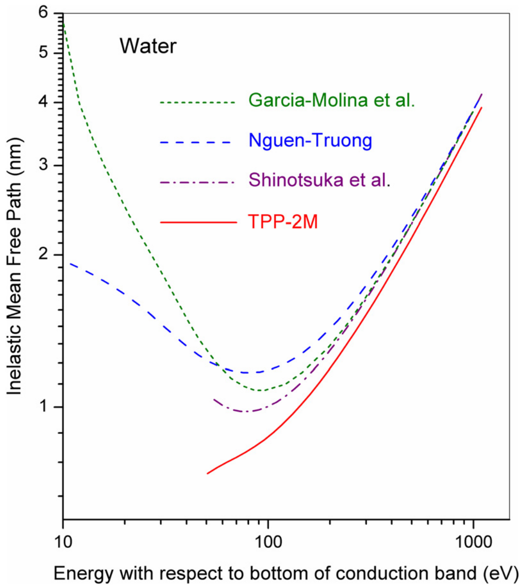

FIG. 29. Comparisons of the calculated IMFPs for water by Shinotsuka *et al.*,[75,107] Nguyen-Truong,[110] and Garcia-Molina *et al.*[109] with IMFPs from the TPP-2M predictive equations [Eqs. (93) and (94)].

between 10 eV and 1 keV. These IMFPs were calculated with different algorithms and show reasonable consistency at energies above about 200 eV. We note that the IMFPs at energies between 373 eV and 602 eV are between 1.9 nm and 2.7 nm, and these values are appreciably smaller than the EAL2 values of Suzuki *et al.* (between 5.5 nm and 9.6 nm) in Fig. 27 that were identified by the authors as being close to IMFP values. At energies between 50 eV and 200 eV, there are larger differences among the calculated IMFPs in Fig. 29 than at higher energies.

We also show IMFPs from the TPP-2M predictive equation [Eqs. (93) and (94) in Sec. 4] in Fig. 29 to indicate that the predicted IMFPs between 50 eV and 200 eV are smaller than the calculated values. Nevertheless, the TPP-2M IMFPs are consistent with a novel analysis of molecular-dynamics (MD) simulations, SESSA simulations, and XPS experiments of the air–water interface (AWI) by Olivieri *et al.*[111] They investigated the spatial distribution of Na^+ ions near the AWI in dilute (<1 mol/l) aqueous solutions of NaCl, NaBr, and NaI from MD simulations with a non-polarizable force field. These distributions showed different density distributions of the Na^+ and halide ions over a depth of 1.5 nm from the solution surface. XPS experiments were performed with a liquid-jet source at an x-ray energy of 122 eV so that the kinetic energy of the Na 2p photoelectrons was about 86.5 eV with respect to the vacuum level or about 82.5 eV in the solution. At this energy, the information depth for the Na 2p photoelectrons from Eq. (A12) in the Appendix was about 1.6 nm (with $P = 95\%$) for each solution. The XPS measurements were thus sensitive to the calculated Na^+ and halide density profiles near the AWI. The measured relative intensities of the Na 2p photoelectrons from the three halide solutions closely matched those from SESSA simulations within the experimental uncertainties. These simulations were performed with the IMFPs from the TPP-2M equation. Olivieri *et al.* also found that the IMFPs would have to be increased by 150% to be outside their experimental uncertainties, that is, acceptable IMFPs at an energy of about 82.5 eV would have to between 0.7 nm and 1.6 nm. They then concluded that the Suzuki *et al.* EAL1 measurement at 79 eV (1.9 nm) must have been overestimated.

3.3. EAL for determination of marker depths

In Sec. 3.2, we described a formalism for determining the EAL for quantitative analysis. This formalism is based on the assumption that the sample of interest had a uniform composition over the sampling depth for the particular XPS or AES experiment. The sampling or information depth for a particular experiment can be determined from Eq. (A12) in the Appendix.

Many samples of interest, however, are inhomogeneous with compositional variations as a function of depth or of position on the surface. We now consider one example of a depth inhomogeneity, that of a marker or delta layer buried at some depth in a matrix of another material. For example, a thin overlayer material (the marker or delta layer) could be deposited on a planar substrate and then covered by a layer of the substrate material. We are interested in determining the depth, z_{ML}, of the embedded marker layer by XPS. For this application, we are assuming that the matrix material rather than the marker layer determines the transport of photoelectrons from the marker layer to the sample surface. As a guide, we suggest that the thickness of the marker layer should be less than about λ_{in}, where λ_{in} here is the IMFP of the photoelectrons from the marker layer in the matrix material.

As an example, we consider an experiment reported by Tougaard and coworkers.[112–114] A thin layer of gold was deposited on a clean nickel surface. Afterward, consecutive unknown amounts of nickel were deposited. Each evaporation of nickel was followed by a measurement of the Au 4d spectrum of photoelectrons emitted by Al Kα x rays. Peak-shape analysis of these spectra[112–114] provided both the depth of the gold layer and the thickness of this layer. However, elastic collisions of the photoelectrons were initially neglected in the analysis, and an attempt was made later to estimate the influence of this simplification.[114] Monte Carlo simulations of photoelectron transport in the Ni/Au/Ni system provided the ratio of photoelectron intensities obtained for different marker-layer depths, first when the elastic-scattering effects were accounted for and then after the elastic scattering was "switched off," I_x/I_x^{SLA}. The use of this correction procedure distinctly improved the results of the original analysis.[114] This analysis stimulated the later introduction of the term correction factor that was designated as *CF* in determinations of the marker-layer depth from the spectral shape (see Subsection 3 in the Appendix).[23]

A formalism has been developed for the determination of the depth of the marker layer from the photoelectron intensities recorded for the marker-layer material, first after its deposition and then after deposition of some thickness of the substrate material.[6,7,102,115] The derivation is based on the assumption that the marker-layer is infinitely thin. If elastic-scattering effects were negligible, we would expect exponential decay of the photoelectron signal intensity, $I_x^{SLA}(z_{ML})$, with depth of the marker layer, z_{ML} [see Eq. (65)],

$$\begin{aligned} I_x^{SLA}(z_{ML}) &= S\Delta\Omega F_x\left(\frac{d\sigma_x}{d\Omega}\right)N_{ML}\exp\left(-\frac{z_{ML}}{\lambda_{in}\cos\alpha}\right) \\ &= S\Delta\Omega N_{ML}\sigma_x\phi^{SLA}(z_{ML},\alpha), \end{aligned} \tag{84}$$

where N_{ML} is the atom density in the marker layer and σ_x is the total photoemission cross section for the atomic species of this layer. Equation (84) can be transformed to the following form:

$$\lambda_{in} = -\left[\cos\alpha \frac{d\ln\phi^{nel}(z,\alpha)}{dz}\right]. \tag{85}$$

Equation (85) can be used as the basis for a definition of the EAL for marker-layer depth determination. Let us denote $\phi(z_{ML}, \alpha)$ as the emission depth distribution function (EMDDF) when account is taken of elastic-scattering effects by atoms of the matrix material. However, the photoelectron energy and the photoemission cross section correspond to the marker-layer material. The EAL for marker-depth measurements can then be defined by

$$L_{ML} = -\left[\cos\alpha \frac{d\ln\phi(z_{ML},\alpha)}{dz_{ML}}\right]. \tag{86}$$

In practice, the value of the derivative in Eq. (86) can be calculated by numerical differentiation. A simple estimation of the derivative is the following:

$$L_{ML} = \frac{1}{\cos\alpha}\frac{z_2 - z_1}{\ln\phi(z_1,\alpha) - \ln\phi(z_2,\alpha)}, \tag{87}$$

where z_1 and z_2 are depths in the vicinity of the marker-layer depth, i.e., $z_1 < z_{ML} < z_2$. The EAL, L_{ML}, calculated from Eq. (87) can be termed as a local EAL.[6,7]

We now denote the photoelectron intensity from the marker layer after its deposition as $I_x(0)$. If elastic-scattering effects are again neglected, we have

$$I_x^{SLA}(0) = S\Delta\Omega F_x\left(\frac{d\sigma_x}{d\Omega}\right)N_{ML}\phi^{SLA}(0,\alpha). \tag{88}$$

The same intensity measured after deposition of the substrate material with a certain thickness, z_{ML}, is $I_x^{SLA}(z_{ML})$, as given by Eq. (84). We emphasize that λ_{in} in Eqs. (84) and (88) is the IMFP of photoelectrons emitted from the marker layer in the matrix material. The depth z_{ML} can be obtained from Eqs. (84) and (88),

$$\begin{aligned} z_{ML} &= \lambda_{in}\cos\alpha\left[\ln I_x^{SLA}(0) - \ln I_x^{SLA}(z_{ML})\right] \\ &= \lambda_{in}\cos\alpha\left[\ln\phi^{SLA}(0,\alpha) - \ln\phi^{SLA}(z_{ML},\alpha)\right]. \end{aligned} \tag{89}$$

To account for elastic collisions of the photoelectrons, we need to replace λ_{in} in Eq. (89) by the appropriate EAL, L_{ML}.[6,102] The modified equation (89) rewritten with respect to the EAL has the following form:

$$L_{ML} = \frac{1}{\cos\alpha}\frac{z_{ML}}{\ln I_x(0) - \ln I_x(z_{ML})} = \frac{1}{\cos\alpha}\frac{z_{ML}}{\ln\phi(0,\alpha) - \ln\phi(z_{ML},\alpha)}. \tag{90}$$

The EAL, L_{ML}, determined from Eq. (90) was called the practical EAL.[6,102] The values of this EAL can be calculated from Eq. (87) with photoelectron signal intensities and EMDDFs calculated from an advanced theoretical model in which elastic-scattering effects are taken into account (e.g., see theoretical models discussed in Ref. 24). The depth of the marker layer can then be determined from the measured intensities, $I_x(0)$ and $I_x(z_{ML})$, with Eq. (90),

$$z_{ML} = L_{ML}\cos\alpha\ln\left[I_x(z_{ML})/I_x(0)\right]. \tag{91}$$

We see that the EAL in Eq. (90) is related to the EMDDF, as indicated in Fig. 3. To the best of the authors' knowledge, there are no reports on practical applications of the above formalism. This situation is mainly due to the relatively small sampling depth of XPS measurements. There are often major difficulties in the preparation of a sample with a marker layer having monolayer thicknesses; however, the photoelectron signal emitted from the marker-layer should be of measurable intensity. Furthermore, the marker layer should be located within the sampling depth for the XPS measurement conditions. A good measure of the sampling depth is the information depth for a given photoelectron line and experimental configuration (see Subsection 2 in the Appendix). For example, the 99% ID of photoelectrons emitted in the selected elements by Ti Kα radiation ($h\nu$ = 4510 eV) for normal photoelectron emission varies in the range from 15 nm to 35 nm.[24] In the experimental studies of the Ni/Au/Ni system reported by Tougaard and Jablonski,[114] the thickness of the gold marker layer was estimated to be 1.3 nm and the maximum depth equal to 4.15 nm. However, these values were derived from the shape of the Au 4d spectrum in the range from 1020 eV to 1180 eV. The sampling depth in this approach was estimated to be ≈2.5 IMFPs for Au 4d photoelectrons in the Ni matrix.

One should also mention that the marker-depth approach is used in electron-probe microanalysis (EPMA) for the determination of the so-called "$\varphi\rho z$" or "phi-rho-zee" function (tracer method). However, the sampling depth of this technique is considerably larger, by several orders of magnitude, than that for XPS or AES. Furthermore, the marker-layer thickness in measurements by AES or XPS must have a finite uniform thickness to produce a measurable signal intensity, while the theoretical model presented here refers to an infinitely small thickness. Thus, a very difficult compromise is needed. To develop a more realistic model, we need an extensive set of experimental data. An obvious recommendation for such experiments seems to be the use of HAXPES since the sampling depth can be considerably increased by this approach.

Nonetheless, one of the options of the NIST Electron Effective-Attenuation-Length Database (SRD 82)[40] is designed to provide the EAL, L_{ML}, for user-specified experimental conditions. There are two issues that need to be stressed here. First, users of SRD 82 should be aware that the relevant option in this database refers to the limiting case of an infinitely thin marker layer. In this case, the atomic species constituting the marker layer are tacitly assumed not to affect the photoelectron transport, and for this reason, the user is not prompted to indicate the marker-layer material and the thickness of the marker-layer. However, information for the considered layer enters the relevant calculations via selection of photoelectron characteristics (the kinetic energy and the asymmetry parameter).

Second, we have observed very strong variations of the derivative in Eq. (86) close to the surface, i.e., for small values of z_{ML}. Consequently, the practical EAL calculated from Eq. (90) may also vary strongly with the depth near the surface. The values of the practical EAL for larger depths may also be affected by the fact that they are always referred to the surface value of the EMDDF. On the other hand, the local EAL is based on estimation of the derivative of the EMDDF in the vicinity of a given depth, as follows from Eq. (87). The local EAL may also be affected by strong variation of the derivative for small depths; however, for larger depths, the surface value of the EMDDF does not affect the local EAL. Thus, use of the local EAL is recommended for determining marker depths. We note that the surface layer of the substrate material should be continuous, i.e., its thickness should be larger than one monolayer. Thus, the region of small depths can be avoided.

Figure 30 shows the depth dependence of the local and practical EALs determined from SRD 82 for an Au marker layer in a Ni matrix. We consider here measurements of the Au 4d$_{5/2}$ signal intensity for the XPS experiments reported by Tougaard and Jablonski,[114] i.e., $\alpha = 0°$, $\psi = 60°$, Al Kα radiation, the Au 4d$_{5/2}$ energy of 1150 eV, and the Au 4d$_{5/2}$ asymmetry parameter, β, equal to 1.22. The practical EAL, L_{ML}, was calculated with SRD 82 [i.e., from Eq. (90)] for 400 values of depth in the range from $z_{ML} = 0.0125$ nm to $z_{ML} = 5$ nm in steps of 0.0125 nm. The local EAL values were calculated with SRD 82 from Eq. (87) for 401 depths up to 5 nm. The step defining the vicinity of a given depth, $z_2 - z_1$, was always constant and equal to 0.1 nm. Although such fine steps are not physically realistic, they are helpful here for showing similarities and differences of the computed EALs. We see noticeable variations of the practical and local EALs for depths up to about 0.5 nm, which corresponds to a Ni thickness of about two monolayers. The local EALs calculated for depths exceeding 0.5 nm vary weakly with the depth and can be averaged using an external program. The SRD 82 database does not provide this average.

The local EAL, L_{ML}, for depths exceeding 0.5 nm in the example of Fig. 30 is practically identical with the EAL for overlayer-thickness determination, L_{TH}, calculated from Eq. (15). Similar agreement has been observed for some other systems.[6] It is possible that the predictive formula for L_{TH} [Eq. (20)] may also be applicable to L_{ML} although further studies are needed to support this observation.

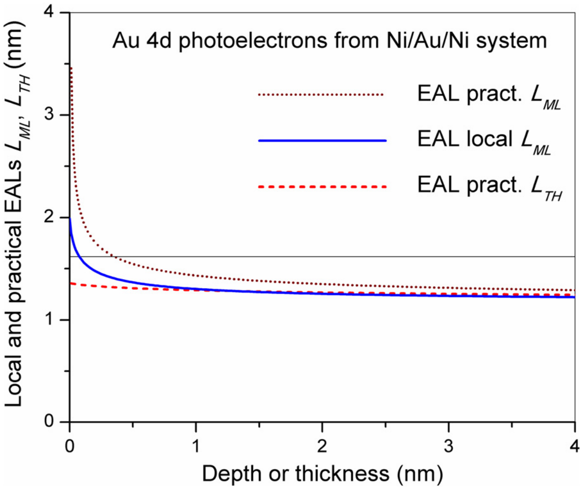

FIG. 30. Dependence of local and practical EALs for the determination of marker-layer depth from Au 4d$_{5/2}$ intensities measured for the Ni/Au/Ni system using the NIST Database SRD 82.[40] For comparison, the thickness dependence of the EAL for overlayer thickness determination is also shown. Solid line: the local EAL, L_{ML}, calculated from Eq. (85); dotted line: the practical EAL, L_{ML}, calculated from Eq. (88); dashed line: the practical EAL for overlayer thickness measurements calculated from Eq. (15). The thin horizonal line indicates the recommended IMFP value for nickel.[120]

3.4. EALs for determination of shell thicknesses of core–shell nanoparticles

XPS has been used for many years to characterize nanoparticles (NPs). Early studies focused on supported catalysts to determine particle size, chemical composition, and chemical state, while more recently, NPs have been developed for biomedical and other applications that involve unsupported core–shell NPs in complex environments. A key parameter in many investigations is the shell thickness of a core–shell NP or, more typically, the average shell thickness of an ensemble of core–shell NPs.

We consider here the use of XPS with unpolarized x rays for determining shell thicknesses of core–shell NPs. We also consider the ideal case of NPs consisting of a spherical core and a concentric spherical shell. Real NPs, however, may be nonspherical, and the core and shell may be excentric. Nevertheless, the ideal case needs to be satisfactorily understood before more complex structures are considered.

Shard[116] developed a series of analytical expressions for determining NP shell thicknesses, T_{NP}, from the ratios of photoelectron intensities excited from the core and shell materials of the NP. The expressions are a parameterization of the results of numerical calculations of XPS intensities from ideally concentric spherical core–shell particles with a range of different core radii, shell thicknesses, material densities, and electron energies. The numerical calculations were performed under the assumption that the photoelectrons travel in straight lines (i.e., the straight-line approximation) and that their attenuation can be described in terms of an exponential decay in intensity with distance traveled through a particular material.

In general, it is necessary to consider elastic-scattering effects with four EALs for the two photoelectron energies and the two materials of a core–shell NP. These EALs are represented as $L_{i,j}$, where i represents the material from which the photoelectrons originated ($i = 1$ for the shell material and $i = 2$ for the core material) and j indicates the material through which the photoelectrons are traveling ($j = a$ for the shell and $j = b$ for the core). For example, $L_{1,a}$ represents an EAL for photoelectrons from the shell traveling in the shell. It was convenient in the parameterization to use $L_{1,a}$ as a scaling parameter and to express all quantities with units of length as ratios to this EAL. This procedure enables a simplicity of expression in the final equations. The radius of the NP core is defined as the product $SL_{1,a}$, where S is the dimensionless ratio of the physical radius of the core to $L_{1,a}$. The parameter S is one of the inputs into the Shard equation, and the dimensionless output, T_{NP}, should be multiplied by $L_{1,a}$ to provide an estimate of the physical thickness of the shell.

The Shard expressions are as follows:

$$T_{NP} = \frac{T_{P\sim 1} + \beta T_0}{1 + \beta}, \tag{92a}$$

where

$$T_{P\sim 1} = \frac{T_{P\to\infty} S}{S + \alpha}, \tag{92b}$$

$$T_0 = S\left[(ABC + 1)^{1/3} - 1\right], \tag{92c}$$

$$T_{S\to\infty} = \frac{0.74A^{3.6}\ln(A)B^{-0.9} + 4.2AB^{-0.41}}{A^{3.6} + 8.9}, \tag{92d}$$

$$\alpha = 1.8/(A^{0.1}B^{0.5}C^{0.4}), \tag{92e}$$

$$\beta = 0.13\alpha^{2.5}/S^{1.5}, \tag{92f}$$

$$A = I_1 I_2^{\infty}/(I_2 I_1^{\infty}), \tag{92g}$$

$$B = L_{1,\alpha}/L_{2,a}, \tag{92h}$$

and

$$C = L_{1,\alpha}/L_{1,b}. \tag{92i}$$

In Eq. (92g), I_1 indicates the photoelectron intensity from the shell and I_2 indicates the photoelectron intensity from the core. The quantities, I_1^{∞} and I_2^{∞}, represent the corresponding intensities from planar semi-infinite materials.

Shard optimized his equation so that inelastic-scattering effects in core–shell NPs could be represented by the EALs obtained from attenuation measurements or calculations for overlayer films on planar substrates. Specifically, EALs developed for describing attenuation of substrate photoelectrons by an overlayer film were recommended for use in the Shard equation (i.e., the EAL we have defined previously as L_{TH} although the subscript will be deleted here for clarity). Unlike the EAL applications described previously, there is no original defining equation involving IMFPs that had been developed on the basis of neglecting the effects of elastic scattering. Instead, one can infer such an equation in which the EALs in Eqs. (92h) and (92i) were replaced by IMFPs.[117]

Shard investigated relative errors in thickness values from his formula for values of B and C each between 0.5 and 2 and found that these errors were less than about 6%.[116] The relative errors were also judged to be satisfactorily small in comparison with the estimated uncertainties of IMFPs (on which the EALs depend) of ≈10%.[5] Further evaluations of the Shard equation have been made from SESSA simulations using Au-core/C-shell, C-core/Au-shell, Cu-core/Al-shell, and Al-core/Cu shell NPs.[118] These material combinations were chosen since they led to suitably large or small (B, C) combination values of (0.88, 2.56), (1.13, 0.39), (2.21, 1.49), and (0.46, 0.68), respectively, for the selected photoelectron signals (Au $4f_{7/2}$, C 1s, Cu $2p_{3/2}$, and Al $2p_{3/2}$). While the results for the Au-core/C-shell NPs are directly relevant to many investigations of Au NPs with various organic coatings, the results for Cu-core/Al-shell and Al-core/Cu-shell NPs are illustrative for XPS characterizations of bimetallic core–shell NPs.

The SESSA simulations were made with Al Kα x rays incident on the NP at an angle of 55° with respect to the analyzer direction, and photoelectron intensities were determined for electrons emitted within 5° of the surface normal.[118] These simulations were performed for core diameters, D, of 1 nm, 2 nm, 5 nm, 10 nm, 20 nm, 50 nm, 100 nm, and 200 nm and for shell thicknesses, T, between 0.25 nm and 3 nm in increments of 0.25 nm.

Figure 31 shows illustrative results of the SESSA simulations for Au-core/C-shell NPs. We show plots of the ratio of the C-shell thickness, $T_{\rm NP}$, from Eq. (92) for each simulation to the actual shell thickness, T, as a function of T.[118] In this example, the values of $T_{\rm NP}/T$ were larger than unity but generally less than 1.1. The average value of the $T_{\rm NP}/T$ results in Fig. 31 was 1.06. Similar simulations for C-core/Au-shell, Cu-core/Al-shell, and Al-core/Cu-shell NPs showed different trends in the plots of $T_{\rm NP}/T$ vs T, but the overall average value of $T_{\rm NP}/T$ was 1.00 with all but 26 of the 768 simulation results giving $T_{\rm NP}/T$ values within 10% of unity.[118] The Shard equation [Eq. (92)] is thus satisfactory for determining shell thicknesses of core–shell NPs with the use of EALs, L_{TH}, describing the attenuation of substrate photoelectrons by an overlayer film.

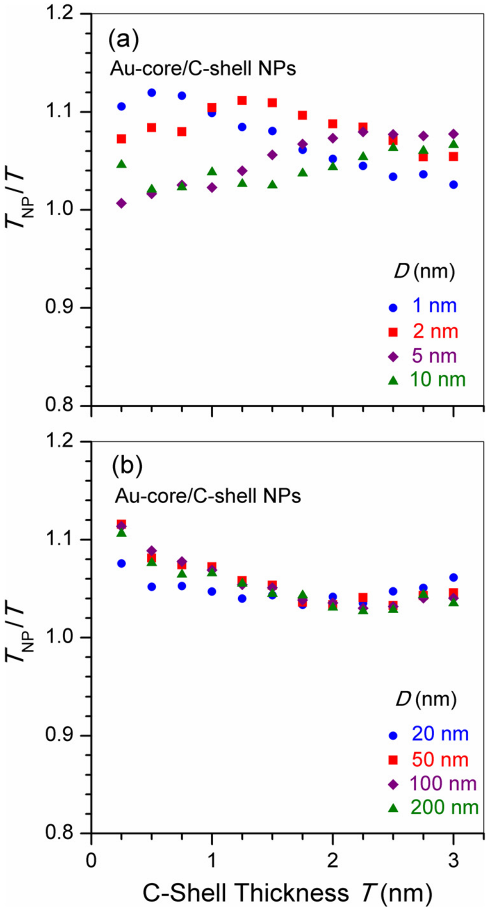

FIG. 31. Plots of the ratio of values of the shell thickness $T_{\rm NP}$ from Eq. (92) to the actual shell thickness, T, as a function of T for Au-core/C-shell NPs from SESSA simulations, as described in the text.[118] (a) Au-core diameters, D, of 1 nm, 2 nm, 5 nm, and 10 nm; (b) Au-core diameters, D, of 20 nm, 50 nm, 100 nm, and 200 nm. Reprinted with permission from Powell *et al.*, J. Phys. Chem. C **122**, 4073–4082 (2018).[118] Copyright 2018 American Chemical Society.

Cant *et al.* extended the Shard approach to core-shell-shell NPs.[119] In this case, iteration is required if both shell thicknesses are unknown.

4. Data for Inelastic Mean Free Paths

We presented many predictive EAL formulas in Sec. 3 for different XPS applications. In each case, the IMFP for a particular material is needed in order to determine the desired EAL. We have previously reviewed calculations and measurements of IMFPs,[2,5,120,121] and a guide for the selection of IMFP data has been prepared recently.[122] We summarize here the useful sources of IMFP data.

The most extensive sources of IMFP data are the calculated IMFPs of Shinotsuka *et al.* for 41 elemental solids[123] and 42 inorganic compounds[75] for electron energies between 50 eV and 200 keV, the calculated IMFPs of Shinotsuka *et al.* for liquid water[75,107] for energies between 50 eV and 30 keV, and the calculated IMFPs of Tanuma *et al.* for a group of 14 organic compounds for energies between 50 eV and 2 keV.[63] These IMFPs were calculated using an algorithm proposed by Penn[124] and with experimental optical constants in most cases or calculated optical data for some compounds.[75] Powell and Jablonski concluded that IMFPs calculated from optical data have uncertainties of up to about 10%.[5] It is possible that they might have smaller uncertainties, but better estimates await the development of better experimental tests.

An approximate form of the relativistic Bethe[125] equation for inelastic scattering of electrons in matter was developed by Shinotsuka *et al.*[123] for describing the dependence of the IMFP, λ_{in}, on electron energy in condensed matter,

$$\lambda_{in} = \frac{\alpha(E)E}{E_p^2[\beta\ln(\gamma\alpha(E)E) - (C/E) + (D/E^2)]}, \tag{93a}$$

where

$$\alpha(E) = \frac{1 + [E/(2m_ec^2)]}{\{1 + [E/(m_ec^2)]\}^2} \approx \frac{1 + E/1\,021\,999.8}{(1 + E/510\,998.9)^2}, \tag{93b}$$

$$E_p = 28.816\left\{\frac{N_v\rho}{M}\right\}^{0.5} \quad (\mathrm{eV}), \tag{93c}$$

where E is the electron energy (in electron volts) above the Fermi level for conductors or above the bottom of the conduction band for nonconductors, m_e is the mass of the electron, c is the speed of light, N_v is the number of valence electrons per atom or molecule, ρ is the density (in g/cm^3), M is the atomic or molecular weight, and β, γ, C, and D are parameters.

Tanuma *et al.*[63] analyzed their early calculations of IMFPs for 27 elemental solids[126] and 14 organic compounds[63] for energies between 50 eV and 2000 eV and developed the following predictive equations for the parameters β, γ, C, and D in Eq. (93):

$$\beta = -1.0 + 9.44/\left(E_p^2 + E_g^2\right)^{0.5} + 0.69\rho^{0.1} \quad (\mathrm{eV^{-1}\,nm^{-1}}), \tag{94a}$$

$$\gamma = 0.191\rho^{-0.5} \quad (\mathrm{eV^{-1}}), \tag{94b}$$

$$C = 19.7 - 9.1U \quad (\mathrm{nm^{-1}}), \tag{94c}$$

$$D = 534 - 208U \quad (\mathrm{eV\,nm^{-1}}), \tag{94d}$$

$$U = \frac{N_v\rho}{M} = \left(E_p/28.816\right)^2, \tag{94e}$$

and where the bandgap energy E_g is expressed in eV. Equations (93) and (94), designated as the TPP-2M equation for estimating IMFPs,[63] have later been found generally satisfactory for energies between 50 eV and 200 keV.[75,107,123] However, for a few materials (diamond, graphite, Cs, cubic-BN, and hexagonal-BN), there were large rms deviations (of 70.7%, 46.6%, 34.7%, 65.6%, and 34.3%, respectively) between the predicted IMFPs and the calculated IMFPs for each material. If these five materials are ignored, the average rms deviations between the predicted IMFPs and calculated IMFPs were 8.9% and 8.7% for the remaining elemental solids and inorganic compounds, respectively. The large rms deviations between the calculated IMFPs and the values from the TPP-2M formula for diamond, graphite, cubic-BN, and hexagonal BN occurred for relatively small values of the parameter β from Eq. (2a), i.e., for $\beta_{\mathrm{TPP\text{-}2M}}$ values less than about 0.13.[75] While the TPP-2M formula is useful for estimating IMFPs in a variety of solids (and also for liquid water[107]) for energies between 50 eV and 200 keV, the accuracy of these estimates is likely to be poorer for energies less than 200 eV.[75,107,123] Recommended values of the parameter N_v for most elements have been published by Tanuma *et al.*[127]

Seah[128] derived another predictive IMFP equation based on an analysis of the IMFP calculations of Tanuma *et al.* for 41 elemental solids,[48] 15 inorganic compounds,[72] and 14 organic compounds.[63] His S1 formula for electron energies between 100 eV and 10 keV is

$$\lambda_{in} = (4 + 0.44Z^{0.5} + 0.104E^{0.872})a^{1.7}/\left[Z^{0.3}(1 - W)\right] \quad (\mathrm{nm}), \tag{95}$$

where Z is the atomic number (or the average atomic number for a compound) and the parameter a is the average atomic spacing defined by Eq. (61b). The term W in Eq. (95) is given by $W = 0.06H$ or $W = 0.02E_g$, where H is the heat of formation of a compound (in eV per atom).[128]

Seah found that the average rms deviations between IMFPs from Eq. (95) and the calculated IMFPs of Tanuma *et al.* were 8.5%, 8.3%, and 7.9% for the groups of elemental solids, inorganic compounds, and organic compounds, respectively.[128] We note that Seah was able to correct the calculated IMFPs of Tanuma *et al.*[72] for the substantial sum-rule errors found for many of the inorganic compounds in their early calculations. The rms deviations of about 8% found by Seah between IMFPs from his S1 formula and those calculated by Tanuma *et al.*[48,63,72] were slightly smaller than those reported by Shinotsuka *et al.*[75,123] Seah's analysis, however, was made for energies above 100 eV, while Shinotsuka *et al.* also considered energies between 50 eV and 100 eV where often larger deviations occur than for higher energies.

Calculation of IMFPs for a material from the TPP-2M formula requires knowledge of three parameters (M, ρ, and N_v) for conductors and a fourth parameter (E_g) for nonconductors. While bandgap energies are available for many compounds,[129–133] we note that evaluations of the earlier TPP-2 formula showed only a weak dependence of IMFPs on E_g.[134] That is, only rough estimates of E_g are needed if specific data do not exist in available resources.[129–133] For example, E_g is generally between 6 eV and 11 eV for highly ionic compounds such as the alkali halides and is often between 1 eV and 9 eV for oxides. Similar calculations of IMFPs from the S1 formula require knowledge of Z (or the average atomic number for a compound), M, and ρ for conductors and either E_g or H for nonconductors. Data for H are available for many inorganic compounds.[135]

Gries[136] developed an earlier predictive IMFP equation based on the calculated IMFPs of Tanuma *et al.*[48,63,72] and an atomistic model. Tanuma *et al.*[137] analyzed the Gries model and pointed out some important limitations. Although use of the Gries equation requires knowledge of a single material parameter (the sample density), it is recommended that IMFPs only be determined from this equation if there is reason to believe that Eqs. (93) and (94) or Eq. (95) will not give satisfactory results.

Finally, we note that IMFPs are available from the NIST SESSA database[42] and from the NIST Electron Inelastic-Mean-Free-Path Database.[138]

5. Concluding Remarks and Recommendations

The EAL is a useful parameter in expressions for different quantitative applications of XPS. It can be used in place of the IMFP to correct those expressions for the effects of elastic scattering of photoelectrons from their point of origin in the sample to their emission from the sample surface.

The most common EAL application is the determination of thicknesses of overlayer films on planar substrates. Reliable measurements of these EALs were often difficult since they required preparation of samples with a thin uniform film of known thickness. The measurements also depended on a number of key assumptions, as described in Sec. 2. The same assumptions also need to be satisfied in overlayer-film thickness measurements by XPS.

Since there were often large scatters in early EAL measurements for the same material,[11–14] we decided to calculate EALs.[6,7] Section 3.1 describes the calculation of EALs for thickness measurements of an overlayer film on a planar substrate, first by XPS with unpolarized x rays (Sec. 3.1.1) and then by XPS with linearly polarized x rays (Sec. 3.1.2). We now summarize our recommendations for these two applications and follow with comments and recommendations for other XPS applications.

5.1. Recommendations of EALs for overlayer-film thickness measurements by XPS with unpolarized x rays

The "magic-angle" experimental configuration (with the angle, ψ, between the direction of the x-ray beam and the photoelectron emission angle fixed at 55°) is preferred; if this is not possible, ψ should be as close as possible to 55°. The photoelectron emission angle should be between 0° and 50°. The values of the EAL, L_{TH}, can then be obtained from a predictive equation such as Eq. (20) or (60) for the three methods of determining film thicknesses described in Secs. 3.1.1.2–3.1.1.4. Information on sources of IMFP data is provided in Sec. 4.

For other XPS configurations and for photoelectron emission angles greater than 50°, EALs can be derived from the NIST Electron Effective-Attenuation-Length Database for photoelectron energies between 50 eV and 2 keV.[40] Alternatively, EALs can be derived from simulated intensities with use of the SESSA software.[42,56,76,139] A photoelectron emission angle close to normal is suggested in order to maximize the range of thickness measurements. An analyst should also ensure that the thickness of the overlayer is close to uniform. An analysis of the spectrum shape using the Tougaard QUASES software[66,82] may be helpful for assessing whether or not the film is uniform.[55]

We recommend the following three methods for determining overlayer-film thicknesses:[53]

1. Measurements of the signal intensity for a single photoelectron line from the overlayer film, I_f, accompanied by a measurement of the signal intensity from the bulk overlayer material, I_f^{∞}, as described in Sec. 3.1.1.2. The EAL, $L_{TH}^{f}(E_f)$, can be calculated from a predictive formula [Eqs. (20) or (60)] for the kinetic energy of photoelectrons from the overlayer. The overlayer thickness should then be calculated from Eq. (35) in which we introduce $R_f^{expt} = I_f/I_f^{\infty}$.
2. Measurements of the signal intensity for a single photoelectron line from the substrate, I_s, accompanied by a measurement of the signal intensity from the uncovered substrate material, I_s^{∞}, as described in Sec. 3.1.1.3. The needed EAL, $L_{TH}^{f}(E_s)$, should be calculated from Eq. (20) or (60) for the overlayer material using the kinetic energy of the selected photoelectron line from the substrate. The overlayer thickness is calculated in this case from Eq. (39) into which we introduce $R_s^{expt} = I_s/I_s^{\infty}$.
3. Measurements of the signal intensity for a selected photoelectron line from the overlayer, I_f, and the intensity of a photoelectron line from the substrate, I_s, as described in Sec. 3.1.1.4. This procedure also requires knowledge of the intensity ratio $I_f^{\infty}/I_s^{\infty}$ measured for the bulk overlayer and substrate materials. In general, we need two values of the EAL for the overlayer material: one for the kinetic energy of photoelectrons from the overlayer, $L_{TH}^{f}(E_f)$, and the other for the kinetic energy of photoelectrons from the substrate, $L_{TH}^{f}(E_s)$. These EALs can be obtained from Eq. (20) or (60). The overlayer thickness should be calculated by solving the nonlinear equation in one unknown given by Eq. (53) into which we introduce the measured parameter, R_{exp}, defined by Eq. (52). However, if the energies of photoelectrons from the substrate and overlayer are almost the same, then the overlayer thickness can be obtained from the simpler equation (51) with a single EAL for the overlayer material, again from Eq. (20) or (60).

The NIST EAL database[40] is a convenient source for obtaining EAL values, particularly if the user's XPS configuration differs from the magic-angle configuration (i.e., $\psi \neq 55°$) or if $\alpha > 50°$. This software is based on an analytical formalism of photoelectron transport (the so-called transport approximation[6]) in which it is assumed that the electron-scattering properties of the overlayer and substrate materials are identical. If the IMFPs and transport mean free paths (TRMFPs) of the substrate and overlayer materials each differ by more than, say, 10%, EALs can be determined from the simulated photoelectron intensities for different overlayer thicknesses, e.g., from use of SESSA[42,56,76] or other Monte Carlo software.[55] The SESSA software is also useful if the overlayer film is non-ideal since simulations can be performed for rectangular islands.[83]

Although Eqs. (20) and (60) are very simple and provide reasonably accurate EALs for the determination of overlayer-film thicknesses at photoelectron energies up to about 4.5 keV, they require knowledge of the single-scattering albedo, ω, for a given solid. For elemental solids, ω can be determined from simple analytical expressions.[44,140] In Ref. 140, the fitted parameter is the ratio of the TRMFP to the IMFP. However, this ratio is closely related to the albedo,

$$\omega = \left[1 + (\lambda_{tr}/\lambda_{in})\right]^{-1}. \qquad (96)$$

In general, ω can be determined from Eq. (7) and IMFP and TRMFP values from NIST databases[40,42] as well as from predictive formulas.[44]

The supplementary material provides TRMFPs and values of ω for energies between 54.6 eV and 29 732.6 eV for the 41 elemental solids and 42 inorganic compounds for which Shinotsuka *et al.* calculated IMFPs.[75,123] Figures S1 and S2 of the supplementary material illustrate the dependences of ω on both photoelectron energy and atomic number for selected elements and inorganic compounds.

5.2. Recommendations of EALs for overlayer-film thickness measurements by XPS with linearly polarized x rays

As explained in Sec. 3.1.2, we recommend the use of Eq. (62) for determining EALs in the measurement of overlayer-film thicknesses by XPS with linearly polarized x rays. Equation (62) was derived from Monte Carlo simulations for the XPS configuration shown in Fig. 22.[92] The simulations were made for photoelectron lines from Si, Cu, Ag, and Au and for photoelectron energies between 100 eV and 10 keV.

5.3. Recommendations of EALs for the determination of surface composition

EALs for the determination of surface composition, L_{QA}, can be obtained from Eqs. (30) and (31) [or the equivalent equation (83)], as recommended in Sec. 3.2. Equations (30) and (31) were derived from calculations of photoelectron intensities from the transport approximation for photoelectron lines from Si, Cu, Ag, and Au excited by Mg and Al Kα x rays. These equations are expected to be valid for XPS configurations close to the magic-angle configuration (i.e., for ψ between 50° and 60°). For other configurations, L_{QA} should be calculated from Eq. (79).

5.4. Recommendations of EALs for determination of marker depths

As described in Sec. 3.3, the values of the EAL, L_{ML}, for the determination of the depth of thin marker or delta layers can be obtained from the NIST Electron Effective-Attenuation-Length Database[40] for user-specified experimental conditions. These EALs should be determined with the values of so-called local EALs in the database.

5.5. Recommendations of EALs for determination of shell thicknesses of core–shell nanoparticles

We described the use of the Shard[116] expressions [Eq. (92)] for measuring shell thicknesses of core–shell NPs in Sec. 3.4. These expressions were optimized so that EALs for the determination of overlayer-film thicknesses, i.e., values of L_{TH}, could be utilized. These EALs can be obtained from the predictive equation [Eq. (20) or (60)] or from the NIST Electron Effective-Attenuation-Length Database.[40] The same approach can be used to determine shell thicknesses of core-shell-shell NPs.[119]

5.6. Comparisons of calculated and measured EALs

Many experiments were performed during the late 1960s and the 1970s to determine what are now known as EALs.[11–14] These EALs were very helpful in providing badly needed information on the surface sensitivity of XPS and the related technique of AES.[5] The EALs also led to the development of useful predictive EAL equations.[14,86,141] Nevertheless, there were often large scatters in the reported EALs for the same material. In addition, there were surprising variations in values of the exponent p often used to describe the energy dependence of the measured EALs, namely, $L_{TH} = kE^p$, where k and p are empirical parameters for a given set of EALs. Powell[86,122] reported the values of p for numerous materials and electron energy ranges. In Ref. 86, the following values were reported: $p = 0.78 \pm 0.05$ for Al (360 eV to 1730 eV), $p = 0.75 \pm 0.03$ for Si (321 eV to 3574 eV), $p = 0.61 \pm 0.02$ for Ge (350 eV to 1404 eV), $p = 0.54 \pm 0.04$ for Au (940 eV to 3208 eV), $p = 0.54 \pm 0.02$ for Al_2O_3 (556 eV to 1404 eV), $p = 0.70 \pm 0.02$ for SiO_2 (719 eV to 3570 eV), $p = 0.73 \pm 0.04$ for NaF (415 eV to 1403 eV), $p = 0.56 \pm 0.03$ for NaCl (415 eV to 1403 eV), and $p = 0.59 \pm 0.03$ for KI (350 eV to 1404 eV). In more recent EAL experiments, Rubio-Zuazo and Castro obtained $p = 0.62 \pm 0.01$ for Au from EAL measurements with linearly polarized x rays on well-characterized samples for photoelectron energies between 1029 eV and 9694 eV.[94] However, the Seah S3 predictive EAL formula [Eq. (61)] indicates that $p = 0.861 \pm 0.002$ for Au and the latter energy range.[83] In the recently published compilation,[122] the values of p from EALs for Au that were calculated from Eq. (20) were 0.871 ± 0.003 for energies between 992.3 eV and 19 330 eV.[122] Nevertheless, a much smaller value of p (0.690 ± 0.011) was found from EALs calculated for Au from Eq. (20) for energies between 492.7 eV and 1480.3 eV. The different p values for the two energy ranges occur because of curvature in plots of L_{TH} vs E on logarithmic scales. This nonlinearity can be explained by advanced theoretical models that are based on the values of the albedo parameter. The energy dependence of the albedo may show a complicated structure, as shown in Figs. S1(b) and S2(b) of the supplementary material.

We believe that the variability in the p values from different EAL experiments and the fact that these p values are less than those expected from the predictive EAL formulas[122] must be associated with different effects of island growth in the deposited overlayer films.[83] The early EAL experiments were performed before the development of scanning tunneling microscopes and low-energy electron microscopes, and experimentalists were then unaware of the possible complexities now known to occur in the early stages of film growth.[142,143] For the example of the Au EAL data of Rubio-Zuazo and Castro[94] shown in Fig. 24 and discussed in Sec. 3.1.2, there is agreement between the measured and calculated values of L_{TH} for energies between 9 keV and 10 keV but increasing disagreement for lower energies. This trend is understandable since the EAL measurements at the higher energies (where the L_{TH} values are over 6 nm) are less sensitive to overlayer-film nonuniformities than the EAL measurements at lower energies where the reported EAL at 1.029 keV was 1.8 ± 0.2 nm. Our consideration of island growth in the Rubio-Zuazo and Castro experiments led to the important conclusion that observations of exponential decreases of substrate photoelectron intensities or exponential increases of overlayer photoelectron intensities during film growth do not necessarily indicate that the overlayer films were uniform during film growth.[83]

We will now summarize the illustrative comparisons we have made between calculated and measured EALs. In Sec. 3.1.1.3, we compared EALs measured for an organic molecular solid, perylene-3,4,9,10-tetracarboxylic dianhydride (PTCDA), by Graber *et al.*[57] with EALs from our predictive formulas for L_{TH} [Eqs. (20) and (62)] for XPS with unpolarized and linearly polarized x rays, respectively.

This set of measurements by Graber *et al.* was attractive because PTCDA has been shown to grow layer-by-layer when deposited on Ag(111) at a sufficiently low temperature. The comparison in Fig. 13 showed general agreement between the measured and calculated EALs although there were two groups of measured EALs, one between 242 eV and 690 eV and the other between 82 eV and 135 eV, which showed systematic differences. We believe that these systematic differences are likely due to diffraction or forward-focusing effects arising from the crystallinity of the Ag(111) substrate.[59–62]

The most accurate determinations of EALs are those of Seah and Spencer[74] who reported average EAL values for Si 2p photoelectrons from the well-characterized films of SiO_2 on a Si substrate,[69–71] as described in Sec. 3.1.1.4. Their final EAL results, in this case for L_{TH}^{ratio}, were 2.996 ± 0.016 nm and 3.448 ± 0.019 nm for XPS with Mg Kα and Al Kα x ray sources, respectively. These EALs were consistent with the corresponding values of L_{TH} calculated by Powell and Jablonski using the transport approximation (as used in the NIST SRD 82 database[40]).[73] Nevertheless, the calculated EALs relate to peak intensities that include shake-up or intrinsic excitations, while these contributions are excluded in the protocol for EAL measurements. Kim and Seah later pointed out that there was an inconsistency between the dependence on SiO_2 film thickness of L_{TH}^{ratio} values calculated by Powell *et al.*[76] (based on the simulated photoelectron intensities from the NIST SESSA database[42]) and the thickness independence of the measured L_{TH}^{ratio} values.[77] This inconsistency is believed to arise from the variation in the fraction of intrinsic or shakeup intensity accompanying the Si 2p photoionization with SiO_2 thickness and/or from variation of inelastic-scattering probabilities in the vicinity of the Si/SiO_2 and SiO_2/vacuum interfaces, also as a function of SiO_2 thickness.[76] Further investigations are needed of these possible effects.

The methodology developed by Seah *et al.*[69] has been extended further by Kim *et al.*[78–80] who reported EALs for thin films of SiO_2, Al_2O_3, and GaAs deposited on Si(100) substrates in XPS experiments with Mg Kα x rays. While their EAL for SiO_2 was consistent with the Seah and Spencer result,[74] their EALs for Al_2O_3 and HfO_2 were reported without estimates of the experimental uncertainties. These EALs are also larger than the corresponding calculated values of L_{TH} by 15% and 33%, respectively. Further investigations are needed of these differences.

In Sec. 3.1.2, we discussed XPS with linearly polarized x rays and described an EAL predictive formula [Eq. (62)] that can provide L_{TH} values for an XPS configuration similar to that shown in Fig. 22. These values are systematically different from those obtained from Eq. (20), as shown in Fig. 23. We also showed in Fig. 24 that the measured EALs of Rubio-Zuazo and Castro[94] for Au were consistent with the predicted EALs at energies between 9 keV and 10 keV, but there were increasing differences at lower energies. These differences were attributed to island formation in the deposited Au film.[83]

We discussed EALs for the determination of surface composition in Sec. 3.2 and a predictive formula for providing L_{QA} values [Eqs. (82) and (83)]. This formula is expected to be valid for XPS configurations close to the so-called magic-angle configuration and for photoelectron emission angles between 0° and 50°. Figure 26 showed a clear difference between L_{TH} and L_{QA} values for a given value of ω.

Figure 27 shows two sets of L_{QA} values for liquid water from the experiments of Suzuki *et al.*[105] These experiments were performed with synchrotron radiation, liquid water from a microjet, and O 1s photoelectron energies between 10 eV and 600 eV. One set of L_{QA} values (designated here as EAL1) was based on the assumption of strong elastic-scattering effects, while the other set (designated here as EAL2) was based on the assumption of negligible elastic-scattering effects. Suzuki *et al.* pointed out that the actual values of L_{QA} should be close to the EAL1 values at low electron energies (where the elastic-scattering effects are expected to be strong) and close to the EAL2 values at high electron energies (where the elastic-scattering effects are expected to be weak). Figure 27 also shows the calculated values of L_{QA} for water from Eqs. (82) and (83) and the IMFP calculations of Shinotsuka *et al.*[75,107] However, we cannot make a direct comparison between the calculated L_{QA} values and the EAL1 and EAL2 values for two reasons. First, the calculations were made for unpolarized x rays, while the experiments were performed with linearly polarized x rays. Second, the calculations were made for a planar sample, and there was a cylindrical sample in the experiments. Nevertheless, the EAL1 values are more than double the water IMFPs[75,107] for energies between 50 eV and 600 eV, while the three EAL2 values at energies between 373 eV and 601 eV are more than three times the calculated IMFPs. Additional IMFP and EAL measurements and calculations are needed for water since such data are important for radiation dosimetry and for investigations of surface reactions on atmospheric aerosols.

5.7. Final remarks

A main result of our work is that the EAL is not a simple material parameter such as the IMFP, which, for a given solid, is a function only of electron energy. In contrast, the EAL generally depends on the defining equation, the XPS configuration, as well as on the material. In addition, the values of the EAL for overlayer-film thickness measurements, L_{TH}, depend on whether XPS is performed with unpolarized or linearly polarized x rays, as shown in Fig. 23. We have also found that the EAL for the determination of surface composition, L_{QA}, is different from L_{TH}, as indicated in Fig. 26. Nevertheless, a preliminary calculation shows that the values of the EAL for determining depths of thin marker layers, L_{ML}, appear to be very similar to the corresponding values of L_{TH}, as shown in Fig. 30.

Figure 3 shows schematically how EALs for different XPS applications can be determined from the emission depth distribution function (EMDDF) and for AES from the excitation depth distribution function (EXDDF). Calculations of the EMDDF are outlined in Figs. 4 and 5 from MC simulations and from use of the transport approximation, respectively. The EMDDF calculations require knowledge of photoionization cross sections, differential elastic-scattering cross sections, transport mean free paths (TRMFPs), and IMFPs. For AES, knowledge is also needed for inner-shell ionization cross sections to determine the EXDDF. The Appendix defines and briefly describes six parameters related to the EMDDF and EXDDF that are useful in AES and XPS analyses: the mean escape depth, the information depth, the CF function, partial escape distributions, partial intensities, and backscattering correction factors. Table 2 lists seven NIST databases that are useful for different quantitative applications of AES and XPS.[144]

A very useful parameter for calculating EALs from predictive formulas, i.e., Eqs. (20), (30), (31), (60), (62), and (83), is the so-called albedo. This parameter, a simple measure of the strength of elastic-scattering effects in a material, depends on the IMFP and

TABLE 2. NIST databases[144] that provide data for various parameters needed for different quantitative applications of AES and XPS: differential elastic-scattering cross sections ($d\sigma_{el}/d\Omega$), total elastic scattering cross sections (σ_{el}), transport mean free paths (λ_{tr}), IMFPs (λ_{in}), EALs for measurement of thin-film thicknesses (L_{TH}), EALs for measurement of surface composition (L_C), mean escape depths (D), emission depth distribution function [$\phi(z, \alpha)$] for depth of emission z and electron emission angle α with respect to the surface normal, backscattering correction factor (R_{BCF}), and cross sections for inner-shell ionization by electron impact (σ_i)

Database	Parameters
NIST Electron Elastic-Scattering Cross-Section Database, Versions 3.2 and 4.0 (SRD 64)[158]	$d\sigma_{el}/d\Omega$, σ_{el}, λ_{tr}
NIST Electron Inelastic-Mean-Free-Path Database (SRD 71)[138]	λ_{in}
NIST Electron Effective-Attenuation-Length Database (SRD 82)[40]	L_{TH}, L_C, D, $\phi(z, \alpha)$
NIST Database for the Simulation of Electron Spectra for Surface Analysis (SRD 100)[42]	$d\sigma_{el}/d\Omega$, σ_{el}, λ_{tr}, λ_{in}, σ_i, R_{BCF}
NIST Backscattering-Correction-Factor Database for Auger Electron Spectroscopy (SRD 154)[157]	R_{BCF}, $\phi(z, \alpha)$
NIST Database of Cross Sections for Inner-Shell Ionization by Electron or Positron Impact (SRD 164)[156]	σ_i

the TRMFP for a given material and electron energy, as indicated by Eq. (7). The TRMFP for a compound can be determined from Eqs. (8) and (9), while IMFPs can be obtained from predictive formulas such as Eqs. (93)–(95). IMFP and TRMFP data can also be found in the NIST EAL[40] and SESSA[42] databases. To facilitate EAL calculations, an extensive tabulation of albedo values is listed in the supplementary material. These values were determined for 41 elemental solids and 42 inorganic compounds for energies between 50 eV and 30 keV.

6. Supplementary Material

See the supplementary material for transport mean free paths and values of the single-scattering albedo, ω, from Eq. (7) for energies between 54.6 eV and 29 732.6 eV for the 41 elemental solids and 42 inorganic compounds for which Shinotsuka *et al.* calculated IMFPs.[75,123] Figures S1 and S2 in the Supplementary Information illustrate the dependences of ω on both photoelectron energy and atomic number for selected elements and inorganic compounds.

Acknowledgments

The authors thank Dr. A. Schöll and Dr. E. Umbach for supplying data and Dr. M. P. Seah, Dr. Toshinori Suzuki, and Dr. Yoshi-Ichi Suzuki for helpful comments on an earlier draft of this manuscript.

7. Data Availability

The data that support the findings of this study are available within this article and its supplementary material.

8. Appendix: Other Parameters Related to the Emission Depth Distribution Function

As indicated in Fig. 3, there are other parameters related to the emission depth distribution function in addition to EALs for different analytical applications that are useful in AES and XPS applications. These parameters are listed here with only basic information (definitions, defining formulas, etc.). More detailed information is available in the cited literature.

8.1. Mean escape depth

The mean escape depth (MED), D, is a parameter that conveniently defines the average sampling depth of AES and XPS for given measurement conditions. This parameter is defined as the "average depth normal to the surface from which the specified particles or radiations escape" (Ref. 1, Definition 4.203),

$$D = \frac{\int_0^\infty z\phi(z,\alpha)dz}{\int_0^\infty \phi(z,\alpha)dz}. \tag{A1}$$

Simple analytical expressions for the MED are available in the literature.[45,46] If elastic-scattering effects are neglected, Eq. (A1) simplifies to

$$D^{SLA} = \lambda_{in}\cos\alpha. \tag{A2}$$

Note that the expression

$$L_{MED} = \frac{1}{\cos\alpha}\frac{\int_0^\infty z\phi(z,\alpha)dz}{\int_0^\infty \phi(z,\alpha)dz} \tag{A3}$$

can be considered as the EAL for the determination of the MED since, after replacing λ_{in} in Eq. (A2) by L_{MED}, the MED given by Eq. (A1) is obtained. It is also frequent practice to introduce the ratio

$$R_{MED} = \frac{D}{D^{SLA}}, \tag{A4}$$

since in this way the elastic-scattering effects can be conveniently visualized. It has been found that that Eq. (A4) can be approximated by a simple predictive formula valid for the magic-angle XPS configuration (angle $\psi = 55°$) and for photoelectron emission angles varying in the range $0° \le \alpha \le 50°$,[45]

$$R_{MED} = 1 - 0.736\omega. \tag{A5}$$

The relevant analysis was performed for selected photoelectron and Auger-electron lines with kinetic energies up to 2016 eV.

Tanuma *et al.*[93] derived a predictive formula for the MED of photoelectrons emitted by linearly polarized x rays. This parameter was calculated for an experimental configuration in which the x-ray beam and the polarization vector were in a plane normal to the sample surface. These calculations were performed in the energy range from 50 eV to 10 000 eV. Tanuma *et al.* also assumed the validity of the dipole approximation. Furthermore, the MEDs were determined for three elements (Si, Cu, and Au) and for arbitrarily assumed values of the asymmetry parameter in the expression for the photoionization cross section (i.e., β values from $\beta = -1$ to $\beta = 2$). Their proposed predictive formula has the following form:

$$D = 0.981 g(\beta)(1 - 0.736\omega)\lambda_{in}\cos\alpha, \tag{A6}$$

where

$$g(\beta) = 1.0 - 0.102\beta + 0.0577\beta^2 - 0.0133\beta^3, \tag{A7}$$

where ω in Eq. (A6) is the single-scattering albedo. The predictive formula given by Eqs. (A6) and (A7) was found to be valid for asymmetry parameters in the range $-0.5 \le \beta \le 2$ and for photoelectron emission angles ranging from 0° to 40°. Jablonski[92] calculated MED values for a similar experimental configuration and for a more realistic model based on non-dipolar photoemission cross sections. These calculations were performed for four elements (Si, Cu, Ag, and Au) and 13 photoelectrons lines. The actual values of all non-dipolar parameters were taken into account. A simple predictive formula was found to be valid for emission angles in the range $0° \le \alpha \le 50°$,

$$R_{MED} = 1 - 0.831\omega. \tag{A8}$$

The relative rms deviation of the calculated MEDs from Eq. (A8) was 1.86%. Equation (A8) is believed to be more accurate than Eq. (A6) for the estimation of MEDs related to the considered experimental geometry.

8.2. Information depth

The information depth (ID) is a useful parameter for defining the sampling depth of an XPS analysis for a given configuration. It is defined as “the maximum depth, normal to the surface, from which useful information is obtained” (Ref. 1, Definition 4.246). Typically, the ID is considered as the depth from which a specified percentage, P, of the signal intensity originates. For a homogeneous solid, the ID designated by S can be calculated by solving a nonlinear equation in one unknown,[45,47]

$$\frac{\int_0^S \phi(z,\alpha)dz}{\int_0^\infty \phi(z,\alpha)dz} = \frac{P}{100}, \tag{A9}$$

where P is often chosen to be 95% or 99%. For the SLA theoretical model, we have

$$S^{SLA} = \lambda_{in}\cos\alpha \ln\left[\frac{1}{1-(P/100)}\right]. \tag{A10}$$

The influence of elastic-electron scattering on the ID is conveniently illustrated by the following ratio:

$$R_{ID} = \frac{S}{S^{SLA}}. \tag{A11}$$

From an analysis of ID values calculated for 12 photoelectron lines and 9 Auger transitions, the following predictive formula was derived:[45]

$$R_{ID} = 1 - 0.787\omega. \tag{A12}$$

This formula is valid for the magic-angle geometry, emission angles, α, ranging from 0° to 50°, and electron energies from 61 eV to 2016 eV.

8.3. The CF function

As mentioned in Sec. 3.3, a useful parameter in determination of the depth of a thin marker layer is the ratio of photoelectron intensities from the marker layer that are obtained from a theoretical model in which elastic-scattering effects are taken into account and from the oversimplified straight-line approximation model in which these effects are neglected.[114] It has been proposed to denote this ratio by[22,23]

$$CF = I_x / I_x^{SLA}. \tag{A13}$$

The photoelectron signal intensities from an infinitely thin marker can be calculated using theoretical models developed for calculations of the emission depth distribution function (EMDDF) in which photoionization cross sections for the marker material are used, and the electron transport is described by the properties of the matrix material. We then have[22,23,145,146]

$$CF = \frac{\phi(z,\alpha)}{\phi^{SLA}(z,\alpha)}. \tag{A14}$$

A simple and convenient predictive formula for the *CF* function was derived from voluminous data on signal intensities obtained from Monte Carlo simulations (10 800 runs for different materials, photoelectron lines, experimental geometries, and marker depths),[22,23,145]

$$\begin{aligned} CF = {} & \exp(-0.157\,764\tau - 1.251\,32) \\ & + \exp(-0.056\,241\,7\tau^2 + 0.006\,988\,49\tau - 0.201\,962), \end{aligned} \tag{A15}$$

where τ is a non-dimensional measure of depth,

$$\tau = \frac{z}{\omega\lambda_{tr}}. \tag{A16}$$

Applications of this formula are limited by the following conditions:

1. The emission angle, α, is close to the surface normal, i.e., $0° \le \alpha \le 30°$.
2. The angle ψ between the x-ray beam and the analyzer axis varies in the range from 45° to 65°.

3. The transport mean free path varies in the range $1.3\lambda_{in} \leq \lambda_{tr} \leq 7\lambda_{in}$.
4. The depth of the marker layer does not exceed 5 nm.
5. The photoelectron kinetic energies corresponded to XPS with Mg Kα radiation; thus, the largest considered kinetic energy for Au $4f_{7/2}$ photoelectrons was 1169 eV.

It turned out that an accurate EMDDF formula (and consequently the *CF* function) can be derived from analytical transport theory initially derived by Tilinin *et al.*[27] and corrected in later reports.[6,7] Very good agreement between this approach and results of Monte Carlo simulations was shown by Jablonski.[147] The values of *CF* are available from the NIST SRD 82 database.[40] These values are calculated from the EMDDF of Eq. (6) with corrected functions $\phi_i(z, \alpha, \omega)$ and $\phi_a(z, \alpha, \theta_x, \psi, \omega)$. The *CF* functions from this source can be obtained for any experimental geometry and for electron energies up to 2 keV.

8.4. PEDs and partial intensities

Werner *et al.*[148] generalized the definition of the EMDDF by introducing a new function that takes inelastic-scattering events of photoelectrons into account. The partial escape distribution (PED) is defined as follows: "… the probability distribution for the process in which an electron generated in a certain depth interval will escape from the surface with a direction in a certain angular interval after experiencing a certain number, n, of inelastic scattering processes in the sample." PEDs for different values of n are useful in the analysis of the spectral shape on the low-energy side of a selected peak from a thin marker layer at a certain depth.[148,149] A convenient expression for calculations of PEDs is[147,150]

$$P_n(z,\alpha) = (-1)^n \frac{\nu^n}{n!}\frac{d^n\phi(z,\alpha)}{d\nu^n}, \tag{A17}$$

where $\nu = (\lambda_{in})^{-1}$.

Simulation of electron spectra using the so-called partial intensity approach[151,152] requires knowledge of partial intensities that are defined as "the total number of electrons in an electron spectrum, originating from a given Auger transition or photoelectric transition, or associated with primary electrons backscattered from a surface per unit of excitation or of backscattering, that reach the detector after participating in a given number of inelastic interactions of a given type" (Ref. 1, Definition 4.323). For a given number of inelastic collisions, n, the partial intensity, C_n, is related to the PED by

$$C_n = \int_0^\infty P_n(z,\alpha)dz. \tag{A18}$$

One can prove that Eq. (A18) can be transformed to a form that is useful when the dependence of the signal intensity on the IMFP is known,[150]

$$C_n = (-1)^n \frac{\nu^n}{n!}\frac{d^n(I_x)}{d\nu^n}. \tag{A19}$$

The values of partial intensities obtained from Eq. (A19) well agree with the values obtained from Monte Carlo simulations.[150,153]

8.5. Backscattering correction factor

The term known initially as the backscattering factor was introduced into the formalism of quantitative AES to correct the calculated signal intensity for an Auger-electron contribution due to inner-shell ionizations from primary electrons that had been backscattered from the "bulk" of a solid to the surface region from which Auger electrons can reach the detector. However, in certain experimental settings, assumptions in early theoretical models of AES turned out to be invalid.[154] Consequently, a generalized term called the backscattering correction factor (BCF) was proposed, which was defined as follows: "factor equal to the ratio of the total Auger-electron current arising from ionizations in the sample caused by both the primary electrons and the backscattered electrons to the Auger electron current arising directly from the primary electrons" (Ref. 1, Definition 7.2).

In one of the notes accompanying this definition, it is stated: "In simple theories, evaluations of the backscattering factor can be based on the assumption that the primary-electron beam is unchanged, in intensity, energy, or direction, within the information depth for Auger-electron emission. This assumption is progressively less useful as the primary energy becomes closer to the core-level ionization energy for the relevant Auger transition or for increasing angles of incidence of the primary electrons. In such cases, a more advanced theory of electron transport should be used." It has been shown that the BCF derived from an advanced theory can be expressed by[154,155]

$$R_{AES} = \int_0^\infty \Phi(E_c, E_0, \theta_0)\phi(z,\alpha)dz, \tag{A20}$$

where $\Phi(E_c, E_0, \theta_0)$ is the excitation depth distribution function (EXDDF) describing the number of ionizations as a function of depth, E_c is the threshold energy for inner-shell ionization, E_0 is the primary-electron energy, and θ_0 is the primary-electron incidence angle with respect to the surface normal. We note that the BCF depends on the EXDDF as well as the EMDDF for the signal electrons.

BCFs can also be estimated from a well-known formula based on a simplified theory of electron transport in which the primary beam is assumed to be unchanged in the surface region,[154]

$$R_{AES} = 1 + \frac{\cos\theta_0}{I_0\sigma_i(E_0)}\int_{E_c}^{E_0}\int_0^{\pi/2} I_B(E,\alpha)\sigma_i(E)\sec\alpha\, d\alpha\, dE, \tag{A21}$$

where $I_B(E, \alpha)$ is the energy and angular distribution of backscattered electrons and $\sigma_i(E)$ is the inner-shell ionization cross section for an electron energy E. The latter parameter can be conveniently taken from the NIST SRD 164 database.[156]

BCF values corresponding to the simplified and advanced theories of electron transport can be obtained from the MC simulations implemented in the NIST SRD 154 database.[157] These BCFs are calculated from Eqs. (A20) and (A21) to facilitate estimation of the systematic error due to the use of the simplified theory, which is typically used in quantitative AES. Furthermore, the NIST SRD 164 database visualizes the shape of the functions $\phi(z, \alpha)$, $\Phi(E_c, E_0, \theta_0)$, and $I_B(E, \alpha)$ during progress of the simulations.

9. References

[1] ISO 18115-1, *Surface Chemical Analysis—Vocabulary, Part 1: General Terms and Terms Used in Spectroscopy* (International Organization for Standardization, Geneva, 2013), https://myavs.avs.org/eweb/StartPage.aspx?Site=AVS and https://www.emsl.pnnl.gov/emslweb/vocabulary.

[2]C. J. Powell and A. Jablonski, "Progress in quantitative surface analysis by X-ray photoelectron spectroscopy: Current status and perspectives," J. Electron Spectrosc. Relat. Phenom. **178-179**, 331–346 (2010).

[3]S. Tougaard, "Energy loss in XPS: Fundamental processes and applications for quantification, non-destructive depth profiling and 3D imaging," J. Electron Spectrosc. Relat. Phenom. **178-179**, 128–153 (2010).

[4]N. S. Faradzhev, S. B. Hill, and C. J. Powell, "Quantitative analysis of trace levels of surface contamination by X-ray photoelectron spectroscopy. Part II: Systematic uncertainties and absolute quantification," Surf. Interface Anal. **49**, 1214–1224 (2017).

[5]C. J. Powell and A. Jablonski, "Surface sensitivity of X-ray photoelectron spectroscopy," Nucl. Instrum. Methods Phys. Res. **601**, 54–65 (2009).

[6]A. Jablonski and C. J. Powell, "The electron attenuation length revisited," Surf. Sci. Rep. **47**, 33–92 (2002).

[7]C. J. Powell and A. Jablonski, "Electron effective attenuation lengths for applications in Auger electron spectroscopy and X-ray photoelectron spectroscopy," Surf. Interface Anal. **33**, 211–229 (2002).

[8]B. L. Henke, "Ultrasoft X-ray reflection, refraction, and production of photoelectrons (100-1000-eV region)," Phys. Rev. A **6**, 94–104 (1972).

[9]C. S. Fadley, R. J. Baird, W. Siekhaus, T. Novakov, and S. Å. L. Bergström, "Surface analysis and angular distributions in X-ray photoelectron spectroscopy," J. Electron Spectrosc. Relat. Phenom. **4**, 93–137 (1974).

[10]C. S. Fadley, "Solid state—and surface—analysis by means of angular-dependent X-ray photoelectron spectroscopy," in *Progress in Solid State Chemistry*, edited by G. Somorjai and J. McCaldin (Pergamon Press, New York, 1976), Vol. 11, pp. 265–343.

[11]C. J. Powell, "Attenuation lengths of low-energy electrons in solids," J. Electron Spectrosc. Relat. Phenom. **44**, 29–46 (1974).

[12]C. R. Brundle, "Application of electron spectroscopy to surface studies," J. Vac. Sci. Technol. **11**, 212–224 (1974).

[13]I. Lindau and W. E. Spicer, "Probing depth in photoemission and Auger-electron spectroscopy," J. Electron Spectrosc. Relat. Phenom. **3**, 409–413 (1974).

[14]M. P. Seah and W. A. Dench, "Quantitative electron spectroscopy of surfaces: A standard data base for electron inelastic mean free paths in solids," Surf. Interface Anal. **1**, 2–11 (1979).

[15]M. L. Tarng and G. K. Wehner, "Escape length of Auger electrons," J. Appl. Phys. **44**, 1534–1540 (1973).

[16]C. J. Powell and A. Jablonski, "Evaluation of calculated and measured electron inelastic mean free paths near solid surfaces," J. Phys. Chem. Ref. Data **28**, 19–62 (1999).

[17]A. Jablonski, "Elastic scattering and quantification in AES and XPS," Surf. Interface Anal. **14**, 659–685 (1989).

[18]W. H. Gries and W. Werner, "Take-off angle and film thickness dependences of the attenuation length of X-ray photoelectrons by a trajectory reversal method," Surf. Interface Anal. **16**, 149–153 (1990).

[19]P. J. Cumpson, "Elastic scattering corrections in AES and XPS: I. Two rapid Monte Carlo methods for calculating the depth distribution function," Surf. Interface Anal. **20**, 727–741 (1993).

[20]A. Jablonski and C. J. Powell, "Comparisons of practical attenuation lengths obtained from different algorithms for application in XPS," Surf. Sci. **520**, 78–96 (2002).

[21]W. S. M. Werner, "Towards a universal curve for electron attenuation: Elastic scattering data for 45 elements," Surf. Interface Anal. **18**, 217–228 (1992).

[22]A. Jablonski and S. Tougaard, "Practical correction formula for elastic electron scattering effects in attenuation of Auger electrons and photoelectrons," Surf. Interface Anal. **26**, 17–29 (1998).

[23]A. Jablonski and S. Tougaard, "Evaluation of validity of the depth-dependent correction formula (CF) for elastic electron scattering effects in AES and XPS," Surf. Interface Anal. **26**, 374–384 (1998).

[24]A. Jablonski, "Emission depth distribution function for photoelectrons emitted by laboratory hard X-ray radiation sources," J. Electron Spectrosc. Relat. Phenom. **195**, 26–42 (2014).

[25]A. Jablonski and H. Ebel, "Comparison of electron attenuation lengths and escape depths with inelastic mean free paths," Surf. Interface Anal. **11**, 627–632 (1988).

[26]W. S. M. Werner and I. S. Tilinin, "Attenuation of electrons in non-crystalline solids," Surf. Sci. **268**, L319–L324 (1992).

[27]I. S. Tilinin, A. Jablonski, J. Zemek, and S. Hucek, "Escape probability of signal photoelectrons from non-crystalline solids: Influence of anisotropy of photoemission," J. Electron Spectrosc. Relat. Phenom. **87**, 127–140 (1997).

[28]S. Hucek, J. Zemek, and A. Jablonski, "Escape probability of O 1s photoelectrons leaving copper oxide," J. Electron Spectrosc. Relat. Phenom. **85**, 257–262 (1997).

[29]J. Zemek, S. Hucek, A. Jablonski, and I. S. Tilinin, "Escape probability of s-photoelectrons leaving aluminium and copper oxides," Surf. Interface Anal. **26**, 182–187 (1998).

[30]J. Zemek and S. Hucek, "Experiments to determine the escape probability of photoelectrons," Fresenius' J. Anal. Chem. **363**, 156–159 (1999).

[31]S. Hucek, J. Zemek, A. Jablonski, and I. S. Tilinin, "Emission depth distribution function of Al 2s photoelectrons in Al_2O_3," Surf. Rev. Lett. **7**, 109–114 (2000).

[32]J. Zemek, P. Jiricek, S. Hucek, A. Jablonski, and B. Lesiak, "Escape probability of photoelectrons from silver sulphide," Surf. Sci. **473**, 8 (2001).

[33]W. S. M. Werner, "Electron transport for spectrum analysis and experiment design," J. Electron Spectrosc. Relat. Phenom. **178-179**, 154–177 (2010).

[34]I. S. Tilinin and W. S. M. Werner, "Escape probability of Auger electrons from noncrystalline solids: Exact solution in the transport approximation," Phys. Rev. B **46**, 13739–13746 (1992).

[35]M. B. Trzhaskovskaya, V. I. Nefedov, and V. G. Yarzhemsky, "Photoelectron angular distribution parameters for elements Z=1 to Z=54 in the photoelectron energy range 100-5000 eV," At. Data Nucl. Data Tables **77**, 97–159 (2001).

[36]M. B. Trzhaskovskaya, V. I. Nefedov, and V. G. Yarzhemsky, "Photoelectron angular distribution parameters for elements Z=55 to Z=100 in the photoelectron energy range 100-5000 eV," At. Data Nucl. Data Tables **82**, 257–311 (2002).

[37]M. B. Trzhaskovskaya, V. K. Nikulin, V. I. Nefedov, and V. G. Yarzhemsky, "Non-dipole second order parameters of the photoelectron angular distribution for elements z=1-100 in the photoelectron energy range 1-10 keV," At. Data. Nucl. Data Tables **92**, 245 (2006).

[38]S. Chandrasekhar, *Radiative Transfer* (Dover Publications, Inc., New York, 1960).

[39]A. Jablonski, "The Chandrasekhar function revisited," Comput. Phys. Commun. **196**, 416–428 (2015).

[40]C. J. Powell and A. Jablonski, NIST Electron Effective-Attenuation-Length Database, Version 1.3, Standard Reference Data Program Database 82, US Department of Commerce, National Institute of Standards and Technology, Gaithersburg, MD, 2011, https://www.nist.gov/srd/nist-standard-reference-database-82.

[41]A. Jablonski and C. J. Powell, "Improved algorithm for calculating transport cross sections of electrons with energies from 50 eV to 30 keV," Phys. Rev. B **76**, 085123 (2007).

[42]W. S. M. Werner, W. Smekal, and C. J. Powell, NIST Database for the Simulation of Electron Spectra for Surface Analysis, Version 2.1, Standard Reference Data Program SRD 100, U.S. Department of Commerce, National Institute of Standards and Technology, Gaithersburg, MD, 2017, https://www.nist.gov/srd/nist-standard-reference-database-100.

[43]W. Smekal, W. S. M. Werner, and C. J. Powell, "Simulation of electron spectra for surface analysis (SESSA): A novel software tool for quantitative auger-electron spectroscopy and X-ray photoelectron spectroscopy," Surf. Interface Anal. **37**, 1059–1067 (2005).

[44]A. Jablonski, "Photoelectron transport in the surface region of solids: Universal analytical formalism for quantitative applications of electron spectroscopies," J. Phys. D: Appl. Phys. **48**, 075301 (2015); Erratum **49**, 289501 (2016).

[45]A. Jablonski and C. J. Powell, "Practical expressions for the mean escape depth, the information depth, and the effective attenuation length in auger-electron spectroscopy and x-ray photoelectron spectroscopy," J. Vac. Sci. Technol., A **27**, 253–261 (2009).

[46]A. Jablonski and C. J. Powell, "Effective attenuation lengths for photoelectrons emitted by high-energy laboratory sources," J. Electron Spectrosc. Relat. Phenom. **199**, 27–37 (2015).

[47]A. Jablonski, "Parameterization of HAXPES photoelectrons with kinetic energies up to 10 keV," Appl. Surf. Sci. **346**, 503–519 (2015).

[48] S. Tanuma, C. J. Powell, and D. R. Penn, "Calculations of electron mean free paths. IX. Data for 41 elemental solids over the 50 eV to 30 keV range," Surf. Interface Anal. **43**, 689–713 (2011).

[49] M. P. Seah and I. S. Gilmore, "Simplified equations for correction parameters for elastic scattering effects in AES and XPS for Q, β and attenuation lengths," Surf. Interface Anal. **31**, 835–846 (2001).

[50] M. P. Seah, "Simple universal curve for the energy-dependent electron attenuation length for all materials," Surf. Interface Anal. **44**, 1353–1359 (2012).

[51] A. Jablonski and S. Tougaard, "Comparison of the attenuation lengths and the inelastic mean free path for photoelectrons in silver," J. Vac. Sci. Technol., A **8**, 106–116 (1990).

[52] A. Jablonski, "Photoemission from ultrathin overlayers," J. Electron Spectrosc. Relat. Phenom. **185**, 498–508 (2012).

[53] A. Jablonski, "Evaluation of procedures for overlayer thickness determination from XPS intensities," Surf. Sci. **688**, 14–24 (2019).

[54] A. Jablonski and C. J. Powell, "Effective attenuation lengths for quantitative determination of surface composition by Auger-electron spectroscopy and X-ray photoelectron spectroscopy," J. Electron Spectrosc. Relat. Phenom. **218**, 1–12 (2017).

[55] A. Jablonski and J. Zemek, "Overlayer thickness determination by XPS using the multiline approach," Surf. Interface Anal. **41**, 193–204 (2009).

[56] C. J. Powell, W. S. M. Werner, W. Smekal, and G. Tasneem, "Effective attenuation lengths for photoelectrons in thin films of silicon oxynitride and hafnium oxynitride on silicon," Surf. Interface Anal. **45**, 628 (2013).

[57] T. Graber, F. Forster, A. Schöll, and F. Reinert, "Experimental determination of the attenuation length of electrons in organic molecular solids: The example of PTCDA," Surf. Sci. **605**, 878–882 (2011).

[58] L. Kilian, E. Umbach, and M. Sokolowski, "Molecular beam epitaxy of organic films investigated by high resolution low energy electron diffraction (SPA-LEED): 3,4,9,10-perylenetetracarboxylicacid-dianhydride (PTCDA) on Ag(111)," Surf. Sci. **573**, 359–378 (2004).

[59] W. F. Egelhoff, "X-ray photoelectron and Auger-electron forward scattering: A new tool for studying epitaxial growth and core-level binding-energy shifts," Phys. Rev. B **30**, 1052 (1984).

[60] W. F. Egelhoff, "X-ray photoelectron and Auger electron forward scattering: A new tool for surface crystallography," Crit. Rev. Solid State Mater. Sci. **16**, 213–235 (1990).

[61] H. E. Bishop, "The effects of photoelectron diffraction on quantitative X-ray photoelectron spectroscopy," Surf. Interface Anal. **17**, 197–202 (1991).

[62] M. P. Seah and S. J. Spencer, "Energy dependence of the electron attenuation length in silicon dioxide," Meas. Sci. Technol. **22**, 115602 (2011).

[63] S. Tanuma, C. J. Powell, and D. R. Penn, "Calculations of electron inelastic mean free paths. V. Data for 14 organic compounds over the 50-2000 eV range," Surf. Interface Anal. **21**, 165–176 (1994).

[64] F. Salvat, A. Jablonski, and C. J. Powell, "ELSEPA: Dirac partial-wave calculation of elastic scattering of electrons and positrons by atoms, positive ions and molecules," Comput. Phys. Commun. **165**, 157–190 (2005).

[65] M. P. Seah, "Ultrathin SiO_2 on Si. VI. Evaluation of uncertainties in thickness measurement using XPS," Surf. Interface Anal. **37**, 300–309 (2005).

[66] Certain commercial products are identified to specify the experimental conditions. This identification does not imply that the products are recommended or endorsed by the National Institute of Standards and Technology, or that they are necessarily the most suitable for the purposes described.

[67] M. P. Seah and R. White, "Ultrathin SiO_2 on Si. III. Mapping the layer thickness efficiently by XPS," Surf. Interface Anal. **33**, 960 (2002).

[68] J. M. Hill, D. G. Royce, C. S. Fadley, L. F. Wagner, and F. J. Grunthaner, "Properties of oxidized silicon as determined by angular-dependent X-ray photoelectron spectroscopy," Chem. Phys. Lett. **44**, 225 (1976).

[69] M. P. Seah, S. J. Spencer, F. Bensebaa, I. Vickridge, H. Danzebrink, M. Krumrey, T. Gross, W. Oesterle, E. Wendler, B. Rheinländer, Y. Azuma, I. Kojima, N. Suzuki, M. Suzuki, S. Tanuma, D. W. Moon, H. J. Lee, H. M. Cho, H. Y. Chen, A. T. S. Wee, T. Osipowicz, J. S. Pan, W. A. Jordaan, R. Hauert, U. Klotz, C. van der Marel, M. Verheijen, Y. Tamminga, C. Jeynes, P. Bailey, S. Biswas, U. Falke, N. V. Nguyen, D. Chandler-Horowitz, J. R. Ehrstein, D. Muller, and J. A. Dura, "Critical review of the current status of thickness measurements for ultrathin SiO_2 on Si: V. Results of a CCQM pilot study," Surf. Interface Anal. **36**, 1269 (2004).

[70] M. P. Seah, W. E. S. Unger, H. Wang, W. Jordaan, Th. Gross, J. A. Dura, D. W. Moon, P. Totarong, M. Krumrey, R. Hauert, and M. Zhiqiang, "Ultra-thin SiO_2 on Si: IX. Absolute measurements of the amount of silicon oxide as a thickness of SiO_2 on Si," Surf. Interface Anal. **41**, 430 (2009).

[71] M. P. Seah and S. J. Spencer, "Ultrathin SiO_2 on Si. II. Issues in quantification of the oxide thickness," Surf. Interface Anal. **33**, 640 (2002).

[72] S. Tanuma, C. J. Powell, and D. R. Penn, "Calculations of electron inelastic mean free paths: III. Data for 15 inorganic compounds over the 50-2000 eV range," Surf. Interface Anal. **17**, 927–939 (1991).

[73] C. J. Powell and A. Jablonski, "Effects of elastic-electron scattering on measurements of silicon dioxide film thicknesses by X-ray photoelectron spectroscopy," J. Electron Spectrosc. Relat. Phenom. **114-116**, 1139–1143 (2001).

[74] M. P. Seah and S. J. Spencer, "Ultrathin SiO_2 on Si. VII. Angular accuracy in XPS and an accurate attenuation length," Surf. Interface Anal. **37**, 731 (2005).

[75] H. Shinotsuka, S. Tanuma, C. J. Powell, and D. R. Penn, "Calculations of electron inelastic mean free paths. XII. Data for 42 inorganic compounds over the 50 eV to 200 keV range with the full Penn algorithm," Surf. Interface Anal. **51**, 427 (2019).

[76] C. J. Powell, W. S. M. Werner, and W. Smekal, "Refined calculations of effective attenuation lengths for SiO_2 film thicknesses by X-ray photoelectron spectroscopy," Appl. Phys. Lett. **89**, 252116 (2006).

[77] K. J. Kim and M. P. Seah, "Ultrathin SiO_2 on Si. VIII. Accuracy of method, linearity and attenuation lengths for XPS," Surf. Interface Anal. **39**, 512 (2007).

[78] K. J. Kim, Y.-S. Kim, J. S. Jang, J. W. Kim, and K. W. Kim, "A mutual calibration method to certify the thickness of nanometre oxide films," Metrologia **45**, 507 (2008).

[79] K. J. Kim, J. S. Jang, J.-H. Lee, Y.-J. Jee, and C.-S. Jun, "Determination of the absolute thickness of ultrathin Al_2O_3 overlayers on Si(100) substrate," Anal. Chem. **81**, 8519 (2009).

[80] K. J. Kim, S. M. Lee, J. S. Jang, and M. Moret, "Thickness measurement of a thin hetero-oxide film with an interfacial oxide layer by X-ray photoelectron spectroscopy," Appl. Surf. Sci. **258**, 3552 (2012).

[81] S. Gurban, G. Gergely, J. Toth, D. Varga, A. Jablonski, and M. Menyhard, "Experimental determination of the inelastic mean free path (IMFP) of electrons in selected oxide films applying surface excitation correction," Surf. Interface Anal. **38**, 624 (2006).

[82] S. Tougaard, QUASES-Tougaard: Software for Quantitative XPS/AES of Surface Nano-Structures by Analysis of the Peak Shape and Background, QUASES Tougaard ApS, Odense, Denmark, 2011, http://www.quases.com.

[83] C. J. Powell and A. Jablonski, "Effective attenuation length dependence on photoelectron kinetic energy for gold from 1 keV to 10 keV: Role of island growth in overlayer experiments," J. Electron Spectrosc. Relat. Phenom. **236**, 27–32 (2019).

[84] P. J. Cumpson and M. P. Seah, "Elastic scattering corrections in AES. II. Estimating attenuation lengths and conditions required for their valid use in overlayer/substrate experiments," Surf. Interface Anal. **25**, 430–446 (1997).

[85] C. D. Wagner, L. E. Davis, and W. M. Riggs, "The energy dependence of the electron mean free path," Surf. Interface Anal. **2**, 53–55 (1980).

[86] C. J. Powell, "The energy dependence of electron attenuation lengths," Surf. Interface Anal. **7**, 256–262 (1985).

[87] J. Schweppe, R. D. Deslattes, T. Mooney, and C. J. Powell, "Accurate measurement of Mg and Al $K\alpha_{1,2}$ X-ray energy profiles," J. Electron Spectrosc. Relat. Phenom. **67**, 463–478 (1994).

[88] L. Kövér, "X-ray photoelectron spectroscopy using hard X-rays," J. Electron Spectrosc. Relat. Phenom. **178-179**, 241–257 (2010).

[89] C. S. Fadley and S. Nemšák, "Some future perspectives in soft- and hard- X-ray photoemission," J. Electron Spectrosc. Relat. Phenom. **195**, 409–422 (2014).

[90] *Hard X-Ray Photoelectron Spectroscopy (HAXPES)*, edited by J. C. Woicik (Springer, Cham; Heidelberg; New York; Dordrecht; London, 2016).

[91] R. D. Deslattes, E. G. Kessler, P. Indelicato, L. de Billy, E. Lindroth, and J. Anton, "X-ray transition energies: New approach to a comprehensive evaluation," Rev. Mod. Phys. **75**, 35 (2003).

[92] A. Jablonski, "Modeling and parameterization of photoelectrons emitted in condensed matter by linearly polarized synchrotron radiation," Surf. Sci. **667**, 121–137 (2018).

[93]S. Tanuma, H. Yoshikawa, H. Shinotsuka, and R. Ueda, "Calculations of mean escape depths of photoelectrons in elemental solids excited by linearly polarized X-rays for high-energy photoelectron spectroscopy," J. Electron Spectrosc. Relat. Phenom. **190**, 127–136 (2013).

[94]J. Rubio-Zuazo and G. R. Castro, "Effective attenuation length dependence on photoelectron kinetic energy for Au from 1 keV to 15 keV," J. Electron Spectrosc. Relat. Phenom. **184**, 384–390 (2011).

[95]A. Jablonski, "Database of correction parameters for the elastic scattering effects in XPS," Surf. Interface Anal. **23**, 29–37 (1995).

[96]A. Jablonski and J. Zemek, "Angular distribution of photoemission from amorphous and polycrystalline solids," Phys. Rev. B **48**, 4799–4805 (1993).

[97]A. Jablonski and C. J. Powell, "Elastic-electron-scattering effects on angular distribution in x-ray-photoelectron spectroscopy," Phys. Rev. B **50**, 4739–4748 (1994).

[98]A. Jablonski and C. J. Powell, "Elastic photoelectron-scattering effects in quantitative X-ray photoelectron spectroscopy," Surf. Sci. **606**, 644–651 (2012).

[99]A. Jablonski, "Angular distribution of photoelectrons emitted by the laboratory soft and hard X-ray radiation sources," J. Electron Spectrosc. Relat. Phenom. **189**, 81–95 (2013).

[100]A. Jablonski and I. S. Tilinin, "Towards a universal description of elastic scattering effects in XPS," J. Electron Spectrosc. Relat. Phenom. **74**, 207–229 (1995).

[101]A. Jablonski, "Universal quantification of elastic scattering effects in AES and XPS," Surf. Sci. **364**, 380–395 (1996).

[102]A. Jablonski and C. J. Powell, "Effective attenuation lengths in electron spectroscopies," J. Alloys Compd. **362**, 26–32 (2004).

[103]A. Jablonski, "Determination of surface composition by X-ray photoelectron spectroscopy taking into account elastic photoelectron collisions," Anal. Sci. **26**, 155–164 (2010).

[104]D. P. Woodruff, "Non-dipole effects in high-energy photoelectron emission; Identification and quantification using X-ray standing waves," Nucl. Instr. Meth. Phys. Res. A. **547**, 187–195 (2015).

[105]Y.-I. Suzuki, K. Nishizawa, N. Kurahaski, and T. Suzuki, "Effective attenuation length of an electron in liquid water between 10 and 600 eV," Phys. Rev. E **90**, 010302 (2014).

[106]B. Winter and M. Faubel, "Photoemission from liquid aqueous solutions," Chem. Rev. **106**, 1176–1211 (2006).

[107]H. Shinotsuka, B. Da, S. Tanuma, H. Yoshikawa, C. J. Powell, and D. R. Penn, "Calculations of electron inelastic mean free paths. XI. Data for liquid water for energies from 50 eV to 30 keV," Surf. Interface Anal. **49**, 238–252 (2017).

[108]D. Emfietzoglou, I. Kyriakou, R. Garcia-Molina, and I. Abril, "Inelastic mean free paths of low-energy electrons in condensed media: Beyond the standard models," Surf. Interface Anal. **49**, 4–10 (2017).

[109]R. Garcia-Molina, I. Abril, I. Kyriakou, and D. Emfietzoglou, "Inelastic scattering and energy loss of swift electron beams in biologically relevant materials," Surf. Interface Anal. **49**, 11–17 (2017).

[110]H. T. Nguyen-Truong, "Low-energy electron inelastic mean free paths for liquid water," J. Phys.: Condens Matter **30**, 155101 (2018).

[111]G. Olivieri, K. M. Parry, R. D'Auria, D. J. Tobias, and M. A. Brown, "Specific anion effects at the aqueous solution-air interface: MD simulations, SESSA calculations, and photoelectron spectroscopy experiments," J. Phys. Chem. B **122**, 910–918 (2018).

[112]S. Tougaard, H. S. Hansen, and M. Neumann, "Test on validity of recent formalism for quantitative XPS/AES," Surf. Sci. **244**, 125–134 (1991).

[113]S. Tougaard, "Accuracy of the non-destructive surface nanostructure quantification technique based on analysis of the XPS or AES peak shape," Surf. Interface Anal. **26**, 249–269 (1998).

[114]S. Tougaard and A. Jablonski, "Quantitative XPS: Influence of elastic electron scattering in quantification by peak shape analysis," Surf. Interface Anal. **25**, 404–408 (1997).

[115]S. Tanuma, in *Surface Analysis by Auger and X-Ray Photoelectron Spectroscopy*, edited by D. Briggs and J. T. Grant (IM Publications and SurfaceSpectra Ltd., Chichester, Manchester, UK, 2003), p. 259.

[116]A. G. Shard, "A straightforward method for interpreting XPS data from core-shell nanoparticles," J. Phys. Chem. C **116**, 16806–16813 (2012).

[117]C. J. Powell, W. S. M. Werner, A. G. Shard, and D. G. Castner, "Evaluation of two methods for determining shell thicknesses of core-shell nanoparticles by X-ray photoelectron spectroscopy," J. Phys. Chem. C **120**, 22730–22738 (2016).

[118]C. J. Powell, W. S. M. Werner, H. Kalbe, A. G. Shard, and D. G. Castner, "Comparisons of analytical approaches for determining shell thicknesses of core-shell nanoparticles by X-ray photoelectron spectroscopy," J. Phys. Chem. C **122**, 4073–4082 (2018).

[119]D. J. H. Cant, Y.-C. Wang, D. G. Castner, and A. G. Shard, "A technique for calculation of shell thicknesses for core-shell-shell nanoparticles from XPS data," Surf. Interface Anal. **48**, 274–282 (2016).

[120]A. Jablonski, "Analytical theory of elastic electron backscattering from elements, alloys and compounds: Comparison with experimental data," J. Electron Spetrosc. Relat. Phenom. **206**, 24–45 (2016).

[121]C. J. Powell and A. Jablonski, "Evaluation of electron inelastic mean free paths for selected elements and compounds," Surf. Interface Anal. **29**, 108–114 (2000).

[122]C. J. Powell, "Practical guide for inelastic mean free paths, effective attenuation lengths, mean escape depths, and information depths in X-ray photoelectron spectroscopy," J. Vac. Sci. Technol., A **38**, 023209 (2020).

[123]H. Shinotsuka, S. Tanuma, C. J. Powell, and D. R. Penn, "Calculations of electron inelastic mean free paths. X. Data for 41 elemental solids over the 50 eV to 200 keV range with the relativistic Penn algorithm," Surf. Interface Anal. **47**, 871–888 (2015).

[124]D. R. Penn, "Electron mean free path calculations using a model dielectric function," Phys. Rev. B **35**, 482–486 (1987).

[125]H. Bethe, "Zur theorie des durchgangs schneller korpuskularstrahlen durch materie," Ann. Phys. **397**, 325–400 (1930).

[126]S. Tanuma, C. J. Powell, and D. R. Penn, "Calculations of electron inelastic mean free paths. II. Data for 27 elements over the 50-2000 eV range," Surf. Interface Anal. **17**, 911–926 (1991).

[127]S. Tanuma, C. J. Powell, and D. R. Penn, "Calculation of electron inelastic mean free paths (IMFPs). VII. Reliability of the TPP-2M IMFP predictive equation," Surf. Interface Anal. **35**, 268–275 (2003).

[128]M. P. Seah, "An accurate and simple universal curve for the energy-dependent electron inelastic mean free path," Surf. Interface Anal. **44**, 497–503 (2012).

[129]*American Institute of Physics Handbook*, 3rd ed., edited by D. E. Gray (McGraw-Hill, New York, 1972), pp. 9–17.

[130]W. H. Strehlow and E. L. Cook, "Compilation of energy band gaps in elemental and binary compound semiconductors and insulators," J. Phys. Chem. Ref. Data **2**, 163–193 (1973).

[131]*CRC Handbook of Chemistry and Physics*, 95th ed., edited by W. M. Haynes (CRC Press, Boca Raton, 2014), pp. 12-90–12-99.

[132]C. Kittel, *Introduction to Solid State Physics*, 6th ed. (John Wiley, New York, 1986), p. 185.

[133]C. M. Wolfe, J. Holonyak, and G. E. Stillman, *Physical Properties of Semiconductors* (Prentice-Hall, Englewood Cliffs, 1989).

[134]S. Tanuma, C. J. Powell, and D. R. Penn, "Calculations of electron inelastic mean free paths (IMFPs). IV. Evaluation of calculated IMFPs and the predictive IMFP formula TPP-2 for electron energies between 50 and 2000 eV," Surf. Interface Anal. **20**, 77–89 (1993).

[135]O. Kubaschewski and C. B. Alcock, *Metallurgical Thermochemistry*, 5th ed. (Pergamon Press, Oxford, 1979).

[136]W. H. Gries, "Calculations of the electron inelastic mean free paths of X-ray photoelectrons and Auger electrons," Surf. Interface Anal. **24**, 38–50 (1996).

[137]S. Tanuma, C. J. Powell, and D. R. Penn, "Calculations of electron inelastic mean free paths (IMFPs). VI. Analysis of the Gries inelastic scattering model and predictive IMFP equation," Surf. Interface Anal. **25**, 25–35 (1997).

[138]C. J. Powell and A. Jablonski, NIST Electron Inelastic-Mean-Free-Path Database, Version 1.2, Standard Reference Data Program Database 71, US Department of Commerce, National Institute of Standards and Technology, Gaithersburg, MD, 2010, https://www.nist.gov/srd/nist-standard-reference-database-71.

[139]C. J. Powell, A. Jablonski, W. S. M. Werner, and W. Smekal, "Characterization of thin films on the nanometer scale by Auger electron spectroscopy and X-ray photoelectrons spectroscopy," Appl. Surf. Sci. **239**, 470–480 (2005).

[140] A. Jablonski and C. J. Powell, "Evaluation of correction parameters for elastic-scattering effects in X-ray photoelectron spectroscopy and Auger-electron spectroscopy," J. Vac. Sci. Technol., A **15**, 2095–2106 (1997).

[141] C. J. Powell, "The quest for universal curves to describe the surface sensitivity of electron spectroscopies," J. Electron Spectrosc. Relat. Phenom. **47**, 197–214 (1988).

[142] A. Barbier, "Generalized model for interface description," Surf. Science **406**, 69–81 (1998).

[143] C. Argile and G. E. Rhead, "Adsorbed layer and thin-film growth modes monitored by Auger-electron spectroscopy," Surf. Sci. Rep. **10**, 277–356 (1989).

[144] See https://www.nist.gov/srd/surface-data for more information on and access to the NIST databases listed in Table 2.

[145] A. Jablonski and S. Tougaard, "Escape probability of electrons from solids. Influence of elastic electron scattering," Surf. Sci. **432**, 211–227 (1999).

[146] A. Jablonski, "Elastic photoelectron scattering effects in the XPS analysis of stratified samples," J. Phys. D: Appl. Phys. **45**, 315302 (2012).

[147] A. Jablonski, "Role of the emission depth distribution function in quantification of electron spectroscopies," Surf. Sci. **586**, 115–128 (2005).

[148] W. S. M. Werner, I. S. Tilinin, H. Beilschmidt, and M. Hayek, "Simultaneous background subtraction and depth profile determination from AES/XPS measurements," Surf. Interface Anal. **21**, 537–545 (1994).

[149] I. S. Tilinin, A. Jablonski, and S. Tougaard, "Emission-depth dependence of the signal photoelectron energy spectrum," Surf. Interface Anal. **25**, 119–131 (1997).

[150] A. Jablonski, "A note on calculations of photoelectron partial intensities for energies reaching 4000 eV," J. Electron Spectrosc. Relat. Phenom. **234**, 34–46 (2019).

[151] W. S. M. Werner, "Electron transport in solids for quantitative surface analysis," Surf. Interface Anal. **31**, 141–176 (2001).

[152] W. S. M. Werner, "Simulation of electron spectra for surface analysis using the partial-intensity approach (PIA)," Surf. Interface Anal. **37**, 846–860 (2005).

[153] M. Novák, N. Pauly, and A. Dubus, "Polarization and dipole effects in hard X-ray photoelectron spectroscopy," J. Electron Spectrosc. Relat. Phenom. **185**, 4–12 (2012).

[154] A. Jablonski, "Remarks on the definition of the backscattering factor in AES," Surf. Sci. **499**, 219–228 (2002).

[155] A. Jablonski and C. J. Powell, "The backscattering factor in Auger electron spectroscopy: New approach for an old subject," Surf. Sci. **574**, 219–232 (2005).

[156] X. Llovet, F. Salvat, D. Bote, F. Salvat-Pujol, A. Jablonski, and C. J. Powell, NIST Database of Cross Sections for Inner-Shell Ionization by Electron or Positron Impact, Version 1.0 Standard Reference Data Program, Database 164, US Department of Commerce, National Institute of Standards and Technology, Gaithersburg, MD, 2011, https://www.nist.gov/srd/nist-standard-reference-database-164.

[157] A. Jablonski and C. J. Powell, NIST Backscattering-Correction-Factor Database for Auger Electron Spectroscopy, Version 1.1, Standard Reference Data Program Database 154, US Department of Commerce, National Institute of Standards and Technology, Gaithersburg, MD, 2015, https://www.nist.gov/srd/nist-standard-reference-database-154.

[158] F. Salvat, A. Jablonski, C. J. Powell, and A. Y. Lee, NIST Electron Elastic-Scattering Cross-Section Database, Version 4.0, Standard Reference Data Program Database 64, US Department of Commerce, National Institute of Standards and Technology, Gaithersburg, MD, 2016, https://srdata.nist.gov/srd64/.